

## ABSTRACT

Title of dissertation:       **MULTIPLE ENERGY DISSIPATION STRATEGIES  
OF BASE ISOLATED STRUCTURES UNDER BLAST  
AND EARTHQUAKE**

Ruiyang Zhang, Master of Science, 2014

Dissertation directed by:   Assistant Professor, Brian M. Phillips  
Department of Civil and Environmental Engineering

Terrorist attacks have become a growing threat worldwide in recent years. Explosive devices, the weapon of choice for a majority of terrorist attacks, significantly threaten civilian and military personnel. Accordingly it is very important to protect critical buildings against blast loads with the main goal of preventing loss of life of the occupants. The research detailed within this dissertation will investigate innovative smart structures, including the mitigation of damage and loss of life under blast loading through base isolated structures combined with supplemental passive control devices without compromising the innate seismic protection that base isolation provides. The focus of this dissertation is the development and simulation of multiple control strategies for multi-story structures subjected to surface blasts and seismic excitations. The goal is to study and improve the response of base isolated structures under blast loadings and simultaneously keep the same level or better performance under earthquakes through alternative energy dissipation systems.

MULTIPLE ENERGY DISSIPATION STRATEGIES OF BASE ISOLATED  
STRUCTURES UNDER BLAST AND EARTHQUAKE

by

Ruiyang Zhang

Thesis submitted to the Faculty of the Graduate School of the  
University of Maryland, College Park in partial fulfillment  
of the requirements for the degree of  
Master of Science  
2014

Advisory Committee:

Professor Brian M. Phillips, Chair  
Professor Sherif M. Aggour  
Dr. Chung C. Fu

© Copyright by

Ruiyang Zhang

2014

## ACKNOWLEDGEMENTS

I would like to express my gratitude to my advisor, Professor Brian M. Phillips, for his excellent guidance, expert advice, patience, encouragement, and support of my research throughout my graduate studies at the University of Maryland, College Park. His academic insight and passion have greatly inspired me in many ways.

I would also like to thank the efforts of my committee members, Professor Sherif M. Aggour and Professor Chung C. Fu. All their support and comments are greatly appreciated.

## TABLE OF CONTENTS

LIST OF FIGURES .....	v
LIST OF TABLES .....	viii
CHAPTER 1 INTRODUCTION .....	1
1.1 Background and Motivation.....	1
1.2 Overview of Dissertation .....	3
CHAPTER 2 LITERATURE REVIEW .....	6
2.1 Blast Loading .....	6
2.2 Structural Control Technology.....	10
2.3 Chapter Summary.....	15
CHAPTER 3 BACKGROUND OF THE STRUCTURE SYSTEMS .....	16
3.1 5-story Structure System .....	17
3.2 8-story Structure System .....	23
3.3 Chapter Summary.....	31
CHAPTER 4 EXTERNAL LOADINGS.....	32
4.1 Near-Field Earthquake Ground Motions.....	32
4.2 Blast loads .....	34
4.2.1 Empirical Chart-based Approach.....	37
4.2.2 Empirical Equation-based Approach .....	38
4.2.3 Numerical Method .....	42
4.3 Chapter Summary.....	53
CHAPTER 5 MULTIPLE STRUCTURAL CONTROL STRATEGIES .....	54
5.1 Base Isolation Systems.....	54
5.2 Base Isolation with Additional Control Devices.....	67
5.2.1 Base Isolation System with TMD (IS-TB, IS-TR) .....	71
5.2.2 Base Isolation System with Cubic NES on the Base (IS-CN).....	72

5.2.3	Base Isolation System with Nonlinear Bumpers (IS-NB) .....	73
5.3	Chapter Summary.....	77
CHAPTER 6 RESULTS AND DATA ANALYSIS .....		78
6.1	Evaluation Criteria .....	78
6.2	Responses of Multiple Control Systems for the 5-story Structure.....	80
6.3	Responses of Multiple Control Systems for the 8-story Structure.....	103
6.4	Chapter Summary.....	116
CHAPTER 7 CONCLUSIONS AND RECOMMENDATIONS .....		118
7.1	Conclusions .....	118
7.1.1	Conclusions on 5-story Structure.....	118
7.1.2	Conclusions on 8-story Structure.....	119
7.2	Future Studies.....	120
REFERENCES .....		121

## LIST OF FIGURES

Figure 2.1: Exponential decay of pressure time history (UFC 3-340-02, 2008) .....	8
Figure 2.2: Positive phase shock wave parameters for a hemispherical TNT surface explosion (UFC 3-340-02, 2008).....	10
Figure 3.1: Schematic of 5-story base isolated structure model .....	17
Figure 3.2: (a) Isolation plan; (b) FEM model of superstructure; and (c) elevation view with devices (S. Narasimhan et al., 2006) .....	30
Figure 4.1: Time histories of earthquake records .....	33
Figure 4.2: Surface burst blast environment .....	36
Figure 4.3: Geometry of the 5-story structure under explosion.....	38
Figure 4.4: Time history of the blast overpressure on the 5-story structure .....	41
Figure 4.5: Time history of the blast loadings on the 5-story structure .....	42
Figure 4.6: 1-D spherically symmetric model in AUTODYN .....	44
Figure 4.7: 1-D spherically symmetric model with end condition of 18s in AUTODYN .....	45
Figure 4.8: 1-D spherically symmetric model with end condition of 10s in AUTODYN .....	45
Figure 4.9: Gage points on the 5-story structure model in AUTODYN.....	46
Figure 4.10: Gage points on the 8-story structure model in AUTODYN.....	47
Figure 4.11: Blast wave propagation around the 5-story structure in AUTODYN .....	48
Figure 4.12: Blast wave propagation around the 8-story structure in AUTODYN .....	48
Figure 4.13: Time histories of blast pressures of 100 kg TNT at the gage points on the 5-story structure in AUTODYN .....	49
Figure 4.14: Blast loadings of 50 kg TNT and 100 kg TNT on the 5-story structure .....	50
Figure 4.15: Comparison of blast loadings from empirical equation-based approach and numerical method.....	51
Figure 4.16: Blast loadings of 2000 kg TNT on the 8-story structure .....	52
Figure 5.1: Force-displacement characteristics of bearings (S. Narasimhan et al., 2006) .....	55
Figure 5.2: Model of the LRB in Simulink.....	58

Figure 5.3: Model of the FPB in Simulink .....	58
Figure 5.4: Hysteresis loop of the linear elastomeric bearings .....	59
Figure 5.5: Hysteresis loop of the LRB .....	59
Figure 5.6: Hysteresis loop of the FPB .....	60
Figure 5.7: Schematic of shifts by rotation .....	61
Figure 5.8: Biaxial Bouc-Wen model in Simulink .....	67
Figure 5.9: Schematic of 5-story base isolated structure with supplemental devices.....	68
Figure 5.10: Simulink diagram of base isolated system with supplemental device .....	70
Figure 5.11: Simulink diagram of the TMD .....	72
Figure 5.12: Simulink diagram of the cubic NES.....	73
Figure 5.13: Example of pyramidal nonlinear bumper (Luo et al., 2014) .....	74
Figure 5.14: Schematic of the installation of the nonlinear bumper on 8-story structure .....	75
Figure 5.15: Simulink diagram of the nonlinear bumper.....	76
Figure 5.16: Force vs. displacement of the nonlinear bumper.....	76
Figure 6.1: Performance of base isolation on maximum superstructure interstory drift under multiple excitations.....	84
Figure 6.2: Performance of base isolation on maximum superstructure absolute acceleration under multiple excitations .....	84
Figure 6.3: Time history of the superstructure absolute acceleration under explosion of 50 kg TNT.....	85
Figure 6.4: The base shears of base isolation under multiple excitations.....	86
Figure 6.5: Performance of the IS-TR and IS-TB under Northridge earthquake .....	87
Figure 6.6: Performance of the IS-TR and IS-TB under explosion of 50 kg TNT.....	87
Figure 6.7: Performance of IS-CN on $J_1$ with varying stiffness .....	88
Figure 6.8: Performance of IS-CN on $J_2$ with varying stiffness .....	88
Figure 6.9: Performance of IS-CN on $J_3$ with varying stiffness .....	89
Figure 6.10: Performance of IS-CN on $J_4$ with varying stiffness .....	89
Figure 6.11: Performance of IS-CN on $J_5$ with varying stiffness .....	89
Figure 6.12: Performance of IS-CN on $J_6$ with varying stiffness .....	90
Figure 6.13: Performance of IS-CN on $J_7$ with varying stiffness .....	90
Figure 6.14: Performance of IS-CN on $J_8$ with varying stiffness .....	90





## LIST OF TABLES

Table 3.1: Parameters of 5-story base-isolated structural model.....	18
Table 3.2: Natural periods of the superstructure (seconds) .....	29
Table 4.1: Characteristics of the near-field records .....	34
Table 4.2: Conversion factors for explosives .....	36
Table 6.1: Symbols of different systems.....	81
Table 6.2: Performance of traditional control strategies.....	82
Table 6.3: Responses of multiple control systems under blast and earthquakes .....	95
Table 6.4: Reductions on different criteria .....	100
Table 6.5: Responses of multiple control systems under blast and earthquakes in $x-d$ .....	110
Table 6.6: Responses of multiple control systems under blast and earthquakes in $y-d$ .....	111
Table 6.7: Reductions on different criteria in $x-d$ .....	113
Table 6.7: Reductions on different criteria in $y-d$ .....	114

# CHAPTER 1 INTRODUCTION

## 1.1 Background and Motivation

In recent years, terrorist activities and threats have become a growing problem all over the world. The use of extremely powerful explosive devices in terrorist attacks on civilian and military targets has become an increasing threat to the safety and well-being of society. Explosive devices produce a supersonic shock wave, which is a high pressure area that expands rapidly outward from the explosive center as a sphere or semi-sphere of compressed gases, causing catastrophic damage to buildings and their occupants. . The protection of buildings and occupants against the terrorist acts involves prediction, prevention, and mitigation of such events.

If security measures are breached, the energy absorption and dissipation provided by the structures at both local and global levels can help mitigate damage and loss of life. In the case of short standoff distances, surrounding partition walls, floor systems, and connections are severely overloaded and will experience damage. If the damage does not lead to progressive collapse, the global structure may be saved, though is likely to require demolition and reconstruction. On the other hand, for medium to long standoff distances, it is feasible that walls, floors, and connections may survive initial local overloads from the blast. In such cases, the blast may also load the global energy dissipation system of the structure, where it is feasible to absorb and safely dissipate the kinetic energy. This research will focus on the latter case, protecting structures from medium to long standoff distance blasts through improved global energy absorption and dissipation.

Structural control technology has been widely accepted as an effective way for the protection of structures against seismic hazards. Base isolation is one of the most popular structural control technologies used to enhance the performance of structures subjected to severe ground excitations. The isolation bearings employed at the base level of a structure naturally reduce its fundamental natural frequency to avoid the predominant frequencies of the ground motion, but concurrently result in large base displacements. The combination of base isolation with other passive devices, i.e., tuned mass damper (TMD), creates the possibility of achieving a balanced level of control performance, reducing both floor accelerations as well as base displacements. The potential for such structural control strategies under blast loading is investigated in this dissertation.

The research detailed within this dissertation will investigate innovative smart structures, including the mitigation of damage and loss of life under blast loading through base isolated structures without compromising the innate seismic protection that base isolation provides. The focus of this dissertation is the development and simulation of multiple control strategies for multi-story structures subjected to surface blasts and seismic excitations. The goal is to study and improve the responses of the structures under blast loadings and simultaneously keep the same level of performance or better under earthquakes through alternative energy dissipation systems. A 5-story simple structure and an 8-story full-scale structure are adopted in this study.

The 5-story simple frame structure is established to prototype control alternatives while the 8-story benchmark structure used matches realistic dynamic characteristics of a representative full-scale structure in Los Angeles, California. The superstructures of both systems are considered to be linear elastic. The base isolation system consists of three

alternative types of isolation elements so that any combination of these can be used for a particular simulation. For the 8-story building, lateral motion in two directions as well as torsion of the structure is considered. The isolation bearings are modeled in multi-directions and able to dissipate energy from bi-directional dynamic loads. Beyond the base isolated systems, supplemental devices, such as tuned mass dampers (TMD), are investigated. In addition, new energy dissipation systems such as nonlinear energy sinks (NES) and nonlinear bumpers are proposed and analyzed. The performance of all control systems are investigated under both blast loadings and seismic excitations for both structures.

## **1.2 Overview of Dissertation**

This dissertation investigates innovative smart structures in detail, including the mitigation of explosion on base-isolated structures and the seismic protection of buildings. The focus of this dissertation is the development and simulation of multiple control strategies for multiple degrees of freedom structures subjected to the surface burst and seismic excitations. The goal of this research is to study and improve the base isolation system under explosions and concurrently maintain the performance of the base isolation under seismic excitations.

Chapter 2 reviews the previous studies on blast loading and structural control technologies. First, knowledge about explosions is briefly addressed. Structural control technologies including base isolation are subsequently introduced. Finally, the benefits and shortcomings of base isolation and modified base isolation systems are summarized.

Chapter 3 provides the information about the structure systems used in this study. First, a simple 5-story structure with one degree-of-freedom on each floor is presented. This lumped-parameter model is assumed to remain linear-elastic during external dynamic excitations. In addition, the three-dimensional 8-story structure is introduced to represent a full-scale building in California. The superstructure of this building is assumed to remain linear-elastic, and the base and floors are assumed to be rigid in the horizontal plane. Three degrees-of-freedom are used to represent each floor at the center of mass. The base isolated system totally consists of 27 degrees-of-freedom. Finally, the equations of motion under blast loads and earthquake loads are derived and given for these structural systems.

Chapter 4 presents the external dynamic excitations applied on the structure systems in this study, including both explosions and earthquakes. Four earthquake records are provided and used as the base input for this study. The earthquakes are El Centro ( $M_w$  6.4, 1979), Northridge ( $M_w$  6.7, 1994), Kobe ( $M_w$  6.8, 1995), and Tohoku ( $M_w$  9.0, 2011). For blast loading, the methods to estimate the explosive pressure are introduced, including both empirical and numerical methods.

Chapter 5 describes the multiple structural control strategies used in this study, including base isolation and the combination of base isolation and supplemental devices. First, for the base isolation system, three types of base isolators are introduced, including linear elastomeric bearings, friction pendulum bearings, and lead rubber bearings. A biaxial Bouc-Wen model is presented for the 8-story structure, used to represent the nonlinear behavior of both friction pendulum bearings and lead rubber bearings. The supplemental devices, such as tuned mass dampers (TMD), nonlinear energy sinks (NES),

and nonlinear bumpers, are introduced. The configurations of different combinations of additional devices are also presented.

Chapter 6 presents the responses of the 5-story structure and the 8-story structure under multiple external excitations. First, evaluation criteria are provided to compare the performance between multiple control devices. Base isolation is verified to be functional and provide good response reductions under blast loadings. However, base isolation leads to a large base displacement which could damage the base isolators and structure itself. Thus, extra passive devices are installed on the base isolation system to achieve favorable overall responses.

Chapter 7 summarizes the research presented in this dissertation. Additionally, a number of research areas for future studies are proposed.

## CHAPTER 2 LITERATURE REVIEW

This chapter presents a literature review of blast loading, structural control technologies, and base isolation systems with supplemental devices.

### 2.1 Blast Loading

Many of the damaging effects of an explosion come from the shock wave created when the atmosphere surrounding the explosion is pushed back due to a compressive pulse travelling outward from the center of the explosion (Kinney, 1985). The front of the wave, also known as the shock front, has an overpressure much higher than the atmosphere behind it and thus immediately decays as the shock propagates outward (Beshara, 1994). The release of energy from a detonation leads to a sharp pressure increasing from the ambient pressure to a peak incident pressure. As the blast wave propagates through the air, the air behind shock front has lower velocity because the pressure is smaller than the incident pressure. When the blast wave encounters an obstacle normal to the direction of wave propagation, the pressure becomes reflected pressure.

The most commonly used approach to scale blast waves based on their distance and weight is the cube root scaling law, otherwise known as Hopkinson's law (Baker, 1973). This law states that two different weights of the same explosive have same blast characteristics at some scaled distances in similar atmospheric conditions. The Hopkinson scaling distance  $Z$  is defined as:



$$Z = \frac{R}{W^{1/3}} \quad (2.1)$$

where  $R$  is the distance from the blast center to the interest of point on the structure and  $W$  is the weight of charge.

Brode (1955) estimated the peak overpressure  $P_s$  due to spherical blast based on Hopkins scaling distance:

$$P_s = \frac{670}{Z^3} + 100, \text{ kPa} \quad (P_s > 1000 \text{ kPa}) \quad (2.2)$$

$$P_s = \frac{97.5}{Z} + \frac{145.5}{Z^2} + \frac{585}{Z^3} - 1.9, \text{ kPa} \quad (10 < P_s < 1000 \text{ kPa}) \quad (2.3)$$

Newmark and Hansen (1961) proposed the peak overpressure in terms of standoff distance and weight of charge at the ground level:

$$P_s = 6784 \frac{W}{R^3} + 93 \sqrt{\frac{W}{R^3}}, \text{ bar} \quad (2.4)$$

Another expression of peak overpressure was proposed by Mills (1987):

$$P_s = \frac{1772}{Z^3} - \frac{114}{Z^2} + \frac{108}{Z}, \text{ kPa} \quad (2.5)$$

During the wave propagation, the pressure may drop below ambient pressure, causing suction. A blast has an overpressure phase called the positive phase and an under-pressure phase known as the negative phase as shown in Figure 2.1.

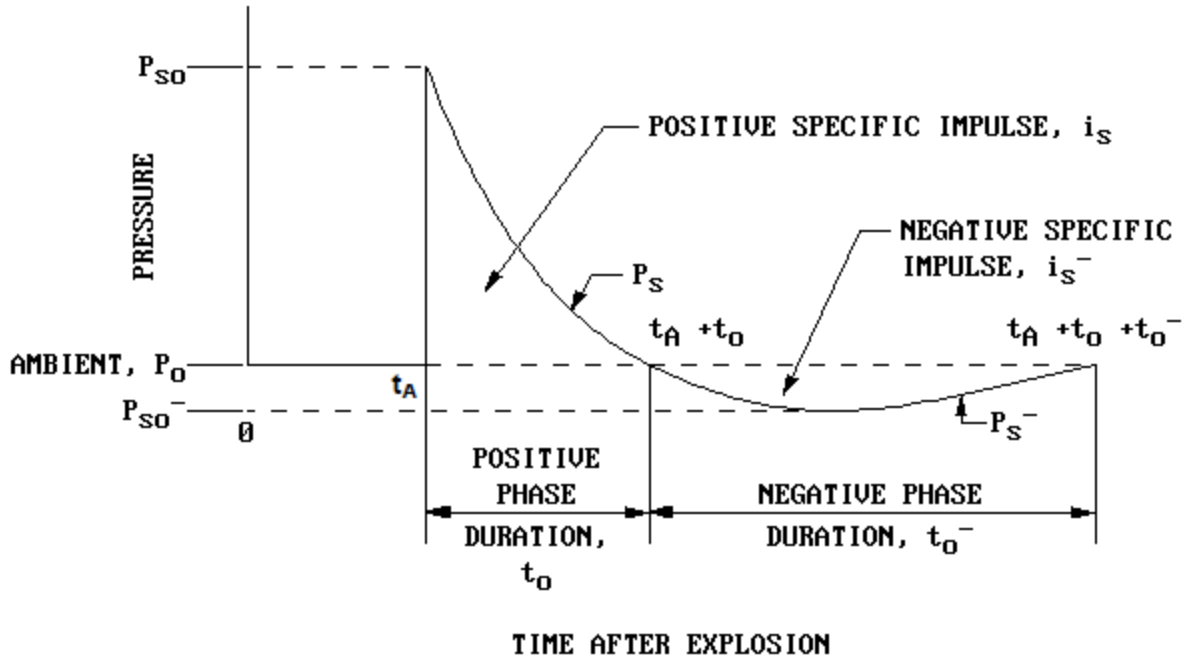


Figure 2.1 Exponential decay of pressure time history (UFC 3-340-02, 2008)

The pressure time history  $P(t)$  of blast wave was proposed by several researchers attempting to describe the theoretical curve of Figure 2.1. The simplest form assumes a linear decay given by Baker (1973). Further attempts were made to allow for a negative exponential form as follows (Bulson, 1997):

$$P(t) = P_0 + P_s \left(1 - \frac{t}{T_s}\right) \exp\left(-\gamma \frac{t}{T_s}\right) \quad (2.6)$$

where  $P(t)$  is the pressure in time;  $\gamma$  is the parameter controlling the rate of wave amplitude decay; and  $T_s$  is the duration of the positive phase. The parameters  $\gamma$  and  $T_s$  are defined as (Smith, 1994 and Lam, 2004).

$$\gamma = Z^2 - 3.7Z + 4.2 \quad (2.7)$$

$$T_s = W^{1/3} 10^{\left[-2.75+0.271\log\left(\frac{R}{W^{1/3}}\right)\right]} \quad (2.8)$$

Lam (2004) also proposed the reflected overpressure  $P_r$ , with a coefficient  $C_r$  given by

$$C_r = 3 \left( \sqrt[4]{\frac{P_s}{101}} \right) \quad (2.9)$$

$$P_r = C_r \cdot P_s \quad (2.10)$$

where  $P_s$  is the peak incident overpressure in unit of kPa.

Rankin and Hugoniot (1870) introduced the equation for reflected overpressure  $P_r$ .

$$P_r = 2P_s \left[ \frac{7P_0 + 4P_s}{7P_0 + P_s} \right] \quad (2.11)$$

where  $P_0$  is ambient air pressure in kPa (101 kPa typically).

UFC 3-340-02 (2008) provided peak reflected overpressure, peak incident overpressure, arrival time, positive time duration, wave velocity and the impulse of incident and reflected overpressure in terms of scaled standoff distance. The shock wave parameters for a hemispherical TNT blast are shown in Figure 2.2.

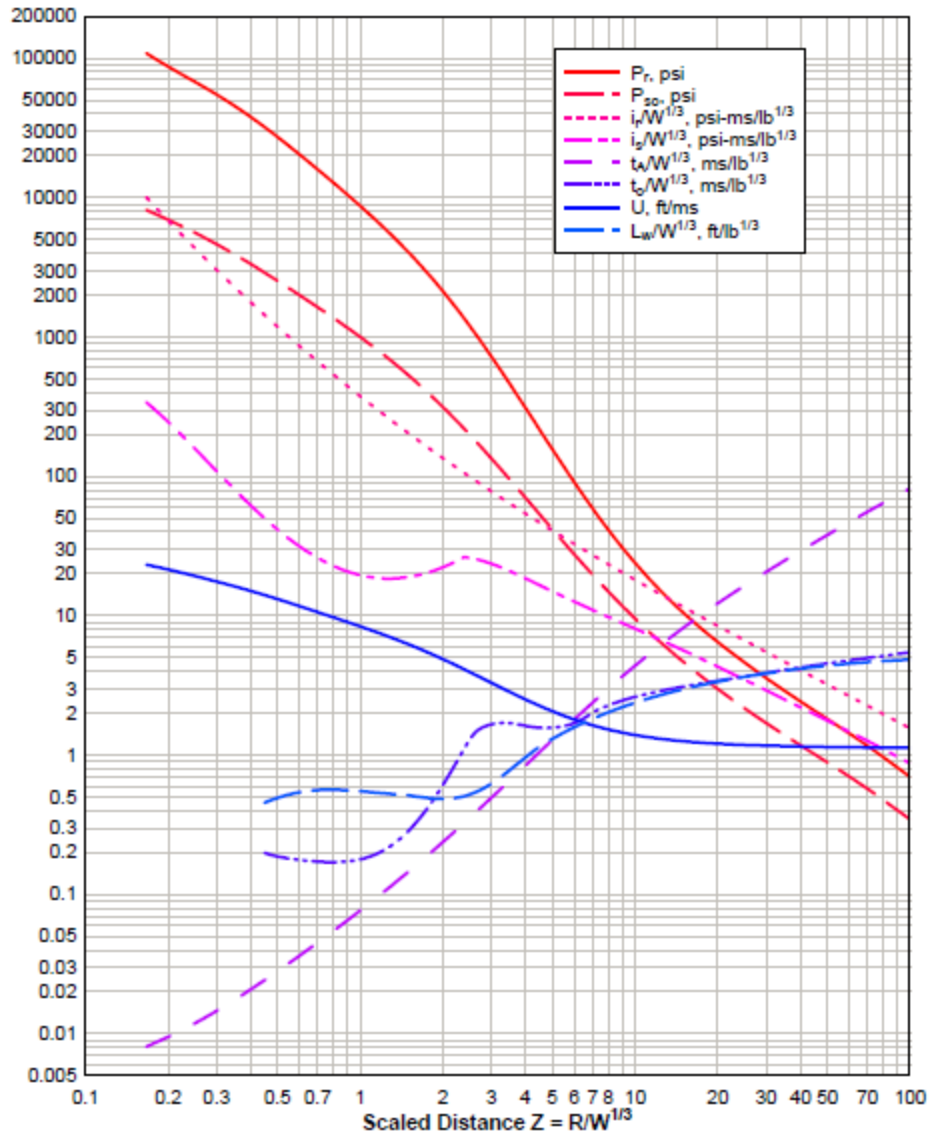


**Figure 2.2 Positive phase shock wave parameters for a hemispherical TNT surface explosion (UFC 3-340-02, 2008)**

## 2.2 Structural Control Technology

Experience and records of past earthquakes highlight the widespread potential failure of structures leading to great loss of life and economic losses. The Northridge earthquake with a magnitude of 6.7 occurred in the U.S. on January 17, 1994 resulting in

\$20 billion losses. The Kobe earthquake with a magnitude of 6.8 occurred in Japan on January 17, 1995, resulting in more than 6,000 people killed and over 200,000 buildings damaged or destroyed. The 1999 Chi-Chi earthquake in Taiwan with a magnitude of 7.6 caused the deaths of 2,500 people and the collapse of 50,000 buildings. The magnitude 9.0 Tōhoku earthquake occurred in Japan on March 11, 2011, resulting in 16,000 deaths as well as 130,000 buildings totally collapsed. These events reveal the duty of researchers and engineers to find solutions to mitigate the effects of extreme events for the protection of structures and thereby human lives.

Structural control technology, as an important research branch of the smart structural technologies, has drawn much more attentions from researchers for several advantages such as improving safety and serviceability and preventing catastrophic collapse of structures due to extreme loadings. The basic idea behind structural control is to efficiently dissipate kinetic energy, alter the dynamics of the structure (e.g., by shifting the natural frequencies), or add energy to produce more favorable responses during earthquakes or other extreme excitations. Structural control can be achieved through passive, active, or semi-active control devices, or a combination of any of the three. Structural control strategies focus on the protection of structures to avoid structural responses that exceed prescribed limits.

Passive control systems applied to structures are the conventional control strategy for seismic protection due to their simplicity and robustness. A large number of passive control systems have been developed and installed in structures to enhance the performance under seismic excitations. Passive control devices may be grouped into three types: energy dissipaters, tuned dampers, and base isolators. Energy dissipaters enhance

the energy dissipation capacity by converting kinetic energy into heat energy. Mahmoodi (1969) proposed the concept of viscoelastic dampers (VEDs). Zhang (1989) experimentally and analytically investigated the performance of VEDs in reducing the seismic responses of steel structures. In early the 1990s, added stiffness damping devices (ADAS) and triangular plates (TADAS) were proposed by Whittaker et al. (1991) and Tsai et al. (1993). Tuned dampers work on the principle of transferring energy to the damper among the vibrating modes. Tuned mass damper (TMD) was initially introduced to control the displacement responses of the structures subjected to wind-introduced vibrations (McNamara, 1977; Luft, 1979). The performance of TMDs under seismic excitations was investigated and it concluded that the TMDs were not effective in reducing the maximum responses in tall buildings (Sladek and Klinger, 1983). Soong and Dargush (1997) summarized the progress of the passive control strategies with civil engineering implementations. However, many challenges and difficulties still exist in passive control techniques (Soong and Constantinou, 1994). Passive devices are often tuned to protect the structure from a particular dynamic loading magnitude and frequency content, and thus the performance of these devices is suboptimal for other loading scenarios.

Base isolation is one of the most popular passive control techniques. In a base isolation system, the energy transmitted to the superstructure from a ground excitation is attenuated by adding base isolators to reduce the fundamental natural frequency of the structure. Base isolation shifts the fundamental period of the structure out of the range of the dominant magnitudes in excitations and also increases the energy-absorbing capability of the structure (Kelly et al. 1987; Kelly 1997). Although interstory drifts, floor

accelerations and base shears are significantly reduced, the base isolation systems concurrently induce larger base displacements (Kelly 1999; Nagarajaiah and Ferrell 1999; Buckle et al. 2002). The large displacements can lead to challenges such as impact with moat walls or damage to the base isolators. Therefore, effectively reducing the base displacements has become an issue for improvement of the base isolation functionality.

Active control is another structural control strategy, using an external power source to improve the performance of structures under excitations. Generally, compared to passive control devices, active control techniques can provide better performance (Soong and Constantinou, 1994). Yao (1972) first proposed the active control of civil structures. The active control strategies use the force or energy generated from control devices to counteract the energy of the dynamic loadings and control different vibration modes and accommodate a wider range of loading conditions (Housner et al., 1997). The control algorithms need to be reliable and workable through all feasible dynamic excitations (Spencer et al., 1994). Many of experiments have been conducted to verify actively controlled systems, coupled with many real-world implementations on civil structures (Soong and Constantions, 1994; Spencer and Sain, 1997). Spencer and Soong (1999) provide detailed lists of these full-scale implementations of active control techniques. Although active control strategy has been proved as a practical technique by many experiments and implementations, there are still some potential risks existing in real-world applications. For example, the power supply from external sources could be interrupted during natural hazards resulting in erroneous and even damaging control forces applied to the system. Furthermore, disturbances in the measurements of structural

responses or computer error could destabilize the system. Details surrounding the real-world application of active control techniques continue to be an active area of research.

A semi-active control system can be viewed as a controllable passive system which typically requires a small amount of external power to operate. The control forces are dissipative only and selected based on feedback from the response of the structure. Semi-active control systems have positive features of both the passive and active control systems while avoiding some challenging problems. Semi-active devices can be adjusted to get better performance by changing the parameters, such as the power levels, stiffness and the damping values (Spencer and Nagarajaiah, 2003), improving their performance beyond passive systems. Semi-active control systems do not have the potential to destabilize the system (Spencer and Sain 1997; Spencer and Nagarajaiah 2003), avoiding issues associated with active systems. As a result of these strong features, semi-active devices are particularly promising and have received increasing attention and interest from researchers. Numerous research and experiments have been conducted to validate the performance of this smart technology. For example, Kobori et al. (1993) and Kurata et al. (1999, 2000) studied a variable orifice damper applied to a full-scale building. A variable friction damper was proposed to reduce the interstory drifts of buildings under seismic excitations (Dowdell and Cherry, 1994; Inaudi, 1997). Controllable fluid dampers such as electrorheological (ER) and magnetorheological (MR) damper were proposed for the application to civil structures (Dyke et al. 1996).



### **2.3 Chapter Summary**

This chapter reviews a number of previous studies on blast loadings and structural control technologies. Passive base isolation has been widely demonstrated as one effective method to enhance the structural performance under severe seismic excitations. However, these previous studies only verify the performance of base isolation under seismic excitations. There is potential for these popular passive devices to provide global energy dissipation under different loading types. Therefore, the performance of base isolation under explosions is investigated and multiple control devices are proposed to enhance the performance of base isolation system under explosions. Solutions will aim to avoid large base displacement induced by base isolation which can potentially exceed the allowable limit of structural designs.

## CHAPTER 3 BACKGROUND OF THE STRUCTURE SYSTEMS

In this chapter, information on the structural systems used in this study is presented. Two structure models are used to investigate the performance of different control devices to protect the structures from external dynamic loadings. The first structure is a simple 5-story building modeled with one degree-of-freedom (DOF) on each floor. Only behavior of the building in one direction is considered and analyzed. The second structure is an 8-story structure modeled with a total of 24 DOF, three at each story. The superstructures of each building are modeled as linear elastic with nonlinearities concentrated at the base isolation devices or supplemental control devices.

The state space equations of structures are formulated as:

$$\dot{\mathbf{Z}} = \mathbf{A}_s \mathbf{Z} + \mathbf{B}_s \mathbf{u} \quad (3.1)$$

$$\mathbf{y} = \mathbf{C}_s \mathbf{Z} + \mathbf{D}_s \mathbf{u} \quad (3.2)$$

where

$$\mathbf{Z} = \begin{Bmatrix} \mathbf{X} \\ \dot{\mathbf{X}} \end{Bmatrix} \quad \dot{\mathbf{Z}} = \begin{Bmatrix} \dot{\mathbf{X}} \\ \ddot{\mathbf{X}} \end{Bmatrix} \quad \mathbf{y} = \begin{Bmatrix} \mathbf{X} \\ \dot{\mathbf{X}} \\ \ddot{\mathbf{X}}_{\text{abs}} \end{Bmatrix}$$

$\mathbf{u}$  is the input to the structure system, and  $\mathbf{A}_s$ ,  $\mathbf{B}_s$ ,  $\mathbf{C}_s$ , and,  $\mathbf{D}_s$  are state space matrices, which will be introduced for specific structure under specific excitation in the following sections;  $\mathbf{X}$ ,  $\dot{\mathbf{X}}$ , and  $\ddot{\mathbf{X}}$  are the vectors of displacements, velocities and relative accelerations of the structures.

### 3.1 5-story Structure System

The 5-story base-isolated structure used in the study of Kelly et al. (1987) and Johnson et al. (1998) is adopted as a basic representation of simple low-rise structures. The model, shown in both fixed-base and base-isolated configurations in Figure 3.1, is a lumped-parameter model with 1 DOF on each floor. This 5-DOF model is assumed to remain linear-elastic during external dynamic excitations.

The parameters of the base-isolated structure are listed in Table 3.1. The parameters of the fixed-base structure are taken from the superstructure of the base-isolated system. The fundamental period of the fixed base structure is 0.3 seconds and fundamental period of the base-isolated structure is 2.5 seconds.

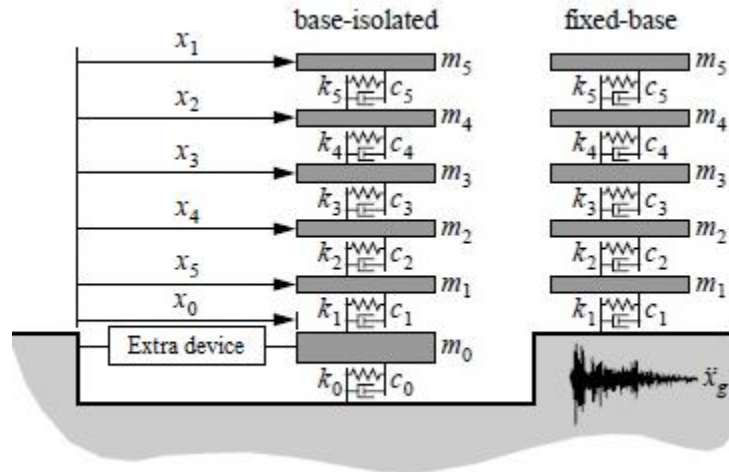


**Figure 3.1 Schematic of 5-story base isolated structure model**

**Table 3.1 Parameters of 5-story base-isolated structure model**

Floor	Floor Mass (kg)	Story Stiffness (kN/m)	Damping Coefficient (kNs/m)
Base	$m_0=6,800$	$k_0=231.5$	$c_0=7,450$
1	$m_1=5,897$	$k_1=33,732$	$c_1=67,000$
2	$m_2=5,897$	$k_2=29,093$	$c_2=58,000$
3	$m_3=5,897$	$k_3=28,621$	$c_3=57,000$
4	$m_4=5,897$	$k_4=24,954$	$c_4=50,000$
5	$m_5=5,897$	$k_5=19,059$	$c_5=38,000$

To calculate the blast loads applied on the structure, the width of the surface subjected to the explosion is assumed to be 12 meters, and the height of each story is assumed to be 3 meters.

### Fixed-base structure equations of motion

Let  $x_i$  ( $i=1, 2, 3, 4, 5$ ) denote the displacement of the fixed-base structure relative to the ground for the  $i$ -th floor. The displacement vector is  $x(t) = [x_1 \ x_2 \ x_3 \ x_4 \ x_5]^T$ .

For the fixed-base 5-story structure, the equations of motion subject to ground excitation  $\ddot{x}_g$  and blast loading  $\mathbf{F}_B$  are expressed as Eq. 3.3 and Eq. 3.4, respectively.

$$\mathbf{M}\ddot{\mathbf{x}} + \mathbf{C}\dot{\mathbf{x}} + \mathbf{K}\mathbf{x} = -\mathbf{M}\Gamma\ddot{x}_g \quad (3.3)$$

$$\mathbf{M}\ddot{\mathbf{x}} + \mathbf{C}\dot{\mathbf{x}} + \mathbf{K}\mathbf{x} = \Lambda_1\mathbf{F}_B \quad (3.4)$$

where  $\mathbf{M}$  is the lumped mass matrix,  $\mathbf{K}$  is the stiffness matrix, and  $\mathbf{C}$  is the damping matrix of the superstructure;  $\mathbf{x}$ ,  $\dot{\mathbf{x}}$ , and  $\ddot{\mathbf{x}}$  are the displacement of the superstructure and its first and second derivative with respect to time, respectively;  $\mathbf{F}_b$  is a  $6 \times 1$  vector of blast loads applied on different stories; and  $\mathbf{\Gamma}$  and  $\mathbf{\Lambda}_1$  are the distribution matrices of external dynamic loadings.

$$\mathbf{F}_b = \begin{bmatrix} F_5 \\ F_4 \\ F_3 \\ F_2 \\ F_1 \\ F_b \end{bmatrix}; \quad \mathbf{\Gamma} = \begin{bmatrix} 1 \\ 1 \\ 1 \\ 1 \\ 1 \end{bmatrix}; \quad \mathbf{\Lambda}_1 = \begin{bmatrix} 1 & 0 & 0 & 0 & 0 & 0 \\ 0 & 1 & 0 & 0 & 0 & 0 \\ 0 & 0 & 1 & 0 & 0 & 0 \\ 0 & 0 & 0 & 1 & 0 & 0 \\ 0 & 0 & 0 & 0 & 1 & 0 \end{bmatrix}$$

The state space matrices of the state space equations in Eq. 3.1 and Eq. 3.2 for the fixed-base structure under earthquakes are given by:

$$u = \ddot{x}_g$$

$$\mathbf{A}_s = \begin{bmatrix} \mathbf{0} & \mathbf{I} \\ -\mathbf{M}^{-1}\mathbf{K} & -\mathbf{M}^{-1}\mathbf{C} \end{bmatrix} \quad \mathbf{B}_s = \begin{bmatrix} \mathbf{0} \\ -\mathbf{\Gamma} \end{bmatrix}$$

$$\mathbf{C}_s = \begin{bmatrix} \mathbf{I} & \mathbf{0} \\ \mathbf{0} & \mathbf{I} \\ -\mathbf{M}^{-1}\mathbf{K} & -\mathbf{M}^{-1}\mathbf{C} \end{bmatrix} \quad \mathbf{D}_s = [\mathbf{0}]$$

The state space matrices of the state space equations in Eq. 3.1 and Eq. 3.2 for the fixed-base structure under blasts are given by:

$$\mathbf{u} = \mathbf{F}_b$$

$$\mathbf{A}_s = \begin{bmatrix} \mathbf{0} & \mathbf{I} \\ -\mathbf{M}^{-1}\mathbf{K} & -\mathbf{M}^{-1}\mathbf{C} \end{bmatrix} \quad \mathbf{B}_s = \begin{bmatrix} \mathbf{0} \\ \mathbf{M}^{-1}\Lambda_1 \end{bmatrix}$$

$$\mathbf{C}_s = \begin{bmatrix} \mathbf{I} & \mathbf{0} \\ \mathbf{0} & \mathbf{I} \\ -\mathbf{M}^{-1}\mathbf{K} & -\mathbf{M}^{-1}\mathbf{C} \end{bmatrix} \quad \mathbf{D}_s = \begin{bmatrix} \mathbf{0} \\ \mathbf{M}^{-1}\Lambda_1 \end{bmatrix}$$

### Base-isolated structure equations of motion

Note that the fixed base structure is the same as the superstructure for the base isolated system. The equations of motion for the base isolated system will therefore be created by introducing an additional degree-of-freedom  $x_b$  to the superstructure equations of motion. The degrees-of-freedom of the superstructure will be considered relative to the base and the degree-of-freedom of the base is relative to the ground.

For the base-isolated system, the isolation bearings are assumed to be linear for the 5-story structure, so the properties can be included in the equations of motion which is shown as follows.

*Under ground excitation:*

$$\text{Superstructure:} \quad \mathbf{M}\ddot{\mathbf{x}} + \mathbf{C}\dot{\mathbf{x}} + \mathbf{K}\mathbf{x} = -\mathbf{M}\Gamma(\ddot{x}_g + \ddot{x}_b) \quad (3.5)$$

$$\text{Base:} \quad m_b\ddot{x}_b + c_b\dot{x}_b + k_b x_b = -m_b\ddot{x}_g - \Gamma^T\mathbf{M}(\ddot{\mathbf{x}} + \Gamma\ddot{x}_g + \Gamma\ddot{x}_b) \quad (3.6)$$

where  $m_b$ ,  $k_b$ ,  $c_b$  are the mass, stiffness, and damping properties of the base and  $\dot{x}_b$  and  $\ddot{x}_b$  are the first and second derivative of base displacement with respect to time, respectively.

Combining Eq. 3.5 and Eq. 3.6, equation of motion of the 5-story base-isolated structure under seismic excitation is:

$$\bar{\mathbf{M}}\ddot{\mathbf{X}} + \bar{\mathbf{C}}\dot{\mathbf{X}} + \bar{\mathbf{K}}\mathbf{X} = -\Phi_1\ddot{x}_g \quad (3.7)$$

where

$$\mathbf{X} = \begin{pmatrix} \mathbf{x} \\ x_b \end{pmatrix} \quad \dot{\mathbf{X}} = \begin{pmatrix} \dot{\mathbf{x}} \\ \dot{x}_b \end{pmatrix} \quad \ddot{\mathbf{X}} = \begin{pmatrix} \ddot{\mathbf{x}} \\ \ddot{x}_b \end{pmatrix}$$

$$\bar{\mathbf{M}} = \begin{bmatrix} \mathbf{M} & \mathbf{M}\Gamma \\ \Gamma^T\mathbf{M} & \Gamma^T\mathbf{M}\Gamma + m_b \end{bmatrix} \quad \Phi_1 = \begin{bmatrix} \mathbf{M}\Gamma \\ \Gamma^T\mathbf{M}\Gamma + m_b \end{bmatrix}$$

$$\bar{\mathbf{K}} = \begin{bmatrix} \mathbf{K} & \mathbf{0} \\ \mathbf{0} & k_b \end{bmatrix} \quad \bar{\mathbf{C}} = \begin{bmatrix} \mathbf{C} & \mathbf{0} \\ \mathbf{0} & c_b \end{bmatrix}$$

Eq. 3.5 and Eq. 3.6 can be rewritten as:

$$\text{Superstructure:} \quad \mathbf{M}(\ddot{\mathbf{x}} + \Gamma\ddot{x}_g + \Gamma\ddot{x}_b) + \mathbf{C}\dot{\mathbf{x}} + \mathbf{K}\mathbf{x} = \mathbf{0} \quad (3.8)$$

$$\text{Base:} \quad \Gamma^T\mathbf{M}(\ddot{\mathbf{x}} + \Gamma\ddot{x}_g + \Gamma\ddot{x}_b) + m_b(\ddot{x}_b + \ddot{x}_g) + c_b\dot{x}_b + k_b x_b = \mathbf{0} \quad (3.9)$$

where the absolute accelerations are:

$$\ddot{\mathbf{x}}_{\text{abs}} = \ddot{\mathbf{x}} + \Gamma\ddot{x}_g + \Gamma\ddot{x}_b \quad (3.10)$$

$$\ddot{x}_{b,abs} = \ddot{x}_b + \ddot{x}_g \quad (3.11)$$

The state space matrices of the state space equations in Eq. 3.1 and Eq. 3.2 are given by:

$$u = \ddot{x}_g$$

$$\mathbf{A}_s = \begin{bmatrix} \mathbf{0} & \mathbf{I} \\ -\overline{\mathbf{M}}^{-1}\overline{\mathbf{K}} & -\overline{\mathbf{M}}^{-1}\overline{\mathbf{C}} \end{bmatrix} \quad \mathbf{B}_s = \begin{bmatrix} \mathbf{0} \\ -\overline{\mathbf{M}}^{-1}\overline{\mathbf{\Phi}}_1 \end{bmatrix}$$

$$\mathbf{C}_s = \begin{bmatrix} \mathbf{I} & \mathbf{0} \\ \mathbf{0} & \mathbf{I} \\ -\overline{\mathbf{M}}_1^{-1}\overline{\mathbf{K}} & -\overline{\mathbf{M}}_1^{-1}\overline{\mathbf{C}} \end{bmatrix} \quad \mathbf{D}_s = [\mathbf{0}]$$

$$\overline{\mathbf{M}}_1 = \begin{bmatrix} \mathbf{M} & \mathbf{0} \\ \mathbf{\Gamma}^T\mathbf{M} & m_b \end{bmatrix}$$

*Under blast loadings:*

$$\text{Superstructure:} \quad \mathbf{M}\ddot{\mathbf{x}} + \mathbf{C}\dot{\mathbf{x}} + \mathbf{K}\mathbf{x} = \mathbf{\Lambda}_1\mathbf{F}_B - \mathbf{M}\mathbf{\Gamma}\ddot{x}_b \quad (3.12)$$

$$\text{Base:} \quad m_b\ddot{x}_b + c_b\dot{x}_b + k_b x_b = (\mathbf{\Gamma}^T\mathbf{\Lambda}_1 + \mathbf{\Lambda}_2)\mathbf{F}_B - \mathbf{\Gamma}^T\mathbf{M}(\ddot{\mathbf{x}} + \mathbf{\Gamma}\ddot{x}_b) \quad (3.13)$$

The combined equation of motion of base-isolated systems under blast can be obtained according to Eq. 3.12 and Eq. 3.13:

$$\overline{\mathbf{M}}\ddot{\mathbf{X}} + \overline{\mathbf{C}}\dot{\mathbf{X}} + \overline{\mathbf{K}}\mathbf{X} = \overline{\mathbf{\Phi}}_2\mathbf{F}_B \quad (3.14)$$

where

$$\overline{\mathbf{\Phi}}_2 = \begin{bmatrix} \mathbf{\Lambda}_1 \\ \mathbf{\Gamma}^T\mathbf{\Lambda}_1 + \mathbf{\Lambda}_2 \end{bmatrix} \quad \mathbf{\Lambda}_2 = [0 \ 0 \ 0 \ 0 \ 0 \ 1]$$

and  $\overline{\mathbf{M}}$ ,  $\overline{\mathbf{C}}$ , and  $\overline{\mathbf{K}}$  can be found in Eqn. 3.7.



To extract the absolute accelerations from the equations of motion, Eq. 3.12 and Eq. 3.13 can be rewritten as:

$$\text{Superstructure:} \quad \mathbf{M}(\ddot{\mathbf{x}} + \mathbf{\Gamma}\ddot{\mathbf{x}}_b) + \mathbf{C}\dot{\mathbf{x}} + \mathbf{K}\mathbf{x} = \mathbf{\Lambda}_1\mathbf{F}_B \quad (3.15)$$

$$\text{Base:} \quad \mathbf{\Gamma}^T\mathbf{M}(\ddot{\mathbf{x}} + \mathbf{\Gamma}\ddot{\mathbf{x}}_b) + m_b\ddot{\mathbf{x}}_b + c_b\dot{\mathbf{x}}_b + k_b\mathbf{x}_b = (\mathbf{\Gamma}^T\mathbf{\Lambda}_1 + \mathbf{\Lambda}_2)\mathbf{F}_B \quad (3.16)$$

where the absolute accelerations are:

$$\ddot{\mathbf{x}}_{\text{abs}} = \ddot{\mathbf{x}} + \mathbf{\Gamma}\ddot{\mathbf{x}}_b \quad (3.17)$$

$$\ddot{\mathbf{x}}_{b,abs} = \ddot{\mathbf{x}}_b \quad (3.18)$$

The state space matrices of the state space equations in Eq. 3.1 and Eq. 3.2 are given by:

$$\mathbf{u} = \mathbf{F}_B$$

$$\mathbf{A}_s = \begin{bmatrix} \mathbf{0} & \mathbf{I} \\ -\overline{\mathbf{M}}^{-1}\overline{\mathbf{K}} & -\overline{\mathbf{M}}^{-1}\overline{\mathbf{C}} \end{bmatrix} \quad \mathbf{B}_s = \begin{bmatrix} \mathbf{0} \\ \overline{\mathbf{M}}^{-1}\mathbf{\Phi}_2 \end{bmatrix}$$

$$\mathbf{C}_s = \begin{bmatrix} \mathbf{I} & \mathbf{0} \\ \mathbf{0} & \mathbf{I} \\ -\overline{\mathbf{M}}_1^{-1}\overline{\mathbf{K}} & -\overline{\mathbf{M}}_1^{-1}\overline{\mathbf{C}} \end{bmatrix} \quad \mathbf{D}_s = \begin{bmatrix} \mathbf{0} \\ \overline{\mathbf{M}}_1^{-1}\mathbf{\Phi}_2 \end{bmatrix}$$

### 3.2 8-story Structure System

An 8-story full-scale structure used in the study of Narasimhan et al. (2006) is adopted in this study to examine the proposed control systems under more realistic building responses. The benchmark structure is designed to match the dynamic

characteristics of a full-scale structure in Los Angeles, California. The building uses a steel-braced frame for lateral support and has dimensions of 82.4 m long by 54.3 m wide in plan and 32.32 m in elevation. The floor plan is L-shaped as shown in Figure 3.2. The superstructure is modeled as a three-dimensional linear elastic system. Both the floors and the base are assumed to be rigid in horizontal plane. Three DOF are used to represent each floor at the center of mass on the superstructure or the base. The base-isolated structure system consists of 27 degrees of freedom combining the superstructure and base isolation. All 24 modes in the original system (e.g., fixed-base case) are used in modeling the superstructure. The floor and base masses, 24 superstructure natural frequencies, and 24 superstructure mass-normalized mode shapes are given in the benchmark structure description. The stiffness matrix of the superstructure is extracted from this information using Eq. 3.19.

$$\psi_j^T K \psi_r = \begin{cases} 0 & \text{for } j \neq r \\ \omega_r^2 & \text{for } j = r \end{cases} \quad (3.19)$$

where  $\psi_j$  and  $\omega_j$  are the eigenvector and eigenvalue of  $j$ -th mode, respectively. The damping ratio is assumed to be 5% in all fixed-base modes. The natural periods for all 24 fixed-base modes are shown in Table 3.2. The natural periods of the base-isolated structure depend on how many base isolators been used as well as their locations. Furthermore, in the case of nonlinear base isolator models, the natural period cannot be determined.

### Fixed base structure equations of motion

The degrees of freedom of the superstructure are denoted as  $\{\mathbf{x}\}_{24 \times 1}$  and the degrees of freedom of the base are denoted as  $\{\mathbf{x}_b\}_{3 \times 1}$ . For the fixed base, the equations of motion are subject to the ground excitation  $\{\ddot{\mathbf{x}}_g\}_{3 \times 1}$  and blast loading  $\{\mathbf{F}_B\}_{27 \times 1}$ , expressed as Eq. 3.20 and Eq. 3.21, respectively.

$$\mathbf{M}\ddot{\mathbf{x}} + \mathbf{C}\dot{\mathbf{x}} + \mathbf{K}\mathbf{x} = -\mathbf{M}\mathbf{\Gamma}\ddot{\mathbf{x}}_g \quad (3.20)$$

$$\mathbf{M}\ddot{\mathbf{x}} + \mathbf{C}\dot{\mathbf{x}} + \mathbf{K}\mathbf{x} = \mathbf{\Lambda}_1 \mathbf{F}_B \quad (3.21)$$

where  $\mathbf{M}$  is the lumped mass matrix,  $\mathbf{K}$  is the stiffness matrix, and  $\mathbf{C}$  is the damping matrix of the superstructure;  $\dot{\mathbf{x}}$  and  $\ddot{\mathbf{x}}$  are the first and second derivative of displacement with respect to time, respectively;  $\mathbf{F}_B$  is a  $27 \times 1$  vector of blast loads applied on different stories;  $\{\mathbf{\Gamma}\}_{24 \times 3}$  and  $\{\mathbf{\Lambda}_1\}_{24 \times 27}$  are the distribution matrices defining the external dynamic loadings on each degree of freedom.

The state space matrices of the state space equations in Eq. 3.1 and Eq. 3.2 for the fixed-base structure under earthquakes are given by:

$$\mathbf{u} = \ddot{\mathbf{x}}_g$$

$$\mathbf{A}_s = \begin{bmatrix} \mathbf{0} & \mathbf{I} \\ -\mathbf{M}^{-1}\mathbf{K} & -\mathbf{M}^{-1}\mathbf{C} \end{bmatrix} \quad \mathbf{B}_s = \begin{bmatrix} \mathbf{0} \\ -\mathbf{\Gamma} \end{bmatrix}$$

$$\mathbf{C}_s = \begin{bmatrix} \mathbf{I} & \mathbf{0} \\ \mathbf{0} & \mathbf{I} \\ -\mathbf{M}^{-1}\mathbf{K} & -\mathbf{M}^{-1}\mathbf{C} \end{bmatrix} \quad \mathbf{D}_s = [\mathbf{0}]$$

The state space matrices of the state space equations in Eq. 3.1 and Eq. 3.2 for the fixed-base structure under blasts are given by:

$$\mathbf{u} = \mathbf{F}_B$$

$$\mathbf{A}_s = \begin{bmatrix} \mathbf{0} & \mathbf{I} \\ -\mathbf{M}^{-1}\mathbf{K} & -\mathbf{M}^{-1}\mathbf{C} \end{bmatrix} \quad \mathbf{B}_s = \begin{bmatrix} \mathbf{0} \\ \mathbf{M}^{-1}\Lambda_1 \end{bmatrix}$$

$$\mathbf{C}_s = \begin{bmatrix} \mathbf{I} & \mathbf{0} \\ \mathbf{0} & \mathbf{I} \\ -\mathbf{M}^{-1}\mathbf{K} & -\mathbf{M}^{-1}\mathbf{C} \end{bmatrix} \quad \mathbf{D}_s = \begin{bmatrix} \mathbf{0} \\ \mathbf{M}^{-1}\Lambda_1 \end{bmatrix}$$

### Base isolated structure equations of motion

For the base-isolated system, the equations of motion under ground excitation and blast loading are shown as follows.

*Under ground excitation:*

$$\text{Superstructure:} \quad \mathbf{M}\ddot{\mathbf{x}} + \mathbf{C}\dot{\mathbf{x}} + \mathbf{K}\mathbf{x} = -\mathbf{M}\Gamma(\ddot{\mathbf{x}}_g + \ddot{\mathbf{x}}_b) \quad (3.22)$$

$$\text{Base:} \quad \mathbf{M}_b\ddot{\mathbf{x}}_b + \mathbf{C}_b\dot{\mathbf{x}}_b + \mathbf{K}_b\mathbf{x}_b = -\mathbf{M}_b\ddot{\mathbf{x}}_g - \Gamma^T\mathbf{M}(\ddot{\mathbf{x}} + \Gamma\ddot{\mathbf{x}}_g + \Gamma\ddot{\mathbf{x}}_b) - \mathbf{f}_B \quad (3.23)$$

where  $\mathbf{M}_b$ ,  $\mathbf{K}_b$ ,  $\mathbf{C}_b$  are the mass, stiffness, and damping properties of the base;  $\dot{\mathbf{x}}_b$  and  $\ddot{\mathbf{x}}_b$  are the first and second derivative of base displacement with respect to time, respectively;  $\{\mathbf{f}_B\}_{3 \times 1}$  is the nonlinear bearing force from the nonlinear base isolators which are addressed in Chapter 5.

According to Eq. 3.22 and Eq. 3.23, equation of motion of the 8-story base-isolated structure under seismic excitation is:

$$\overline{\mathbf{M}}\ddot{\mathbf{X}} + \overline{\mathbf{C}}\dot{\mathbf{X}} + \overline{\mathbf{K}}\mathbf{X} = -\Phi_1\ddot{\mathbf{x}}_g - \Phi_3\mathbf{f}_B \quad (3.24)$$

where

$$\mathbf{X} = \begin{pmatrix} \mathbf{x} \\ \mathbf{x}_b \end{pmatrix} \quad \dot{\mathbf{X}} = \begin{pmatrix} \dot{\mathbf{x}} \\ \dot{\mathbf{x}}_b \end{pmatrix} \quad \ddot{\mathbf{X}} = \begin{pmatrix} \ddot{\mathbf{x}} \\ \ddot{\mathbf{x}}_b \end{pmatrix}$$

$$\overline{\mathbf{M}} = \begin{bmatrix} \mathbf{M} & \mathbf{M}\Gamma \\ \Gamma^T\mathbf{M} & \Gamma^T\mathbf{M}\Gamma + \mathbf{M}_b \end{bmatrix}_{27 \times 27} \quad \overline{\mathbf{K}} = \begin{bmatrix} \mathbf{K} & \mathbf{0} \\ \mathbf{0} & \mathbf{K}_b \end{bmatrix}_{27 \times 27} \quad \overline{\mathbf{C}} = \begin{bmatrix} \mathbf{C} & \mathbf{0} \\ \mathbf{0} & \mathbf{C}_b \end{bmatrix}_{27 \times 27}$$

$$\Phi_1 = \begin{bmatrix} \mathbf{M}\Gamma \\ \Gamma^T\mathbf{M}\Gamma + \mathbf{M}_b \end{bmatrix}_{27 \times 3} \quad \Phi_3 = \begin{bmatrix} \mathbf{0}_{24 \times 3} \\ \mathbf{I}_{3 \times 3} \end{bmatrix}_{27 \times 3}$$

The state space matrices of the state space equations in Eq. 3.1 and Eq. 3.2 are given by:

$$\mathbf{u} = \begin{Bmatrix} \ddot{\mathbf{x}}_g \\ \mathbf{f}_B \end{Bmatrix}$$

$$\mathbf{A}_s = \begin{bmatrix} \mathbf{0} & \mathbf{I} \\ -\overline{\mathbf{M}}^{-1}\overline{\mathbf{K}} & -\overline{\mathbf{M}}^{-1}\overline{\mathbf{C}} \end{bmatrix}_{54 \times 54} \quad \mathbf{B}_s = \begin{bmatrix} \mathbf{0} & \mathbf{0} \\ -\overline{\mathbf{M}}^{-1}\Phi_1 & -\overline{\mathbf{M}}^{-1}\Phi_3 \end{bmatrix}_{54 \times 6}$$

$$\mathbf{C}_s = \begin{bmatrix} \mathbf{I} & \mathbf{0} \\ \mathbf{0} & \mathbf{I} \\ -\overline{\mathbf{M}}_1^{-1}\overline{\mathbf{K}} & -\overline{\mathbf{M}}_1^{-1}\overline{\mathbf{C}} \end{bmatrix}_{81 \times 54} \quad \mathbf{D}_s = \begin{bmatrix} \mathbf{0} & \mathbf{0} \\ \mathbf{0} & -\overline{\mathbf{M}}_1^{-1}\Phi_3 \end{bmatrix}_{81 \times 6}$$

$$\overline{\mathbf{M}}_1 = \begin{bmatrix} \mathbf{M} & \mathbf{0} \\ \Gamma^T\mathbf{M} & \mathbf{M}_b \end{bmatrix}_{27 \times 27}$$

Under blast loadings:

$$\text{Superstructure:} \quad \mathbf{M}\ddot{\mathbf{x}} + \mathbf{C}\dot{\mathbf{x}} + \mathbf{K}\mathbf{x} = \Lambda_1 \mathbf{F}_B - \mathbf{M}\Gamma\ddot{\mathbf{x}}_b \quad (3.25)$$

$$\text{Base:} \quad \mathbf{m}_b\ddot{\mathbf{x}}_b + \mathbf{c}_b\dot{\mathbf{x}}_b + \mathbf{k}_b\mathbf{x}_b = (\Gamma^T \Lambda_1 + \Lambda_2)\mathbf{F}_B - \Gamma^T \mathbf{M}(\ddot{\mathbf{x}} + \Gamma\ddot{\mathbf{x}}_b) - \mathbf{f}_B \quad (3.26)$$

The equation of motion of base-isolated system under blast can be obtained according to Eq. 3.25 and Eq. 3.26:

$$\overline{\mathbf{M}}\ddot{\mathbf{X}} + \overline{\mathbf{C}}\dot{\mathbf{X}} + \overline{\mathbf{K}}\mathbf{X} = \Phi_2 \mathbf{F}_B - \Phi_3 \mathbf{f}_B \quad (3.27)$$

where

$$\Phi_2 = \begin{bmatrix} \Lambda_1 \\ \Gamma^T \Lambda_1 + \Lambda_2 \end{bmatrix}_{27 \times 27} \quad \{\Lambda_2\}_{3 \times 27}$$

The state space matrices of the state space equations in Eq. 3.1 and Eq. 3.2 are given by:

$$\mathbf{u} = \begin{Bmatrix} \mathbf{F}_B \\ \mathbf{f}_B \end{Bmatrix}_{30 \times 1}$$

$$\mathbf{A}_s = \begin{bmatrix} \mathbf{0} & \mathbf{I} \\ -\overline{\mathbf{M}}^{-1}\overline{\mathbf{K}} & -\overline{\mathbf{M}}^{-1}\overline{\mathbf{C}} \end{bmatrix}_{54 \times 54} \quad \mathbf{B}_s = \begin{bmatrix} \mathbf{0} & \mathbf{0} \\ \overline{\mathbf{M}}^{-1}\Phi_2 & -\overline{\mathbf{M}}^{-1}\Phi_3 \end{bmatrix}_{54 \times 30}$$

$$\mathbf{C}_s = \begin{bmatrix} \mathbf{I} & \mathbf{0} \\ \mathbf{0} & \mathbf{I} \\ -\overline{\mathbf{M}}_1^{-1}\overline{\mathbf{K}} & -\overline{\mathbf{M}}_1^{-1}\overline{\mathbf{C}} \end{bmatrix}_{81 \times 54} \quad \mathbf{D}_s = \begin{bmatrix} \mathbf{0} & \mathbf{0} \\ \overline{\mathbf{M}}_1^{-1}\Phi_2 & -\overline{\mathbf{M}}_1^{-1}\Phi_3 \end{bmatrix}_{81 \times 30}$$

**Table 3.2 Natural periods of the superstructure (seconds)**

Floor	East-West (x-d)	North-South (y-d)	Torsion (t-d)
1	0.89	0.78	0.66
2	0.28	0.27	0.21
3	0.15	0.15	0.12
4	0.11	0.11	0.08
5	0.08	0.08	0.07
6	0.07	0.07	0.06
7	0.06	0.06	0.06
8	0.06	0.05	0.05

Three possible types of base isolators, linear elastomeric bearings, friction pendulum bearings, and lead rubber bearings, are established and installed in multi-direction to dissipate energy from external dynamic excitations. The nominal isolation system consists of 92 base isolators as shown in Figure 3.2. The base-isolated structure is introduced in detail in Chapter 5.

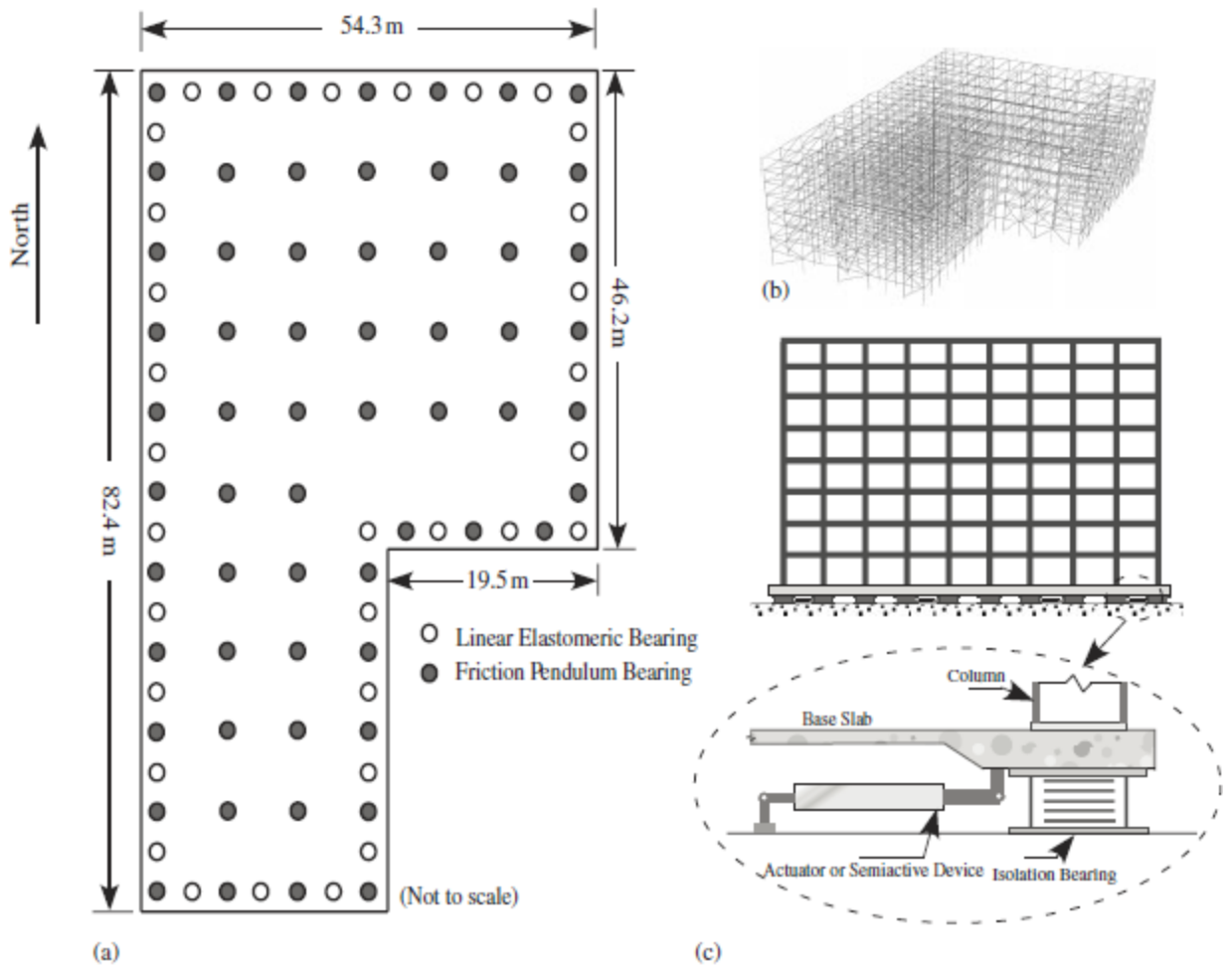


**Figure 3.2 (a) Isolation plan; (b) FEM model of superstructure; and (c) elevation view with devices (S. Narasimhan et al., 2006)**



### **3.3 Chapter Summary**

This chapter describes the structure systems used in this study. First, a simple 5-story structure with one degree of freedom on each floor is presented. This mass lumped model is assumed to be linear elastic. The dimensions and the dynamic properties of this model are given. Second, an 8-story real-scale structure is also presented. The superstructure of this building is modeled as a three-dimensional linear elastic system. The floors and the base are assumed to be rigid in horizontal plane. Three master degrees of freedom are used to represent each floor at the center of mass on the superstructure or the base. The base isolated structure system totally consists of 27 degrees of freedom. The dimensions and the natural periods are given. The equations of motion under blasts and earthquakes are derived and presented for both structure systems.

## CHAPTER 4 EXTERNAL LOADINGS

This chapter presents the external dynamic excitations applied on the structure systems, including both ground motions and blasts. Four strong ground motion records obtained in near-field regions during four large earthquakes are utilized as the base input excitation. The earthquakes are El Centro ( $M_w$  6.4, 1979), Northridge ( $M_w$  6.7, 1994), Kobe ( $M_w$  6.8, 1995), and Tohoku ( $M_w$  9.0, 2011). In addition, explosions with multiple charge weights and stand-off distances are modeled in AUTODYN and blast loadings applied on both structure systems are obtained.

### 4.1 Near-Field Earthquake Ground Motions

In this study, three commonly cited earthquake records, El Centro, Northridge, and Kobe, are utilized as the ground input excitation. In addition, as a recent significant ground motion, Japan Tohoku Earthquake with a magnitude of 9.0 occurred on March 11, 2011, is also taken into account. These four strong motion records with different magnitudes and frequency contents are chosen to investigate the performance of the structure and control devices under different seismic excitations. A description of each station and the characteristic of the near-field records processed at these stations are provided in Table 4.1. The earthquakes used in this study are both in the fault-normal (FN) and fault-parallel (FP) directions as shown in Figure 4.1. Note that the fault-parallel direction is assumed to be corresponding to the East-West direction ( $x-d$ ) of the 8-story structure and the fault-normal is assumed to be corresponding to the North-South

direction ( $y$ - $d$ ) of the 8-story structure. For the 5-story structure, only ground motions in  $x$ -direction (fault parallel) are input to the system.

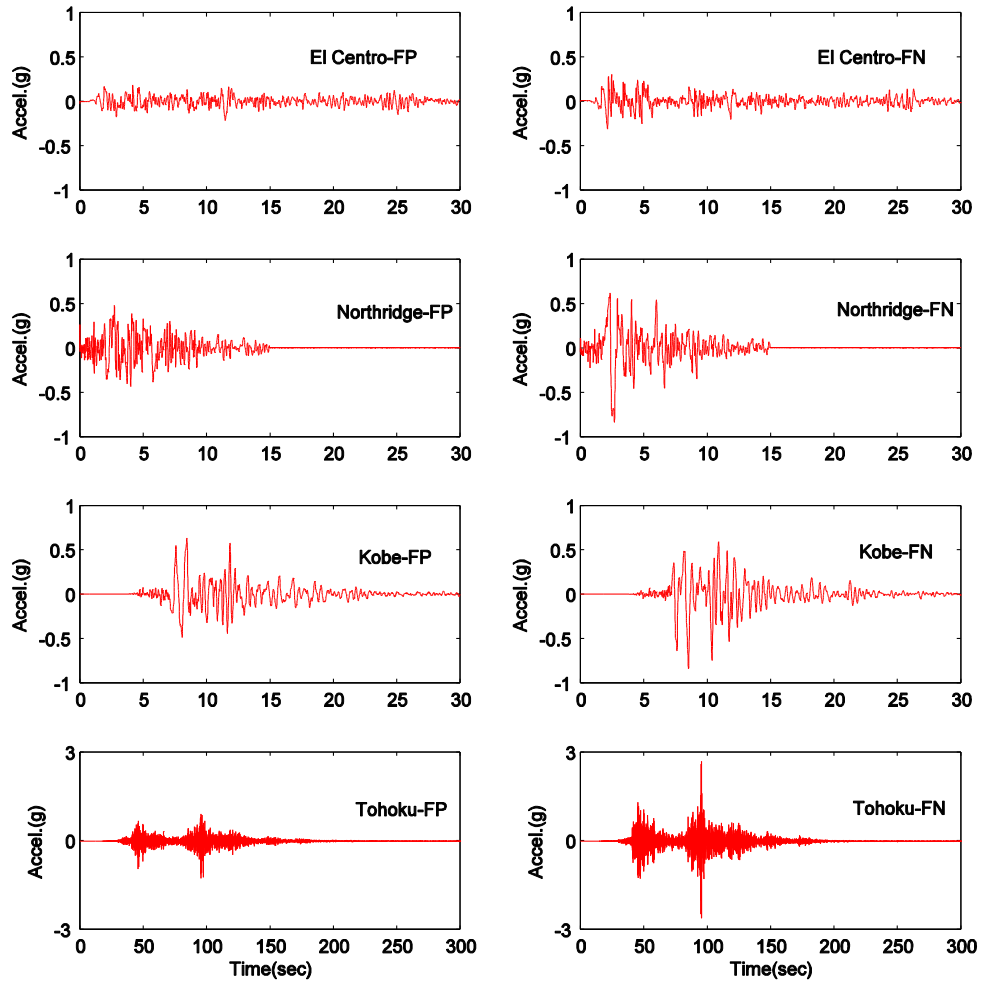


**Figure 4.1** Time histories of earthquake records

**Table 4.1 Characteristic of the near-field records**

Earthquake	Station	Direction	Peak Ground Acceleration (g)
Imperial Valley, 1979	El Centro	E-W	0.22
		N-S	0.31
Northridge, 1994	Rinaldi	E-W	0.48
		N-S	0.84
Kobe, 1995	JMA, Kobe	E-W	0.63
		N-S	0.84
Tohoku, 2011	MYG004	E-W	1.29
		N-S	2.68

## 4.2 Blast Loads

To investigate the behaviors of the structure systems under explosions, blast loads are predicted through both empirical and numerical approaches for both the 5-story building and 8-story building. TNT (Trinitrotoluene) is utilized as the explosive in this study. The explosive wave from a source other than the TNT can be determined by converting the charge of weight into an equivalent charge weight of TNT. This calculation is performed using a conversion factor based on the specific energy of the desired charge and the specific energy of TNT. Specific energy of different explosives and their conversion factors to the TNT are given in Table 4.2. Explosives with two different weights of charge, 50 kg and 100 kg of TNT, are used as the source for the 5-story structure in this study. For the 8-story structure, explosions of 2000 kg TNT are created at two locations in order to create blast loadings in both  $x$  and  $y$  directions. Global

behaviors of the structure systems under explosion are assumed to be dominant, meaning that local failures are not taken into consideration.

Generally there are two burst environments: (1) air burst and (2) surface burst. The air burst is a phenomenon that the explosions occur above the ground surface and at some distance away from the structure so that the initial shock wave hits the ground surface prior to arrival at the structure. As the shock wave continues to propagate, a front known as the Mach front is formed by the interaction between the incident wave and the reflected wave. The reflected wave is the amplified initial wave reflected by the ground. If the charge is located on or very close to the ground surface the explosion is termed surface burst (see Figure 4.2). The initial wave is reflected and reinforced by the ground surface to produce a reflected wave. Unlike the air burst, the reflected wave is merged with the incident wave at the detonation point to form a single wave, which is similar to the Mach front in the air burst, but essentially forms a hemisphere instead. This study will focus on the surface burst only.

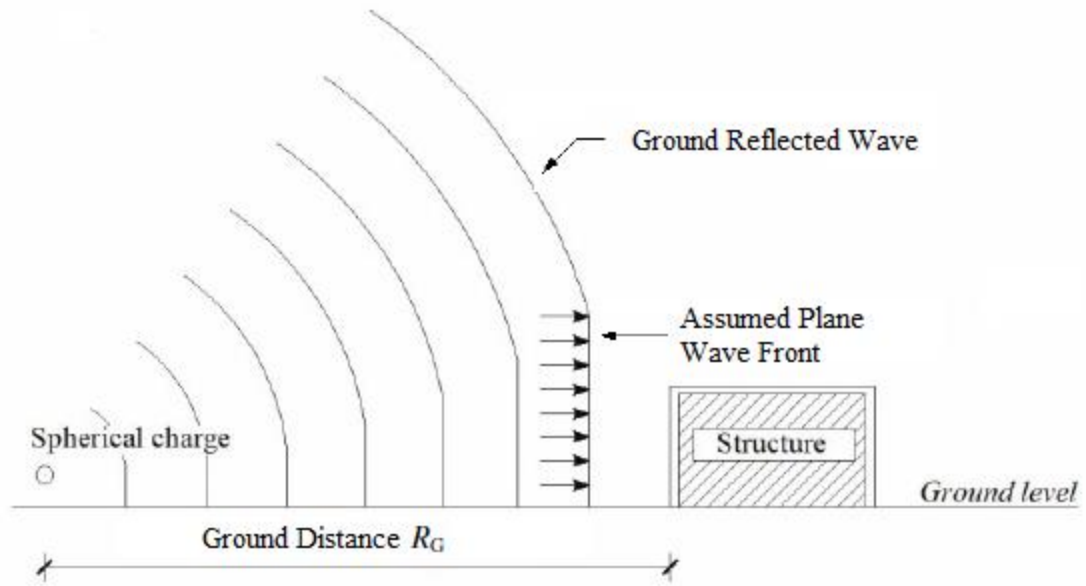


**Figure 4.2 Surface burst blast environment**

**Table 4.2 Conversion factors for explosives**

Explosive	Specific energy $Q_x$ (kJ/kg)	TNT equivalent $Q_x / Q_{TNT}$
C4	6057	1.340
Compound B (60% RDX, 40% TNT)	5190	1.148
HMX	5680	1.256
RDX	5360	1.185
Nitroglycerin	6700	1.481
TNT	4520	1.000
Semtex	5660	1.250

### 4.2.1 Empirical Chart-based Approach

Empirical approach is essentially an approximate method to predict the blast pressures or loads based on the numerous experimental data and on the results of response tests on slabs. Approximate chart-based methods are presented in several technical design manuals such as UFC 3-340-02 (2008). This manual is applicable to the design of protective structures subjected to the high explosive detonations. In this manual, the parameters which are necessary to determine the blast loads, such as structure's configuration and size, weight of charge, and charge location, are presented. A scaling chart that gives the positive phase blast wave parameters for a surface burst of a hemispherical TNT charge is also presented as shown in Figure 2.2. A schematic of the 5-story structure under explosions is shown in Figure 4.3. The procedure for determining the blast wave parameters for a surface blast given in this manual is shown as following:

1. Determine the weight of charge,  $W$ , as TNT equivalent. Select the point of interest on the exterior vertical wall of a building at height  $h$  above the ground.
2. For the point of interest, calculate the standoff distance at height  $h$ ,  $R_h$ , scaled standoff distance,  $Z_h$ , according to the Eq. 4.1 and 4.2.

$$R_h = (R_G^2 + h^2)^{1/2} \quad (4.1)$$

$$Z_h = R_h / W^{1/3} \quad (4.2)$$

3. Read peak reflected overpressure  $P_r$ , peak incident overpressure  $P_{so}$ , arrival time  $t_A$ , positive time duration  $t_0$ , wave velocity  $U$  from Figure 2.2.

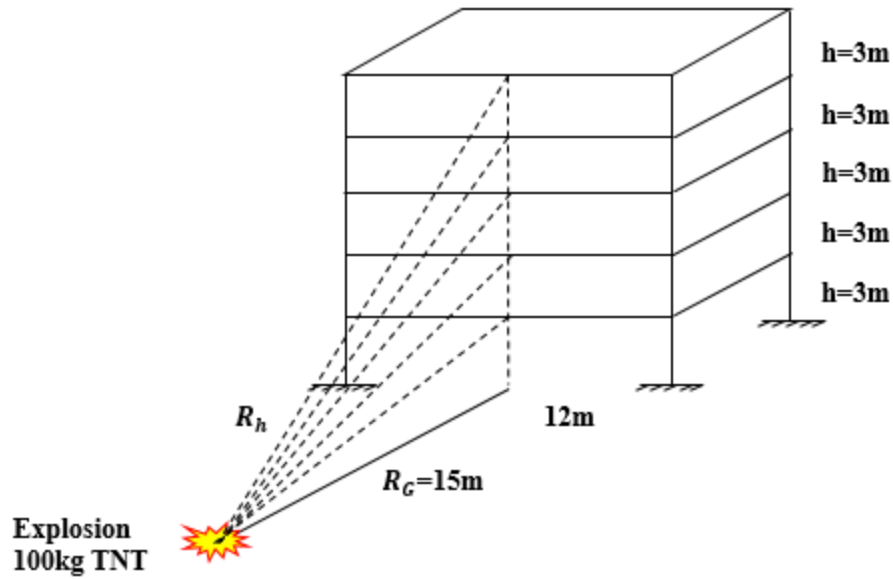


**Figure 4.3 Geometry of the 5-story structure under explosion**

#### **4.2.2 Empirical Equation-based Approach**

Empirical equation-based approach is another conservative method to determine the blast loadings on the structure by using empirical equations. There are various proposals for the calculation of the shock wave parameters which have been proposed in Chapter 2. The benefit of using empirical equations instead of the charts is quick calculations for multiple points of interest, minimizing the time consumed especially for the cases of more complicated structures.

Follow the same first two steps in the previous section, scaled standoff distance,  $Z_h$ , can be determined. An equation used to predict the peak incident overpressure was proposed by Mills (1987) which is shown below.



$$P_{so} = \frac{1772}{Z_h^3} - \frac{114}{Z_h^2} + \frac{108}{Z_h}, \text{ kPa} \quad (4.3)$$

The positive time duration can be obtained by using the following equation proposed by Lam (2004).

$$t_o = W^{1/3} 10^{[-2.75+0.27 \log(Z_h)]} \quad (4.4)$$

Explosive wave front velocity  $U$  is estimated as

$$U = a_0 \cdot \sqrt{\frac{6P_{so} + 7P_0}{7P_0}} \quad (4.5)$$

where  $P_0$  is ambient air pressure in kPa (101 kPa typically),  $a_0$  is the speed of sound in the air which is 335 m/s.

Thus, the arrival time for each point of interest can be easily determined as following:

$$t_A = \frac{R_h}{U} \quad (4.6)$$

The reflected overpressure is defined with a coefficient  $C_r$  given by

$$C_r = 3 \left( \sqrt[4]{\frac{P_s}{101}} \right) \quad (4.7)$$

$$P_r = C_r \cdot P_{so} \quad (4.8)$$

An important parameter in the reflected overpressure is the clearing time  $t_c$  which defines the time taken for the reflected overpressure to decay completely to ambient pressure and it can be estimated as following

$$t_c = \frac{S}{U} \quad (4.9)$$

where  $S$  is the clearing distance, taken as the shortest distance from the point of interest to the free edge of the structure.

Time history of the explosion pressure wave is usually described as an exponential function in the form of Friedlander's equation,

$$P(t) = P_o + P_r \left(1 - \frac{t}{t_0}\right) \exp\left(-\gamma \frac{t}{t_0}\right) \quad (4.10)$$

where  $P(t)$  is the pressure in time;  $\gamma$  is the parameter controlling the rate of wave amplitude decay which is defined as

$$\gamma = Z^2 - 3.7Z + 4.2 \quad (4.11)$$

In this study, the detonation point is put 15 meters away from the center of the base of the structure. The points of interest are set at midpoint of each floor. For the 5-story structure, the time histories of the overpressure under explosions with two weights of charge are shown in Figure 4.4.

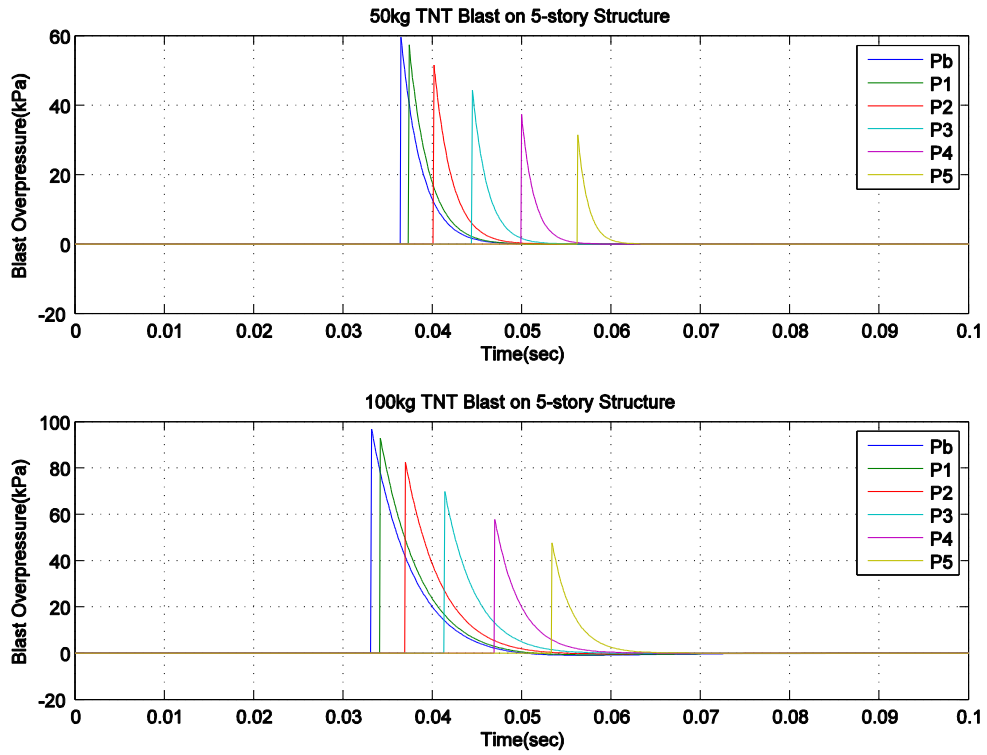


**Figure 4.4 Time history of the blast overpressure on the 5-story structure**

To transform the blast pressures to the dynamic blast loadings on the structure, effective area of each point of interest is taken into account. If points of interest are selected, more accurate estimations can be obtained. For the 5-story structure, only one point of interest is selected on each floor. Therefore, the blast loads obtained are discrete and not smooth. The dynamic blast loadings obtained are shown in Figure 4.5.

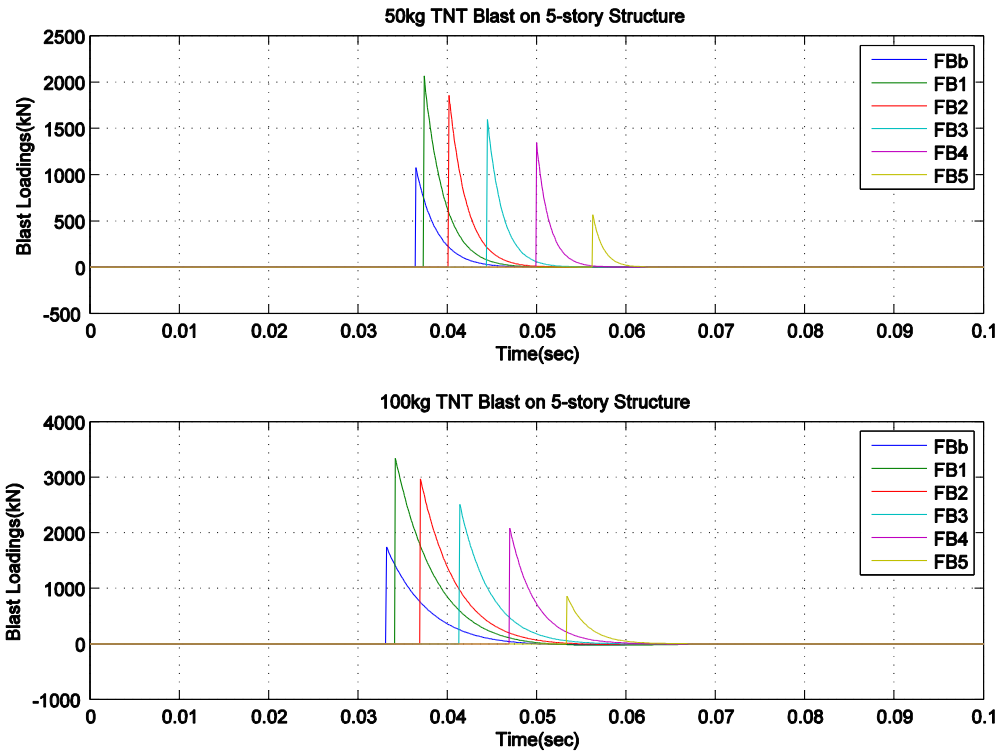


**Figure 4.5 Time history of the blast loadings on the 5-story structure**

### 4.2.3 Numerical Method

The numerical methods used to simulate the blast effects typically are based on a finite volume, finite difference, or finite element method with explicit time integration scheme. In this study, AUTODYN is used to model the explosions and predict the blast loadings on structures.

AUTODYN is fully integrated engineering analysis codes specifically designed for nonlinear dynamic problems and particularly suited to the modeling of impact, penetration, blast and explosion effects. Finite difference, finite volume, finite element

and meshless methods are used depending on the solver or processor being used (Anderson, 1987; Pilley, 1995).

Currently there are several alternative numerical methods available to model different regions of a problem, including Lagrange, Euler, ALE (Arbitrary Lagrange Euler), Shell, and SPH (Smooth Particle Hydrodynamics). Typically, Lagrange is used to model solid continua and structures, and Euler is used to model gases, fluids, and the large distortion of solids. The Euler capacity allows for multi-material flow and material strength to be included which is good at modeling blast detonation. A Shell processor is available for modelling thin structures. Coupling between the processor types is available so that the best processor type for each part of a problem can be used. In addition, various techniques, such as remapping which uses an initial explosion calculation to set up the initial conditions for a subsequent simulation stage, can be used to improve computational efficiency and solution accuracy.

A large number of material equations of state (EOS) and constitutive models are available in AUTODYN. The explosive detonation and expansion is usually modeled using the default JWL (Jones – Wilkins – Lee) EOS for the TNT. This is an empirical material model with parameters typically derived from cylinder test data. In this study, the explosive is initiated at a point and a detonation wave propagates away from the initiation locations into the material at the detonation velocity. In this way the explosive is converted to high pressure detonation products on structures. The model of the explosives is discussed in detail in the following sections.

First, to set the initial conditions for the 3-D analysis of blast wave interaction with the structure, a 1-D model of the hemispherical detonation with a charge weight of 50 kg, 100 kg, or 2000 kg is modeled. Figure 4.6 illustrates the setup of the 1-D model.

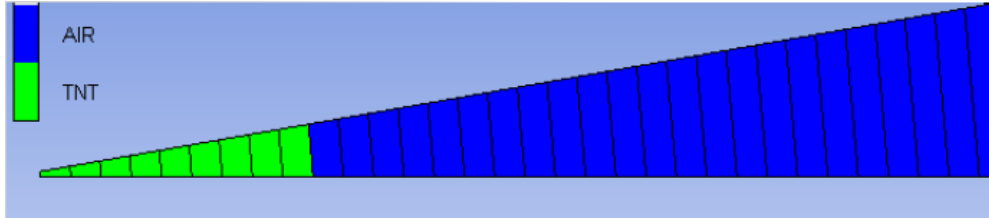


**Figure 4.6 1-D spherically symmetric model in AUTODYN**

Second, the TNT and air material data is loaded in the EXPLOS material library of AUTODYN. The default density of TNT ( $\gamma_{TNT} = 1.63 \text{ g/cm}^3$ ) is used to calculate the radius of a hemispherical charge of TNT. The radii of a 50 kg, 100 kg and 2000 kg charge of TNT are 244.7 mm, 308.3 mm and 836.7mm, respectively. The internal energy of air is set as 2.068e5 kJ to initialize the air at ambient pressure (1 bar).

The 1-D model will be converted to 3-D by rotating the model through 360 degrees in the remapping process after the 1-D simulation completes. The blast wave reaches the end of the mesh at about 18 seconds as shown in Figure 4.7. In this study, the end time of the blast detonation simulation of the 50 kg and 100 kg blast is set as 10 milliseconds instead which is shown in Figure 4.8. Larger distance between the wave front and the structure is observed in Figure 4.8. Next, the solution profile of density, velocity, energy, and pressure is saved as a remap file.

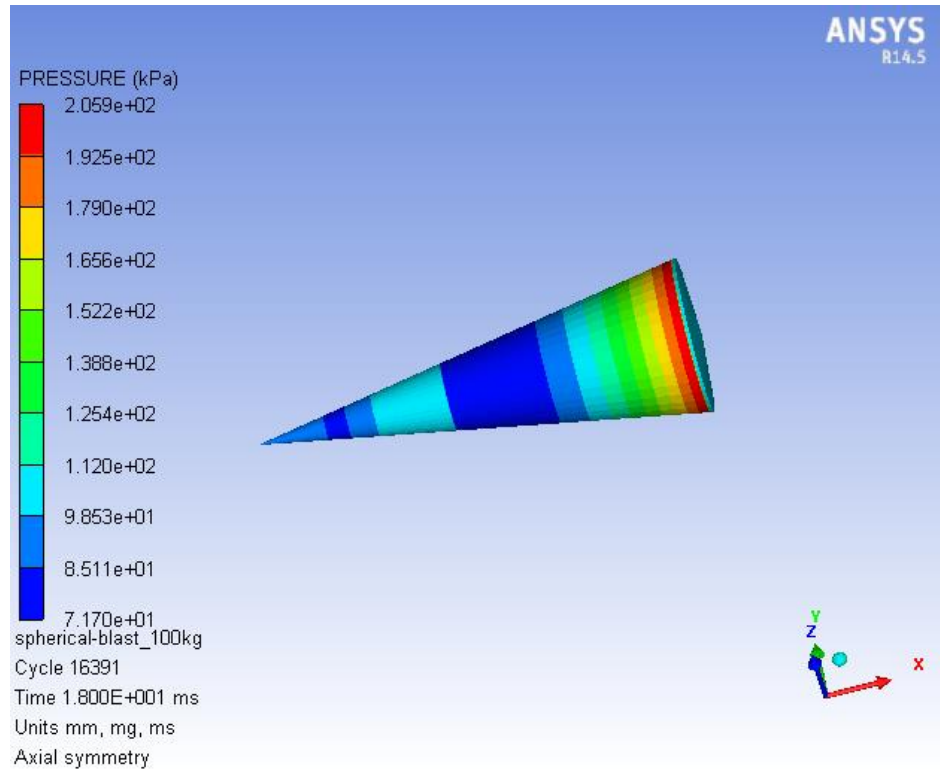


**Figure 4.7 3-D spherically symmetric model with end condition of 18s in AUTODYN**

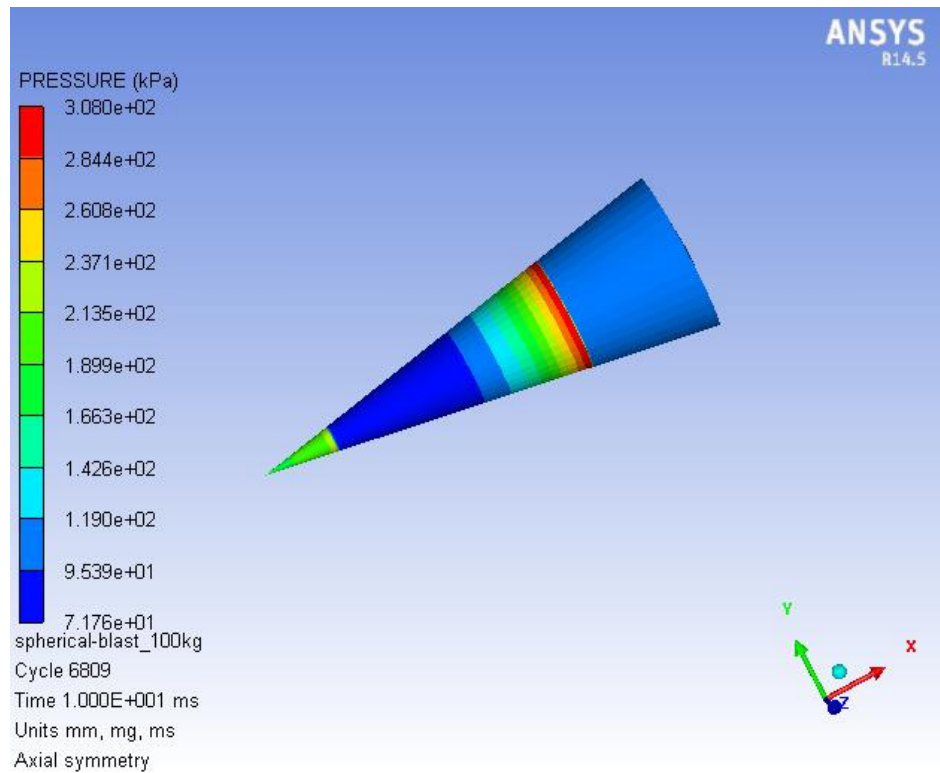


**Figure 4.8 3-D spherically symmetric model with end condition of 10s in AUTODYN**

The data file of the blast detonation is then remapped into the 3-D model consisting of the rigid structure model and the surrounding environment as an initial condition. The gage points are installed on the 5-story and 8-story structures as shown in Figure 4.9 and Figure 4.10. Note that the blast pressures are symmetric with respect to the centerline of the surface, thus, only half of the symmetric gage points are installed.

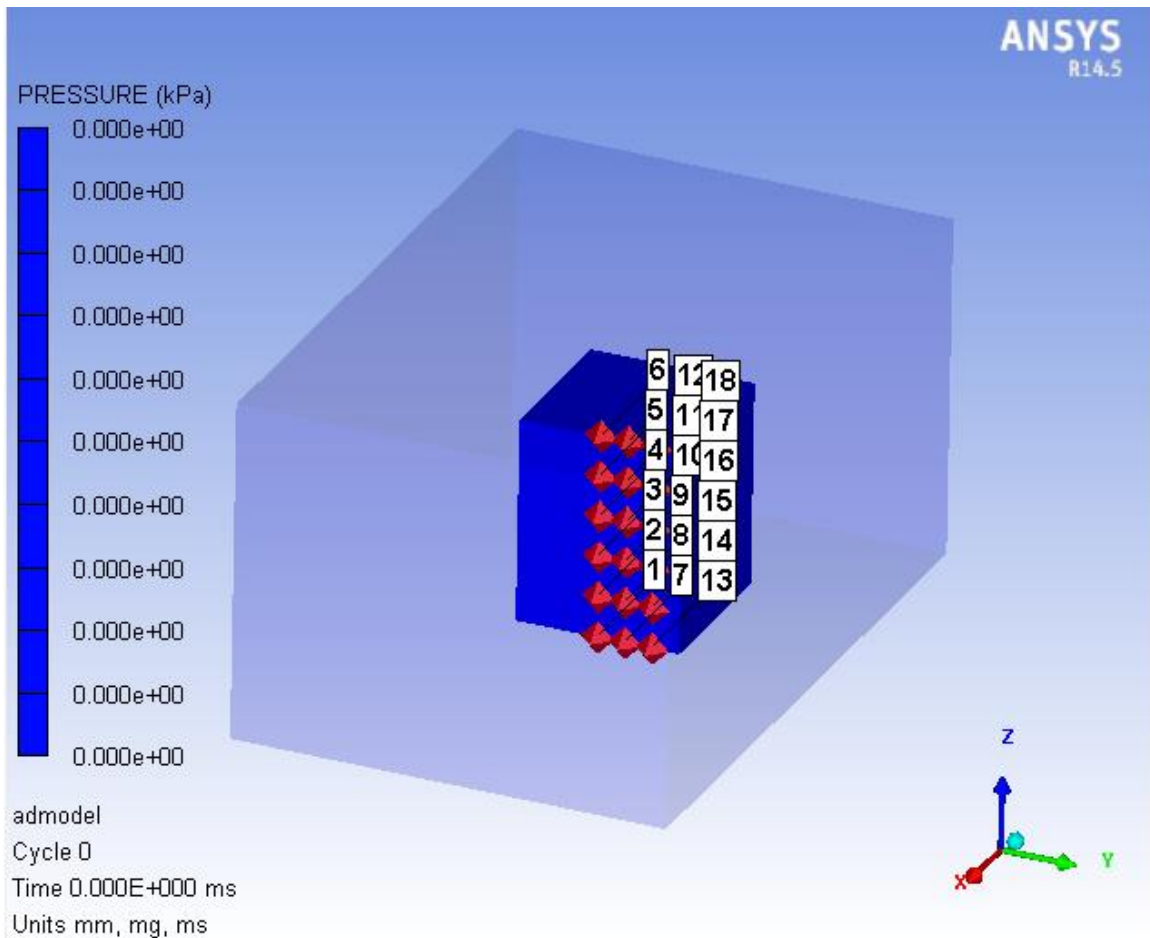


**Figure 4.9 Gage points on the 5-story structure model in AUTODYN**

Figure 4.11 and Figure 4.12 show the simulation of blast wave propagation around the 5-story structure model and the 8-story structure model.





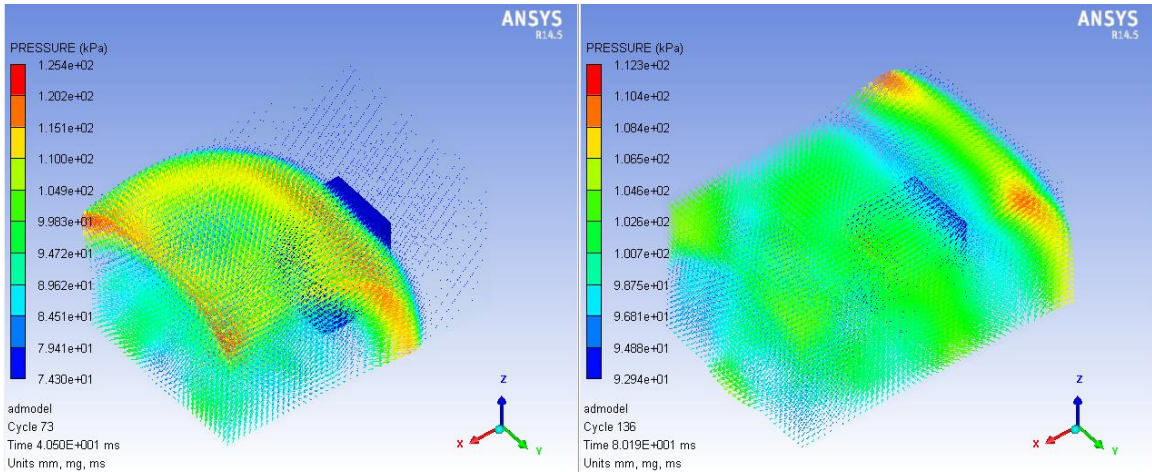


Figure 4.11 Blast wave propagation around the 5-story structure in AUTODYN

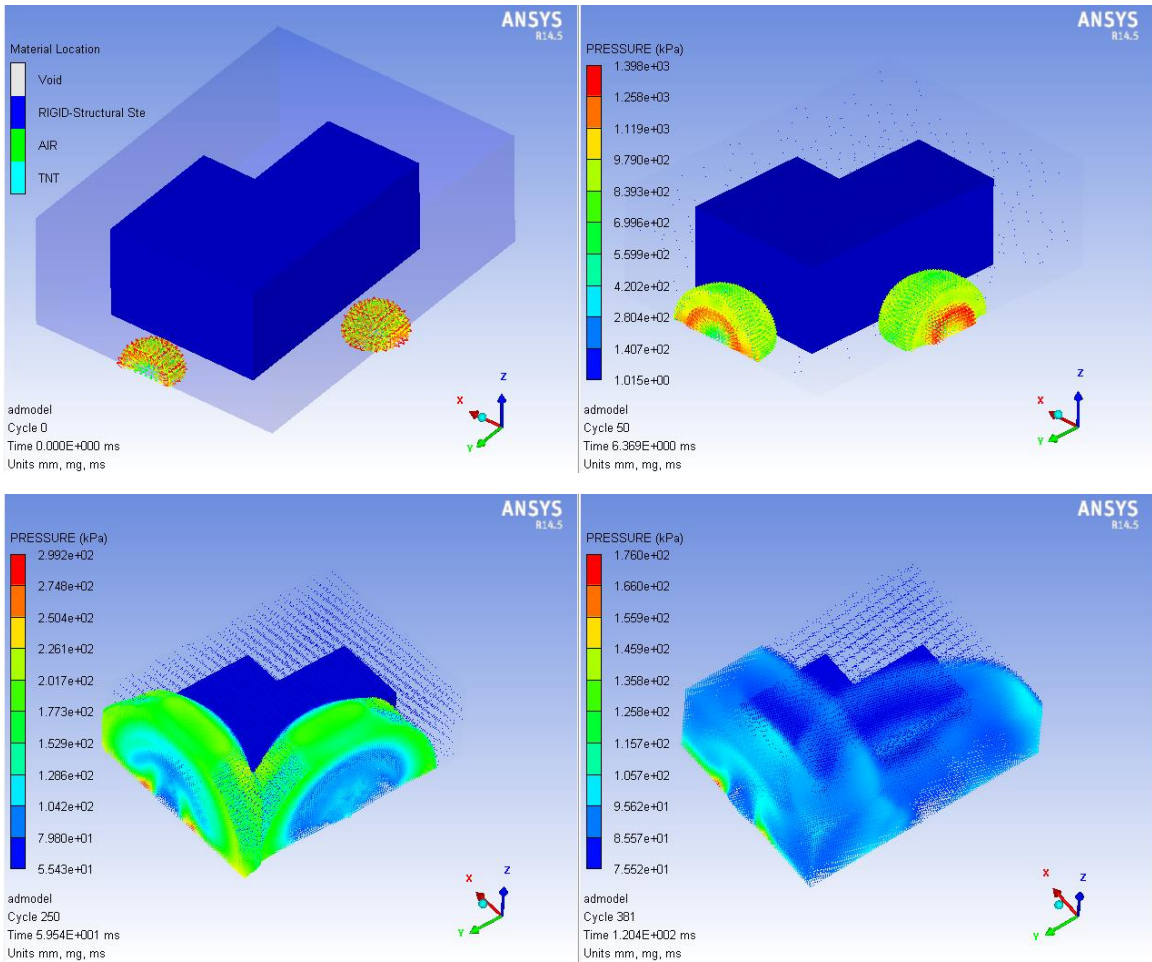
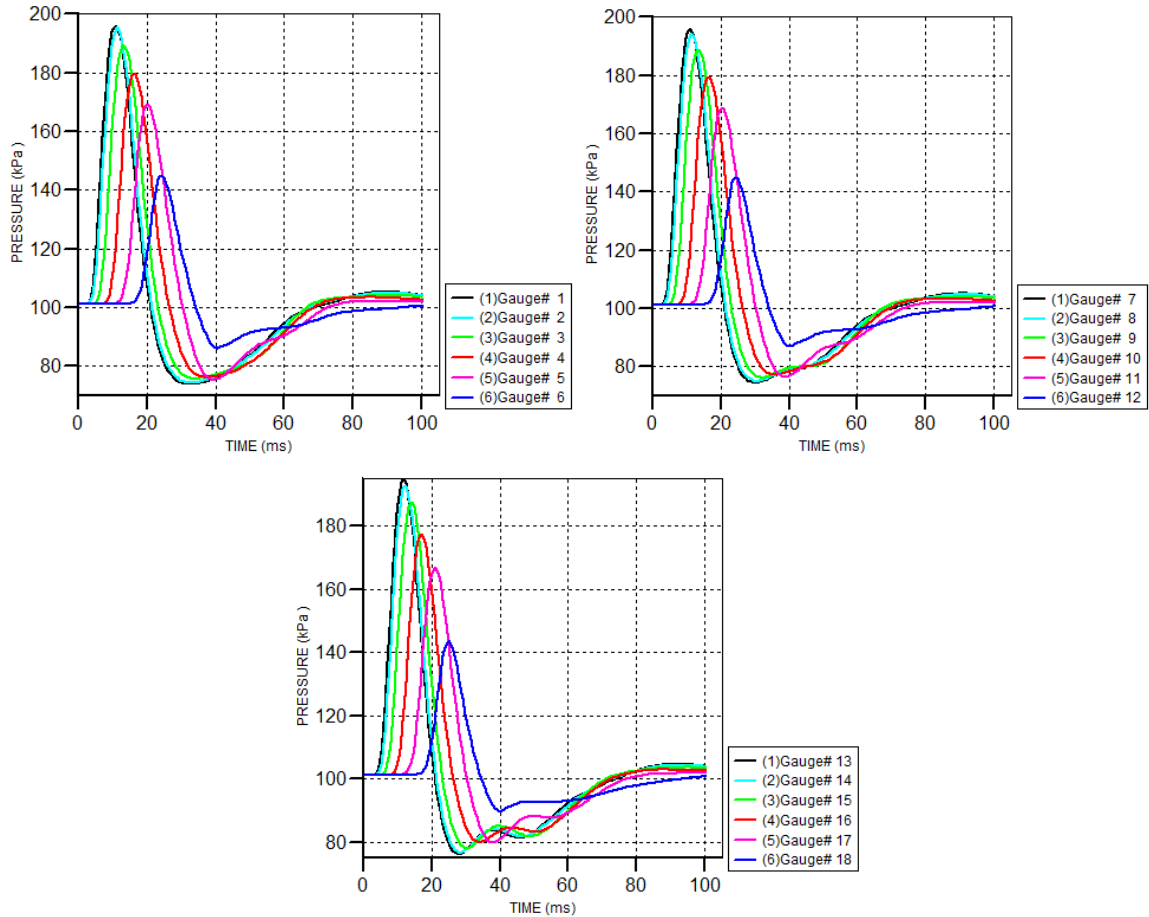
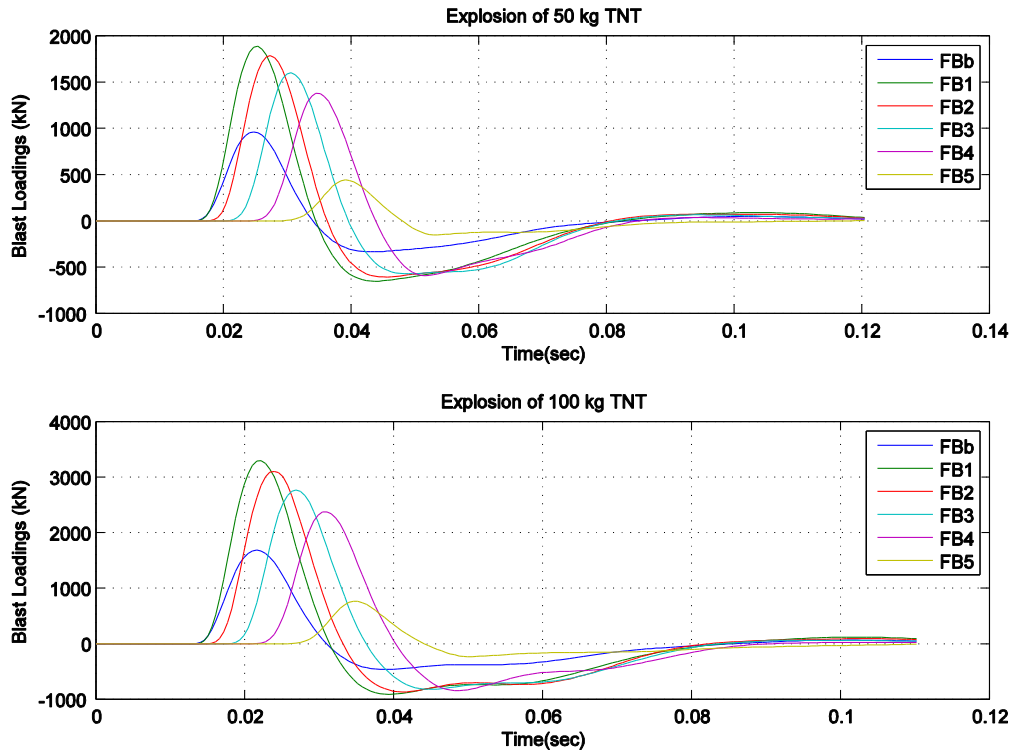


Figure 4.12 Blast wave propagation around the 8-story structure in AUTODYN



**Figure 4.13 Time histories of blast pressures of 100 kg TNT at the gage points on the 5-story structure in AUTODYN**

The time histories of the blast pressures of the gage points on 5-story structure are shown in Figure 4.13. By multiplying the effective area of each gage point, the blast dynamic loadings on the gage points are obtained. The sums of the loads on the gage points at same floor are the dynamic explosive load applied on various floors. The blast loadings of 50 kg TNT and 100 kg TNT on the 5-story structure are shown in Figure 4.14.  $F_{Bb}$  and  $F_{B5}$  are the blast loading applied on the base level and the top floor, respectively.



**Figure 4.14 Blast loadings of 50 kg TNT and 100 kg TNT on the 5-story structure**

Figure 4.15 shows the comparison between the blast loads computed in empirical equation-based approach and numerical approach from Figure 4.6 and Figure 4.14. Note that the solid line represents blast loads from numerical method and the dash line represents the empirical equation-based approach. The same peak level of blast loading is obtained through both methods. However, there is a large different in the arrival time and duration of the blasts between the two methods. Furthermore, smoother curves are observed with larger positive time duration and more reasonable negative phases through numerical method.

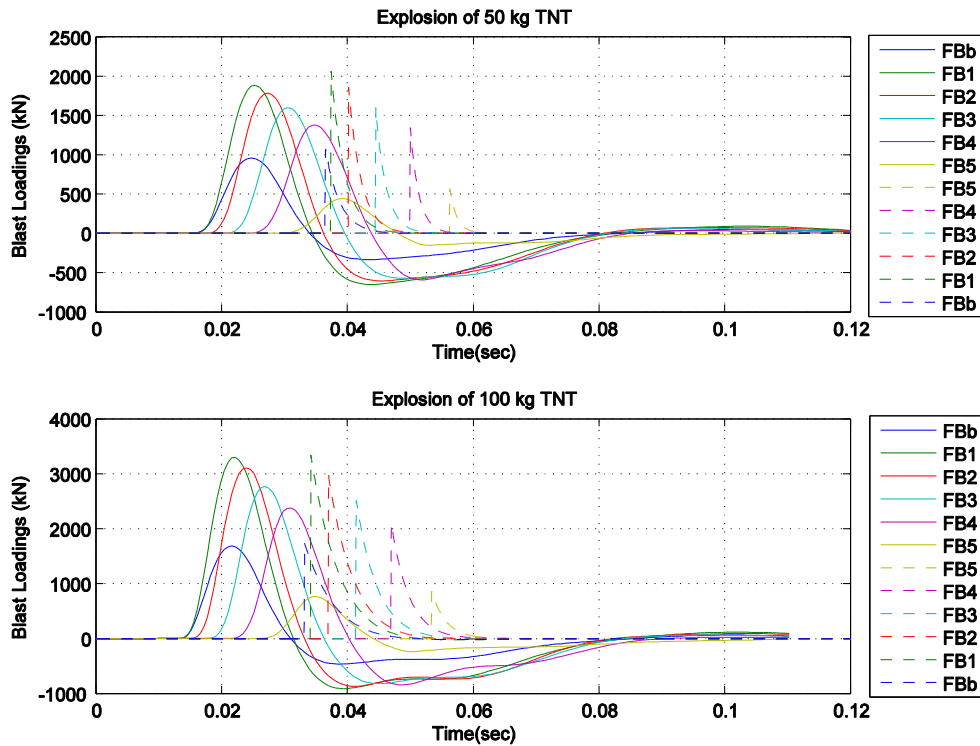


**Figure 4.15 Comparison of blast loadings from empirical equation-based approach and numerical method**

To create blast loadings in two directions for the 8-story structure, the detonations are set at two locations in front of the west and north surface, respectively. The interaction between the explosions in both directions is ignored because the distance of the detonations is large enough. The blast loadings of 2000 kg TNT on the 8-story structure are shown in Figure 4.16. The blast loading in y direction is in negative direction.  $F_{Bb}$  and  $F_{B8}$  are the blast loading applied on the base level and the top floor, respectively.

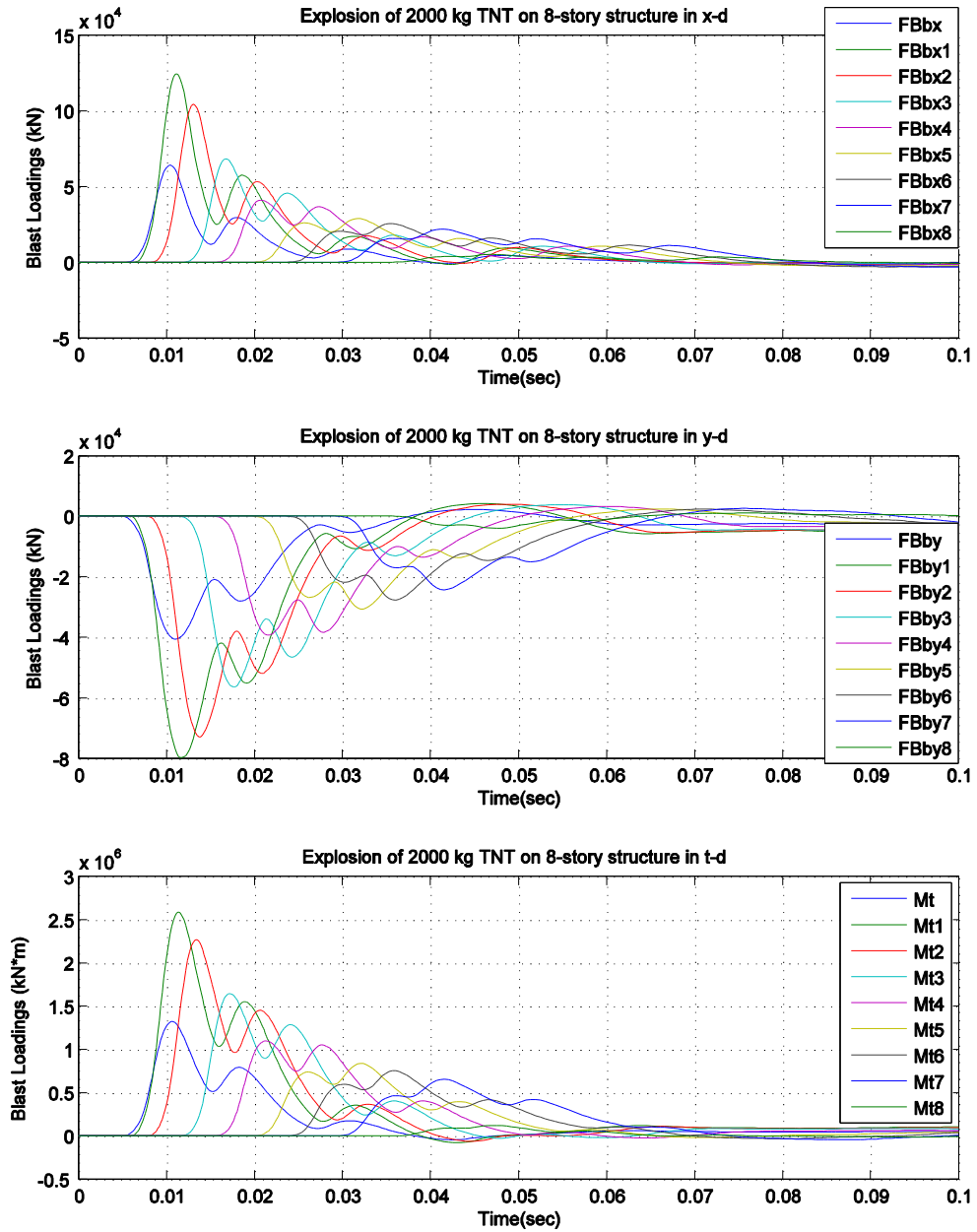


Figure 4.16 Blast loadings of 2000 kg TNT on the 8-story structure

### 4.3 Chapter Summary

In this chapter, the external dynamic excitations applied on the structure systems, including both earthquakes and explosions, are presented. Four strong ground motion records are given and utilized as the base input to study the performance of the control devices under seismic excitations. The earthquakes are El Centro ( $M_w$  6.4, 1979), Northridge ( $M_w$  6.7, 1994), Kobe ( $M_w$  6.8, 1995), and Tohoku ( $M_w$  9.0, 2011). In addition, three methods are introduced to estimate the blast pressures and loadings on the structure. The empirical chart-based and equation-based methods are suitable for estimating the blast pressures on simple structures with fewer points of interest. The most accurate means to estimate the blast pressures is the numerical approach. In this study, the model of explosion is generated and analyzed in AUTODYN. The blast pressures obtained have a smoother curve with a more reasonable negative phase compared to the estimations of the other two approaches. The blast pressures estimated in AUTODYN are used as the explosive excitations to the structure systems.

## CHAPTER 5 MULTIPLE STRUCTURAL CONTROL STRATEGIES

This chapter presents several types of base isolators, including linear elastomeric bearings, friction pendulum bearings, and lead rubber bearings. Multiple supplemental control devices installed on the base isolated structure are also presented, including tuned mass dampers on the base (IS-TB), tuned mass dampers on the roof (IS-TR), cubic nonlinear energy sinks (NES) on the base (IS-CN), and nonlinear bumpers connected to the base (IS-NB).

### 5.1 Base Isolation Systems

Base isolation is a widely accepted method to reduce the transmission of the earthquake energy from the ground into the structure as well as provide energy dissipation. Three types of isolation elements, linear elastomeric bearings (linear bearings), friction pendulum bearings (FPB), and lead rubber bearings (LRB), are considered and modeled such that any combination of these can be used to in the isolation system. Figure 5.1 shows the force-displacement characteristics for linear elastomeric bearings, FPB, and LRB. All bearings are modeled as bi-directional so that they can provide realistic performance for the three-dimensional models such as the 8-story building in this study. For the one-directional models like the 5-story building, the behavior is only considered in one direction. The state space models of both 5-story and 8-story base isolated structures were introduced in Chapter 3.



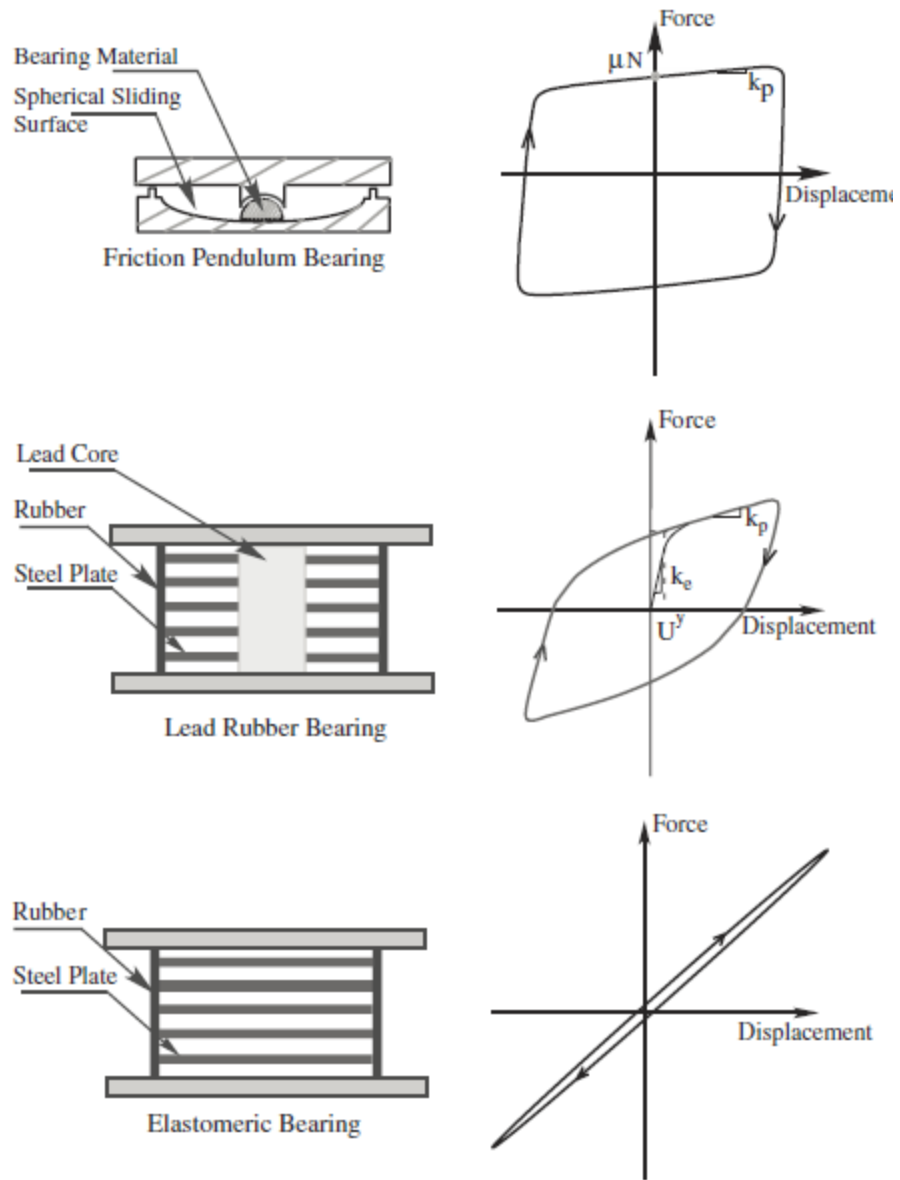


**Figure 5.1 Force-displacement characteristics of bearings (S. Narasimhan et al., 2006)**

The biaxial hysteretic behavior of friction pendulum bearings and lead rubber bearings is modeled by using the biaxial interaction of Bouc-Wen model (Park et al., 1986) as following:

$$U^y \begin{Bmatrix} \dot{z}_x \\ \dot{z}_y \end{Bmatrix} = \alpha \begin{Bmatrix} \dot{U}_x \\ \dot{U}_y \end{Bmatrix} - Z_w \begin{Bmatrix} \dot{U}_x \\ \dot{U}_y \end{Bmatrix} \quad (5.1)$$

$$Z_w = \begin{bmatrix} z_x^2 (\gamma \operatorname{sgn}(\dot{U}_x z_x) + \beta) & z_x z_y (\gamma \operatorname{sgn}(\dot{U}_y z_y) + \beta) \\ z_x z_y (\gamma \operatorname{sgn}(\dot{U}_x z_x) + \beta) & z_y^2 (\gamma \operatorname{sgn}(\dot{U}_y z_y) + \beta) \end{bmatrix} \quad (5.2)$$

where  $\alpha$ ,  $\beta$  and  $\gamma$  are dimensionless quantities,  $z_x$  and  $z_y$  are dimensionless hysteretic variables that are bounded by  $\pm 1$ ;  $U_x$ ,  $U_y$  and  $\dot{U}_x$ ,  $\dot{U}_y$ , are the displacements and velocities at the specific isolation bearings in the  $x$  and  $y$  directions, respectively;  $U^y$  is the yield displacement. The biaxial interaction of both friction pendulum bearings and lead rubber bearings is accounted for in Eq. 5.2. The off-diagonal terms of the matrix in Eq. 5.2 show the biaxial interaction. If they are replaced by zeros, it results in the uniaxial model with two independent elements in two orthogonal directions.

The bearing forces generated from different isolators are shown in the following equations. Eq. 5.3 shows the linear force from the linear elastomeric bearings.

$$\begin{Bmatrix} f_x \\ f_y \end{Bmatrix} = \begin{Bmatrix} k_b U_x + c_v \dot{U}_x \\ k_b U_y + c_v \dot{U}_y \end{Bmatrix} \quad (5.3)$$

where  $k_b$  and  $c_v$  are the stiffness and damping coefficient of the linear elastomeric bearings.

The bearing forces for the LRB are modeled by an elastic-viscoplastic model with a strain hardening in Eq. 5.4.

$$\begin{Bmatrix} f_x \\ f_y \end{Bmatrix} = \begin{Bmatrix} k_p U_x + c_v \dot{U}_x + (k_e - k_p) U^y z_x \\ k_p U_y + c_v \dot{U}_y + (k_e - k_p) U^y z_y \end{Bmatrix} \quad (5.4)$$

where  $k_e$  is the pre-yield stiffness;  $k_p$  is the post-yield stiffness.

The bearing forces for the FPB can be modeled with a flat or spherical sliding surface by using a small yield displacement  $U^y$  because of rigid plastic behavior and large pre-yield stiffness. Setting  $c_v = 0$  and  $(k_e - k_p)U^y = \mu N$ , we can get

$$\begin{cases} f_x \\ f_y \end{cases} = \begin{cases} k_p U_x + \mu N z_x \\ k_p U_y + \mu N z_y \end{cases} \quad (5.5)$$

where  $\mu$  is the coefficient of friction and  $N$  is the average normal force on each bearing (normal force variation is neglected).

Figure 5.2 and Figure 5.3 show the simulation block diagram of the LRB and FPB for the 8-story structure. The inputs to both isolation bearings are the base displacements in  $x$ ,  $y$ , and torsional directions. The linear elastomeric bearings are modeled directly in the state space models of the structure systems. The force-displacement characteristics for simulations of linear elastomeric bearings, LRB, and, FPB of 8-story structure in  $x$  direction under El Centro earthquake are shown in Figure 5.4 through Figure 5.6.

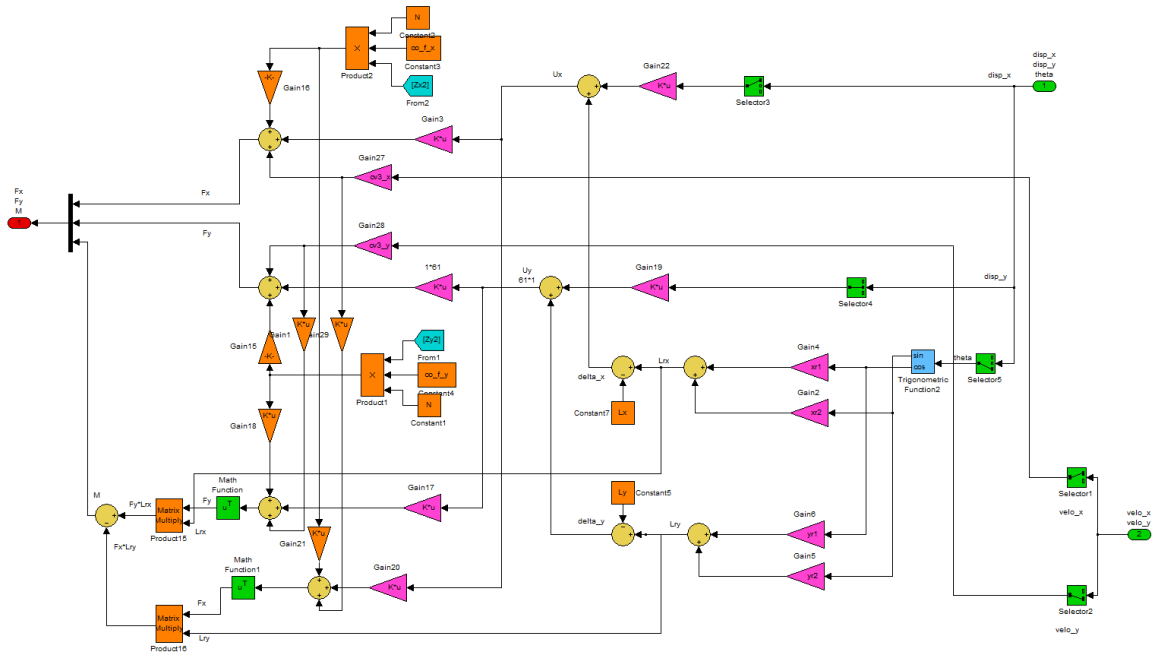


**Figure 5.2 Model of the LRB in Simulink**

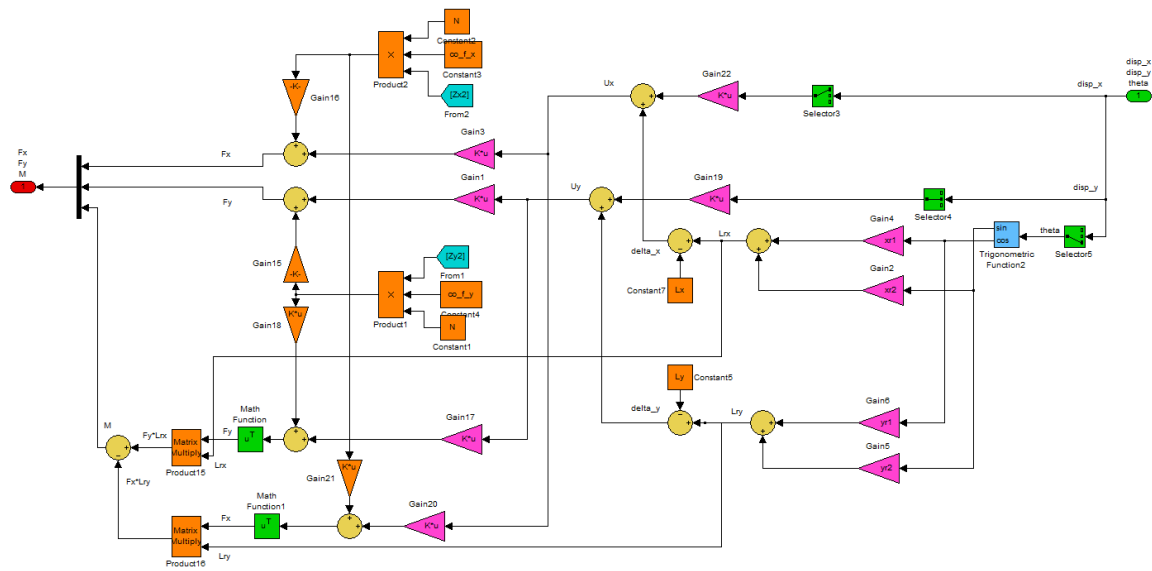


**Figure 5.3 Model of the FPB in Simulink**

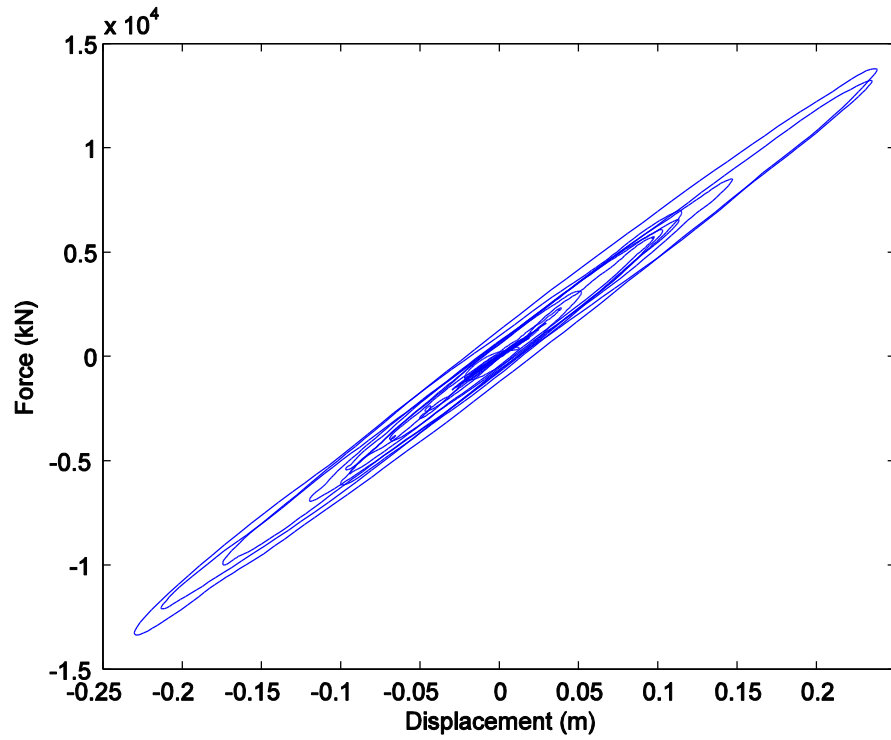


**Figure 5.4 Hysteresis loop of the linear elastomeric bearings**

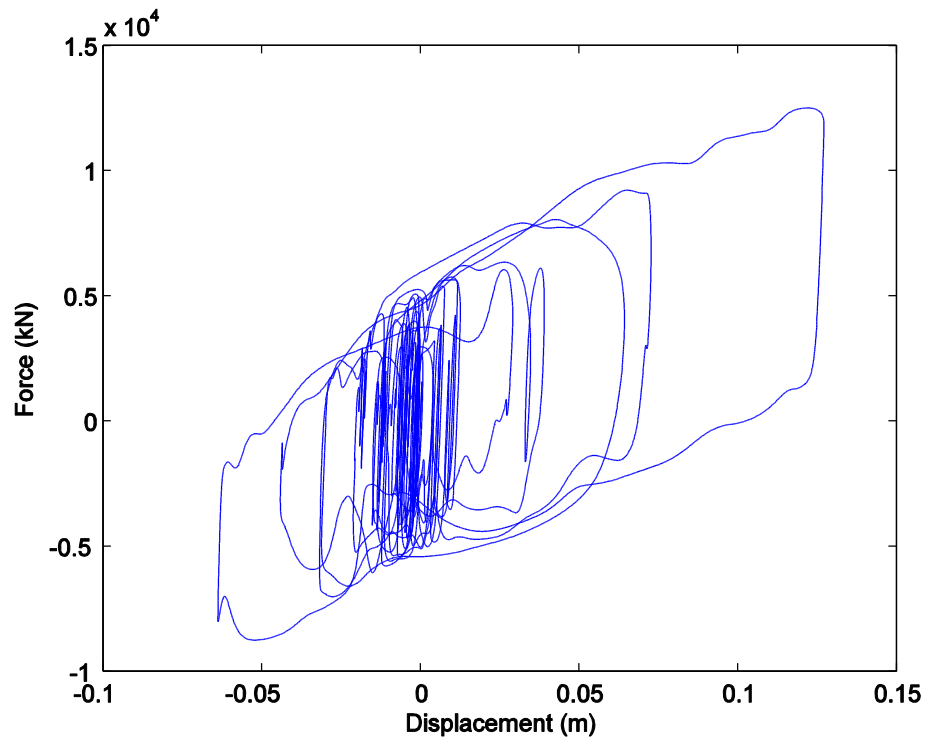


**Figure 5.5 Hysteresis loop of the LRB**

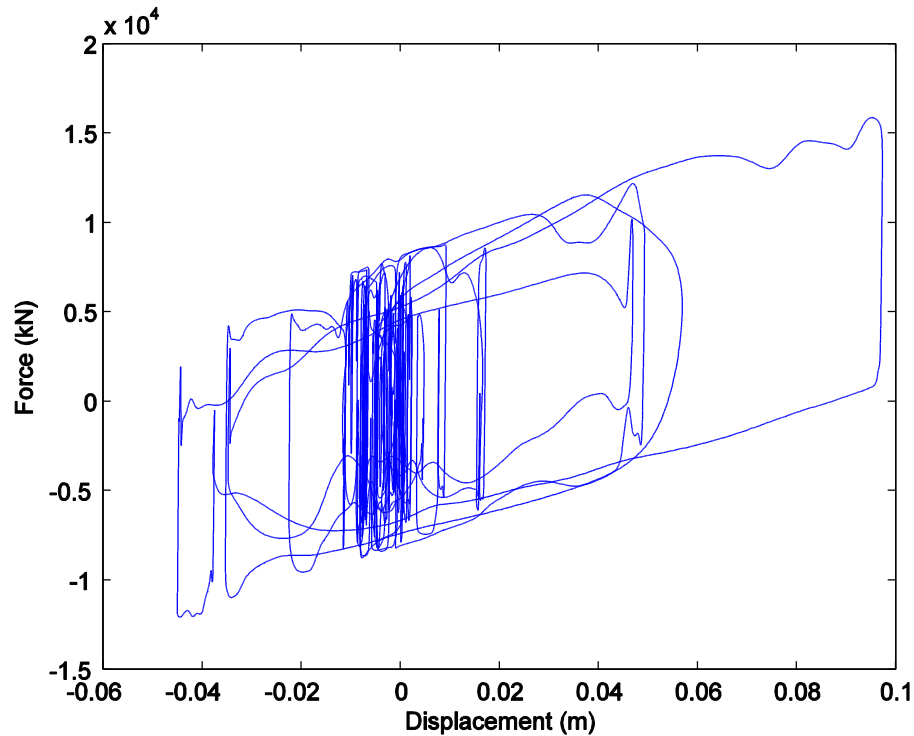


**Figure 5.6 Hysteresis loop of the FPB**

There are total of 92 isolation bearings shown in Figure 3.2. Three types of base isolators are available and potential for any combination of the 92 isolation bearings.

The calculation of the bearing forces for the 8-story structure is complex because the model is three-dimensional which results in different displacements and velocities on each bearing. Therefore, the model of simulation should account for this phenomenon which is addressed as below.

Since there exists torsional behavior during external dynamic loadings, additional shifts caused by base rotation are added to each isolation bearing. Let  $x_i$ ,  $y_i$  denote the coordinates of each base isolator before base rotation occurred, and let  $x_{r,i}$ ,  $y_{r,i}$  denote

the coordinates of which after base rotation. As shown in Figure 5.7,  $P$  is the initial location of one bearing with an initial angle of  $\alpha$  to the  $x$  direction, and  $P_r$  is the final location after base rotates  $\theta$  degrees.

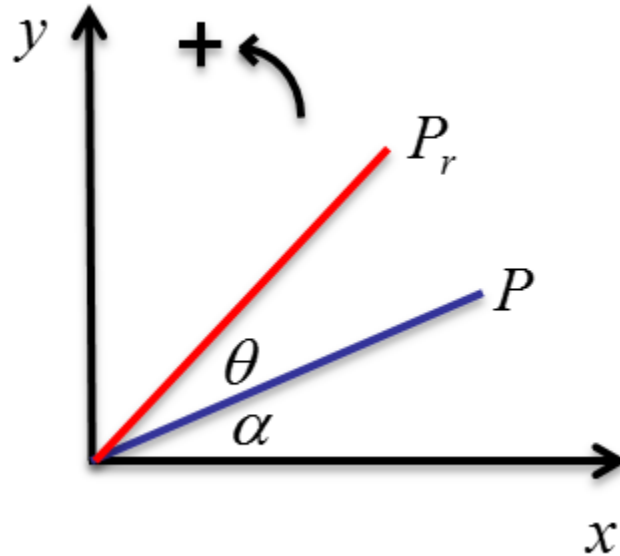


**Figure 5.7 Schematic of shifts by rotation**

Then, the coordinates of the bearing after rotation can be represented by the initial coordinates:

$$\begin{aligned} x_{r,i} &= \sqrt{x_i^2 + y_i^2} \cos(\alpha + \theta) \\ y_{r,i} &= \sqrt{x_i^2 + y_i^2} \sin(\alpha + \theta) \end{aligned} \quad (5.6)$$

where

$$\alpha = \tan^{-1} \frac{y_i}{x_i} \quad (5.7)$$

Let  $L_i = \sqrt{x_i^2 + y_i^2}$ ,

$$\begin{aligned} x_{r,i} &= L_i (\cos \alpha \cos \theta - \sin \alpha \sin \theta) \\ y_{r,i} &= L_i (\sin \alpha \cos \theta + \cos \alpha \sin \theta) \end{aligned} \quad (5.8)$$

Let

$$\begin{aligned} x_{r1} &= L_i \times \cos \alpha \\ x_{r2} &= -L_i \times \sin \alpha \\ y_{r1} &= L_i \times \sin \alpha \\ y_{r2} &= L_i \times \cos \alpha \end{aligned} \quad (5.9)$$

Then the bearing coordinates after rotation can be written as:

$$\begin{aligned} L_{xr} &= x_{r1} \cos \theta + x_{r2} \sin \theta \\ L_{yr} &= y_{r1} \cos \theta + y_{r2} \sin \theta \end{aligned} \quad (5.10)$$

Hence, the shifts of bearings caused by rotation are:

$$\begin{aligned} \Delta x &= L_{xr} - L_x \\ \Delta y &= L_{yr} - L_y \end{aligned} \quad (5.11)$$

The displacements of all non-linear bearings in  $x$  and  $y$  direction are:

$$\begin{aligned} U'_x &= U_x + \Delta x \\ U'_y &= U_y + \Delta y \end{aligned} \quad (5.12)$$

where  $U_x$  and  $U_y$  are the base displacement in  $x$  and  $y$  direction, respectively, without considering the effect of torsional behavior.

If we take the derivative of the displacements, the velocities of all non-linear bearings in  $x$  and  $y$  direction can be obtained as follows:



$$\begin{aligned}
U'_x &= U_x + L_{xr} - L_x \\
\frac{d}{dt}U'_x &= \frac{d}{dt}U_x + \frac{d}{dt}L_{xr} - \frac{d}{dt}L_x \\
V'_x &= V_x - x_{r1}\dot{\theta}\sin\theta + x_{r2}\dot{\theta}\cos\theta \\
V'_x &= V_x + (-x_{r1}\sin\theta + x_{r2}\cos\theta)\dot{\theta}
\end{aligned} \tag{5.13}$$

Similarly,

$$V'_y = V_y + (-y_{r1}\sin\theta + y_{r2}\cos\theta)\dot{\theta} \tag{5.14}$$

To simplify the Simulink file, matrix transformation is used in calculation of all bearing forces. Take the friction pendulum system, for example. The total force generated from the FPB is equal to the sum of the forces of each isolation bearing in  $x$  and  $y$  direction.

$$\begin{aligned}
F_x &= F_{1x} + F_{2x} + \dots + F_{nx} \\
&= (k_p U_{1x} + k_p U_{2x} + \dots + k_p U_{nx}) + (\mu N Z_{1x} + \mu N Z_{2x} + \dots + \mu N Z_{nx}) \\
&= [k_p \ k_p \ \dots \ k_p] \begin{bmatrix} U_{1x} \\ U_{2x} \\ \vdots \\ U_{nx} \end{bmatrix} + [\mu N \ \mu N \ \dots \ \mu N] \begin{bmatrix} Z_{1x} \\ Z_{2x} \\ \vdots \\ Z_{nx} \end{bmatrix}
\end{aligned} \tag{5.15}$$

$$\begin{aligned}
F_y &= F_{1y} + F_{2y} + \dots + F_{ny} \\
&= (k_p U_{1y} + k_p U_{2y} + \dots + k_p U_{ny}) + (\mu N Z_{1y} + \mu N Z_{2y} + \dots + \mu N Z_{ny}) \\
&= [k_p \ k_p \ \dots \ k_p] \begin{bmatrix} U_{1y} \\ U_{2y} \\ \vdots \\ U_{ny} \end{bmatrix} + [\mu N \ \mu N \ \dots \ \mu N] \begin{bmatrix} Z_{1y} \\ Z_{2y} \\ \vdots \\ Z_{ny} \end{bmatrix}
\end{aligned} \tag{5.16}$$

The moment applied on the base is:

$$\begin{aligned}
M &= M_1 + M_2 + \cdots + M_n \\
&= (F_{1y}L_{1rx} - F_{1x}L_{1ry}) + (F_{2y}L_{2rx} - F_{2x}L_{2ry}) + \cdots + (F_{ny}L_{nrx} - F_{nx}L_{nry}) \quad (5.17) \\
&= [F_{1y} \ F_{2y} \ \cdots \ F_{ny}] \begin{bmatrix} L_{1rx} \\ L_{2rx} \\ \vdots \\ L_{nrx} \end{bmatrix} - [F_{1x} \ F_{2x} \ \cdots \ F_{nx}] \begin{bmatrix} L_{1ry} \\ L_{2ry} \\ \vdots \\ L_{nry} \end{bmatrix}
\end{aligned}$$

where

$$\left( \begin{bmatrix} k_p & 0 & \cdots & 0 \\ 0 & k_p & \cdots & 0 \\ \vdots & \vdots & \ddots & \vdots \\ 0 & 0 & \cdots & k_p \end{bmatrix} \begin{bmatrix} U_{1y} \\ U_{2y} \\ \vdots \\ U_{ny} \end{bmatrix} + \begin{bmatrix} \mu N & 0 & \cdots & 0 \\ 0 & \mu N & \cdots & 0 \\ \vdots & \vdots & \ddots & \vdots \\ 0 & 0 & \cdots & \mu N \end{bmatrix} \begin{bmatrix} Z_{1y} \\ Z_{2y} \\ \vdots \\ Z_{ny} \end{bmatrix} \right)^T = \begin{bmatrix} F_{1y} \\ F_{2y} \\ \vdots \\ F_{ny} \end{bmatrix} = [F_{1y} \ F_{2y} \ \cdots \ F_{ny}]$$

For the biaxial Bouc-Wen model, substituting Eq.5.2 to Eq.5.1, we have

$$U^y \dot{Z}_x = \alpha \dot{U}_x - Z_x^2 (\gamma \operatorname{sgn}(\dot{U}_x Z_x) + \beta) \dot{U}_x - Z_x Z_y (\gamma \operatorname{sgn}(\dot{U}_y Z_y) + \beta) \dot{U}_y \quad (5.18)$$

where  $Z_x = [Z_{1x} \ Z_{2x} \ \cdots \ Z_{nx}]^T$ , then we have:

$$U^y \begin{bmatrix} \dot{Z}_{1x} \\ \dot{Z}_{2x} \\ \vdots \\ \dot{Z}_{nx} \end{bmatrix} = \alpha \begin{bmatrix} \dot{U}_{1x} \\ \dot{U}_{2x} \\ \vdots \\ \dot{U}_{nx} \end{bmatrix} - \begin{bmatrix} Z_{1x}^2 (\gamma \operatorname{sgn}(\dot{U}_{1x} Z_{1x}) + \beta) & 0 & \cdots & 0 \\ 0 & Z_{2x}^2 (\gamma \operatorname{sgn}(\dot{U}_{2x} Z_{2x}) + \beta) & \cdots & 0 \\ \vdots & \vdots & \ddots & \vdots \\ 0 & 0 & \cdots & Z_{nx}^2 (\gamma \operatorname{sgn}(\dot{U}_{nx} Z_{nx}) + \beta) \end{bmatrix} \begin{bmatrix} \dot{U}_{1x} \\ \dot{U}_{2x} \\ \vdots \\ \dot{U}_{nx} \end{bmatrix} \\
- \begin{bmatrix} Z_{1x} Z_{1y} (\gamma \operatorname{sgn}(\dot{U}_{1y} Z_{1y}) + \beta) & 0 & \cdots & 0 \\ 0 & Z_{2x} Z_{2y} (\gamma \operatorname{sgn}(\dot{U}_{2y} Z_{2y}) + \beta) & \cdots & 0 \\ \vdots & \vdots & \ddots & \vdots \\ 0 & 0 & \cdots & Z_{nx} Z_{ny} (\gamma \operatorname{sgn}(\dot{U}_{ny} Z_{ny}) + \beta) \end{bmatrix} \begin{bmatrix} \dot{U}_{1y} \\ \dot{U}_{2y} \\ \vdots \\ \dot{U}_{ny} \end{bmatrix}$$

where

$$\begin{aligned}
& \begin{bmatrix} Z_{1x}^2 (\gamma \operatorname{sgn}(\dot{U}_{1x} Z_{1x}) + \beta) & 0 & \cdots & 0 \\ 0 & Z_{2x}^2 (\gamma \operatorname{sgn}(\dot{U}_{2x} Z_{2x}) + \beta) & \cdots & 0 \\ \vdots & \vdots & \ddots & \vdots \\ 0 & 0 & \cdots & Z_{nx}^2 (\gamma \operatorname{sgn}(\dot{U}_{nx} Z_{nx}) + \beta) \end{bmatrix} \begin{bmatrix} \dot{U}_{1x} \\ \dot{U}_{2x} \\ \vdots \\ \dot{U}_{nx} \end{bmatrix} \\
= & \left( \beta \begin{bmatrix} Z_{1x}^2 & 0 & \cdots & 0 \\ 0 & Z_{2x}^2 & \cdots & 0 \\ \vdots & \vdots & \ddots & \vdots \\ 0 & 0 & \cdots & Z_{nx}^2 \end{bmatrix} + \gamma \begin{bmatrix} Z_{1x}^2 \operatorname{sgn}(\dot{U}_{1x} Z_{1x}) & 0 & \cdots & 0 \\ 0 & Z_{2x}^2 \operatorname{sgn}(\dot{U}_{2x} Z_{2x}) & \cdots & 0 \\ \vdots & \vdots & \ddots & \vdots \\ 0 & 0 & \cdots & Z_{nx}^2 \operatorname{sgn}(\dot{U}_{nx} Z_{nx}) \end{bmatrix} \right) \begin{bmatrix} \dot{U}_{1x} \\ \dot{U}_{2x} \\ \vdots \\ \dot{U}_{nx} \end{bmatrix}
\end{aligned}$$

where

$$\begin{bmatrix} Z_{1x}^2 & 0 & \cdots & 0 \\ 0 & Z_{2x}^2 & \cdots & 0 \\ \vdots & \vdots & \ddots & \vdots \\ 0 & 0 & \cdots & Z_{nx}^2 \end{bmatrix} = \operatorname{diag} \begin{bmatrix} Z_{1x}^2 \\ Z_{2x}^2 \\ \vdots \\ Z_{nx}^2 \end{bmatrix}$$

$$\begin{bmatrix} Z_{1x}^2 \\ Z_{2x}^2 \\ \vdots \\ Z_{nx}^2 \end{bmatrix} = \begin{bmatrix} Z_{1x} & 0 & \cdots & 0 \\ 0 & Z_{2x} & \cdots & 0 \\ \vdots & \vdots & \ddots & \vdots \\ 0 & 0 & \cdots & Z_{nx} \end{bmatrix} \begin{bmatrix} Z_{1x} \\ Z_{2x} \\ \vdots \\ Z_{nx} \end{bmatrix} = \left( \operatorname{diag} \begin{bmatrix} Z_{1x} \\ Z_{2x} \\ \vdots \\ Z_{nx} \end{bmatrix} \right) \begin{bmatrix} Z_{1x} \\ Z_{2x} \\ \vdots \\ Z_{nx} \end{bmatrix}$$

$$\begin{bmatrix} Z_{1x}^2 \operatorname{sgn}(\dot{U}_{1x} Z_{1x}) & 0 & \cdots & 0 \\ 0 & Z_{2x}^2 \operatorname{sgn}(\dot{U}_{2x} Z_{2x}) & \cdots & 0 \\ \vdots & \vdots & \ddots & \vdots \\ 0 & 0 & \cdots & Z_{nx}^2 \operatorname{sgn}(\dot{U}_{nx} Z_{nx}) \end{bmatrix} = \operatorname{diag} \begin{bmatrix} Z_{1x}^2 \operatorname{sgn}(\dot{U}_{1x} Z_{1x}) \\ Z_{2x}^2 \operatorname{sgn}(\dot{U}_{2x} Z_{2x}) \\ \vdots \\ Z_{nx}^2 \operatorname{sgn}(\dot{U}_{nx} Z_{nx}) \end{bmatrix}$$

$$\begin{bmatrix} Z_{1x}^2 \operatorname{sgn}(\dot{U}_{1x} Z_{1x}) \\ Z_{2x}^2 \operatorname{sgn}(\dot{U}_{2x} Z_{2x}) \\ \vdots \\ Z_{nx}^2 \operatorname{sgn}(\dot{U}_{nx} Z_{nx}) \end{bmatrix} = \begin{bmatrix} \operatorname{sgn}(\dot{U}_{1x} Z_{1x}) & 0 & \cdots & 0 \\ 0 & \operatorname{sgn}(\dot{U}_{2x} Z_{2x}) & \cdots & 0 \\ \vdots & \vdots & \ddots & \vdots \\ 0 & 0 & \cdots & \operatorname{sgn}(\dot{U}_{nx} Z_{nx}) \end{bmatrix} \begin{bmatrix} Z_{1x}^2 \\ Z_{2x}^2 \\ \vdots \\ Z_{nx}^2 \end{bmatrix}$$

$$\begin{bmatrix} \text{sgn}(\dot{U}_{1x}Z_{1x}) & 0 & \cdots & 0 \\ 0 & \text{sgn}(\dot{U}_{2x}Z_{2x}) & \cdots & 0 \\ \vdots & \vdots & \ddots & \vdots \\ 0 & 0 & \cdots & \text{sgn}(\dot{U}_{nx}Z_{nx}) \end{bmatrix} = \text{diag} \begin{bmatrix} \text{sgn}(\dot{U}_{1x}Z_{1x}) \\ \text{sgn}(\dot{U}_{2x}Z_{2x}) \\ \vdots \\ \text{sgn}(\dot{U}_{nx}Z_{nx}) \end{bmatrix}$$

$$\begin{bmatrix} \text{sgn}(\dot{U}_{1x}Z_{1x}) \\ \text{sgn}(\dot{U}_{2x}Z_{2x}) \\ \vdots \\ \text{sgn}(\dot{U}_{nx}Z_{nx}) \end{bmatrix} = \text{sgn} \left( \begin{bmatrix} \dot{U}_{1x}Z_{1x} \\ \dot{U}_{2x}Z_{2x} \\ \vdots \\ \dot{U}_{nx}Z_{nx} \end{bmatrix} \right)$$

$$\begin{bmatrix} \dot{U}_{1x}Z_{1x} \\ \dot{U}_{2x}Z_{2x} \\ \vdots \\ \dot{U}_{nx}Z_{nx} \end{bmatrix} = \begin{bmatrix} Z_{1x} & 0 & \cdots & 0 \\ 0 & Z_{2x} & \cdots & 0 \\ \vdots & \vdots & \ddots & \vdots \\ 0 & 0 & \cdots & Z_{nx} \end{bmatrix} \begin{bmatrix} \dot{U}_{1x} \\ \dot{U}_{2x} \\ \vdots \\ \dot{U}_{nx} \end{bmatrix}$$

The expression in y direction can be derived in a similar manner. Figure 5.8 shows the biaxial Bouc-Wen model in Simulink. The inputs to the Bouc-Wen model are the velocities at the locations of nonlinear bearings (eg., FPB or LRB). The outputs are the dimensionless hysteretic variables,  $z_x$  and  $z_y$ .

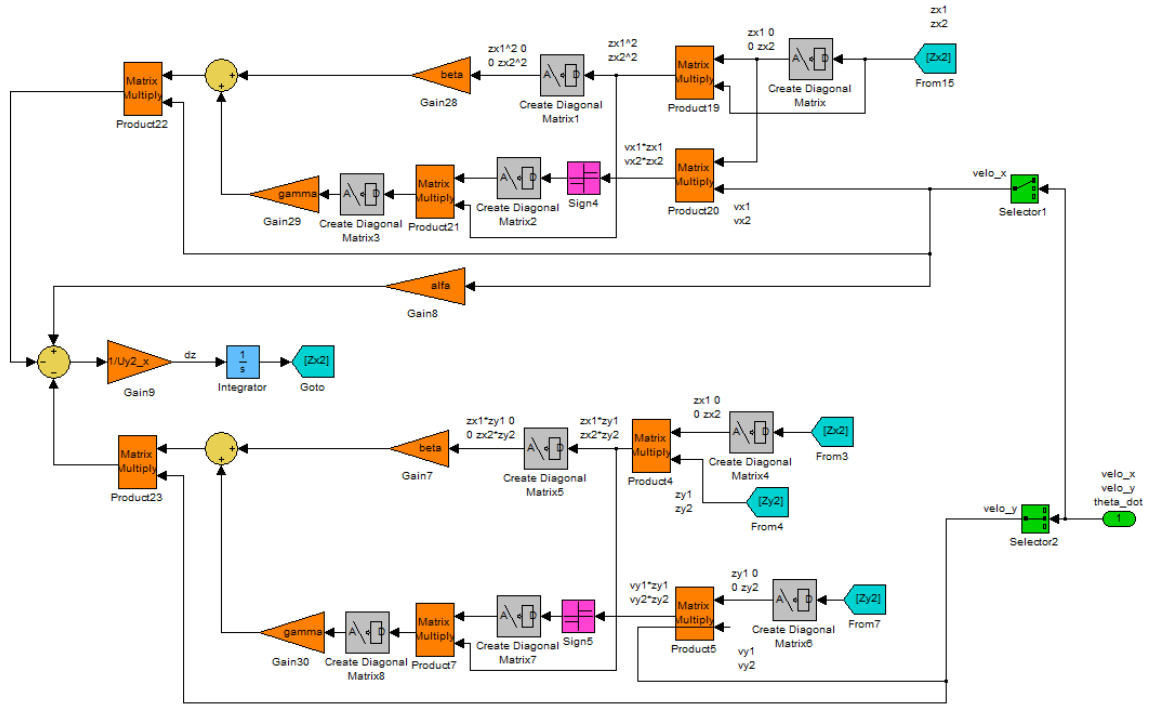


**Figure 5.8 Biaxial Bouc-Wen model in Simulink**

## 5.2 Base Isolation with Additional Control Devices

Base isolation is one of the most popular structural control strategies in enhancing the performance of structures subjected to ground excitations. However, although the interstory drifts, floor accelerations, and base shears are significantly reduced, the base isolation systems concurrently induce larger base displacements which could be detrimental to the isolation bearings. Therefore, supplemental passive devices are added to the base isolated systems to reduce the base displacements. The reason of using passive devices instead of active or semi-active devices is to consider the cost-effectiveness and avoid the malfunction and instability of the active control devices during the intense blast loading. Figure 5.9 shows the schematic of 5-story base isolated structure model with supplemental control devices. The extra devices used in this study

are the tuned mass damper, cubic nonlinear energy sink, and nonlinear force device. All devices are installed on the base except the TMD which is also installed on the top floor to compare with the device on the base. The base isolation bearings are all assumed to be linear elastomeric bearings to simplify the simulation for these exploratory studies. The performance of each device is discussed in Chapter 6 in detail.

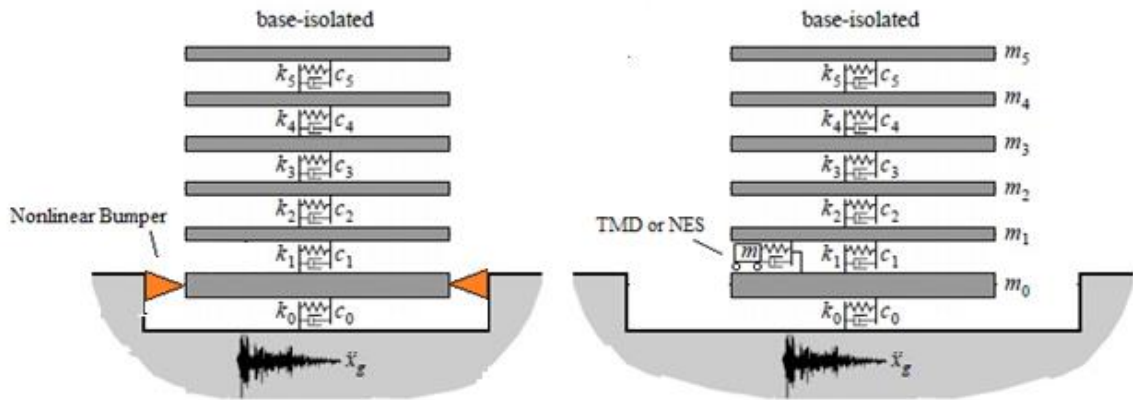


**Figure 5.9 Schematic of 5-story base isolated structure with supplemental devices**

The equations of motion of base isolated systems for both structures with additional devices can be obtained in same way with base isolated systems described in Chapter 3.

**Under ground excitation:**

$$\overline{\mathbf{M}}\ddot{\mathbf{X}} + \overline{\mathbf{C}}\dot{\mathbf{X}} + \overline{\mathbf{K}}\mathbf{X} = -\Phi_1\ddot{x}_g - \Phi_3\mathbf{f}_B - \Phi_4\mathbf{f}_E \quad (5.19)$$

**Under blast loadings:**

$$\overline{\mathbf{M}}\ddot{\mathbf{X}} + \overline{\mathbf{C}}\dot{\mathbf{X}} + \overline{\mathbf{K}}\mathbf{X} = \Phi_2\mathbf{F}_B - \Phi_3\mathbf{f}_B - \Phi_4\mathbf{f}_E \quad (5.20)$$

where  $\Phi_4$  is the distribution matrix defining the forces from extra devices on each degree of freedom,  $\Phi_4 = \Phi_3$  if extra devices are installed on base level;  $\mathbf{f}_E$  is the force provided by extra devices.

$$\bar{\mathbf{M}} = \begin{bmatrix} \mathbf{M} & \mathbf{M}\Gamma \\ \Gamma^T\mathbf{M} & \Gamma^T\mathbf{M}\Gamma + \mathbf{M}_b \end{bmatrix} \quad \bar{\mathbf{M}}_1 = \begin{bmatrix} \mathbf{M} & \mathbf{0} \\ \Gamma^T\mathbf{M} & \mathbf{M}_b \end{bmatrix}$$

$$\bar{\mathbf{K}} = \begin{bmatrix} \mathbf{K} & \mathbf{0} \\ \mathbf{0} & \mathbf{K}_b \end{bmatrix} \quad \bar{\mathbf{C}} = \begin{bmatrix} \mathbf{C} & \mathbf{0} \\ \mathbf{0} & \mathbf{C}_b \end{bmatrix}$$

$$\Phi_1 = \begin{bmatrix} \mathbf{M}\Gamma \\ \Gamma^T\mathbf{M}\Gamma + \mathbf{M}_b \end{bmatrix} \quad \Phi_2 = \begin{bmatrix} \Lambda_1 \\ \Gamma^T\Lambda_1 + \Lambda_2 \end{bmatrix} \quad \Phi_3 = \begin{bmatrix} \mathbf{0} \\ \mathbf{I} \end{bmatrix}$$

The state space matrices of the state space equations in Eq. 3.1 and Eq. 3.2 are given by:

**Under ground excitation:**

$$\mathbf{u} = \begin{Bmatrix} \ddot{\mathbf{x}}_g \\ \mathbf{f}_B \\ \mathbf{f}_E \end{Bmatrix}$$

$$\mathbf{A}_s = \begin{bmatrix} \mathbf{0} & \mathbf{I} \\ -\bar{\mathbf{M}}^{-1}\bar{\mathbf{K}} & -\bar{\mathbf{M}}^{-1}\bar{\mathbf{C}} \end{bmatrix} \quad \mathbf{B}_s = \begin{bmatrix} \mathbf{0} & \mathbf{0} & \mathbf{0} \\ -\bar{\mathbf{M}}^{-1}\Phi_1 & -\bar{\mathbf{M}}^{-1}\Phi_3 & -\bar{\mathbf{M}}^{-1}\Phi_4 \end{bmatrix}$$

$$\mathbf{C}_s = \begin{bmatrix} \mathbf{I} & \mathbf{0} \\ \mathbf{0} & \mathbf{I} \\ -\bar{\mathbf{M}}_1^{-1}\bar{\mathbf{K}} & -\bar{\mathbf{M}}_1^{-1}\bar{\mathbf{C}} \end{bmatrix} \quad \mathbf{D}_s = \begin{bmatrix} \mathbf{0} & \mathbf{0} & \mathbf{0} \\ \mathbf{0} & -\bar{\mathbf{M}}_1^{-1}\Phi_3 & -\bar{\mathbf{M}}_1^{-1}\Phi_4 \end{bmatrix}$$

Under blast loadings:

$$\mathbf{u} = \begin{Bmatrix} \mathbf{F}_B \\ \mathbf{f}_B \\ \mathbf{f}_E \end{Bmatrix}$$

$$\mathbf{A}_s = \begin{bmatrix} \mathbf{0} & \mathbf{I} \\ -\overline{\mathbf{M}}^{-1}\overline{\mathbf{K}} & -\overline{\mathbf{M}}^{-1}\overline{\mathbf{C}} \end{bmatrix} \quad \mathbf{B}_s = \begin{bmatrix} \mathbf{0} & \mathbf{0} & \mathbf{0} \\ \overline{\mathbf{M}}^{-1}\Phi_2 & -\overline{\mathbf{M}}^{-1}\Phi_3 & -\overline{\mathbf{M}}^{-1}\Phi_4 \end{bmatrix}$$

$$\mathbf{C}_s = \begin{bmatrix} \mathbf{I} & \mathbf{0} \\ \mathbf{0} & \mathbf{I} \\ -\overline{\mathbf{M}}_1^{-1}\overline{\mathbf{K}} & -\overline{\mathbf{M}}_1^{-1}\overline{\mathbf{C}} \end{bmatrix} \quad \mathbf{D}_s = \begin{bmatrix} \mathbf{0} & \mathbf{0} & \mathbf{0} \\ \overline{\mathbf{M}}_1^{-1}\Phi_2 & -\overline{\mathbf{M}}_1^{-1}\Phi_3 & -\overline{\mathbf{M}}_1^{-1}\Phi_4 \end{bmatrix}$$

In this study, isolation bearings are all assumed as linear elastomeric bearings, therefore, the term of nonlinear bearing force  $\mathbf{f}_B$  and  $\Phi_3$  can be ignored.

Figure 5.10 shows the Simulink diagram of base isolated system with additional device.

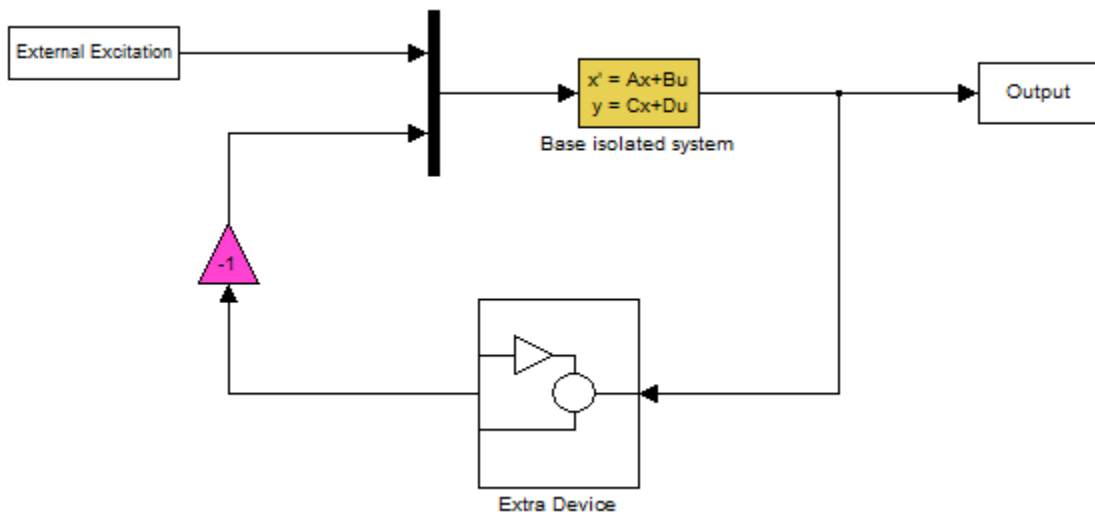


Figure 5.10 Simulink diagram of base isolated system with supplemental device



### 5.2.1 Base Isolation System with TMD (IS-TB, IS-TR)

A tuned mass damper (TMD) is a device consisting of a mass, spring and damper that is attached to a structure in order to reduce the dynamic responses of the structure. The frequency of the damper is tuned to the fundamental structural frequency which is 0.4 Hz for the 5-story base isolated structure and 0.3 Hz and 0.31 Hz for the 8-story base isolated structure in both  $x$  and  $y$  direction. The damper will resonate out of phase with the structural motion and energy is dissipated by the inertia force of the damper acting on the structure. Application of TMD on the upper or top story is an efficient mean to reduce structural responses, in particular for period loading such as wind loading. In addition, TMD is installed on the base level in this study because the main goal is to reduce the base displacement. There is significant motion of the base under the first natural frequency of the structure to which the TMD is tuned. Furthermore, it is easier to introduce additional mass at the base as compared to upper stories.

The equation of motion of the TMD is:

$$m_{TMD}\ddot{x}_{TMD,abs} + c_{TMD}\dot{x}_{TMD} + k_{TMD}x_{TMD} = 0 \quad (3.23)$$

The resisting force  $f_E$  from the TMD is:

$$f_E = k_{TMD}x_{TMD} + c_{TMD}\dot{x}_{TMD} \quad (3.24)$$

where  $m_{TMD}$ ,  $k_{TMD}$ , and  $c_{TMD}$  are the mass, stiffness and damping coefficient of the TMD;

The mass of the TMD is predetermined as either 1% or 6% of the total weight of the structure, and the stiffness is determined to match the first natural frequency of the base-isolated structure; The damping ratio is set as 10%;  $\ddot{x}_{TMD,abs}$  is the absolute acceleration

of the TMD,  $x_{TMD}$  is the displacement of the TMD relative to the base or top floor.

Figure 5.11 shows configuration of the TMD in Simulink.

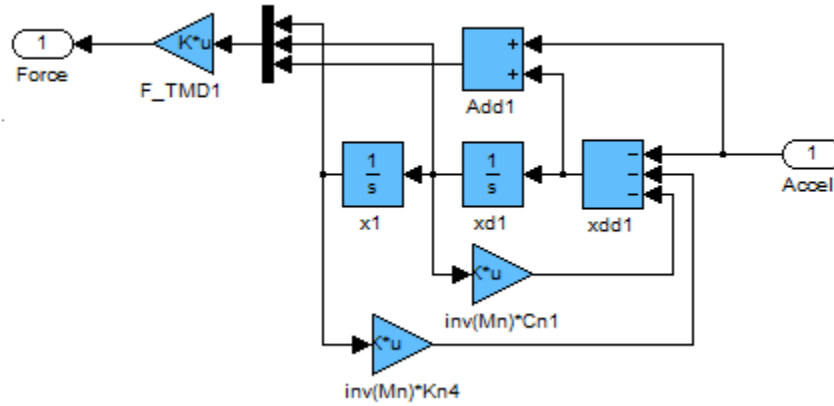


**Figure 5.11 Simulink diagram of the TMD**

### 5.2.2 Base Isolation System with Cubic NES on the Base (IS-CN)

A nonlinear energy sink (NES) is a passive energy dissipation device designed to locally dissipate the vibration energy induced to a structure system due to earthquakes, shock, blast, etc. The NES is a light-weight device coupled to large-scale dynamic structure through a nonlinear stiffness element. It can be regarded as broadband TMD as it is not tuned to a particular frequency. Different designs of the NES were proposed and experimentally tested by researchers, such as the vibro-impact NES (AL-Shudeifat et al., 2013). In this study, the NESs with a cubic spring to provide the nonlinearity has been employed on the base level to reduce the base displacement. The equation of motion and the inertia force are shown in Eq. 5.25 and Eq. 5.26, respectively.

$$m_{NES} \ddot{x}_{NES,abs} + c_{NES} \dot{x}_{NES} + k_{NES} x_{NES}^3 = 0 \quad (5.25)$$

$$f_E = k_{NES} x_{NES}^3 + c_{NES} \dot{x}_{NES} \quad (5.26)$$

where  $m_{NES}$ ,  $k_{NES}$ , and  $c_{NES}$  are the mass, stiffness and damping coefficient of the NES; The mass of the NES is also predetermined as 1% or 6% of the total weight of the structure, and the stiffness is tuned for a specific structure addressed in Chapter 6; The damping ratio is set as 10%;  $x_{NES,abs}$  is the absolute acceleration of the NES,  $x_{NES}$  is the displacement of the NES relative to the base. Figure 5.12 shows configuration of the cubic NES in Simulink.

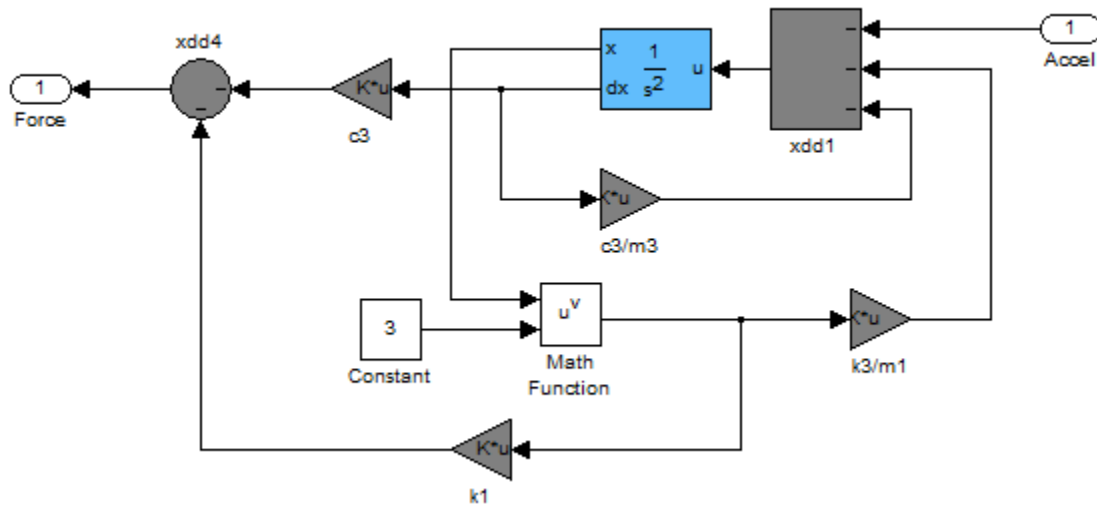


**Figure 5.12 Simulink diagram of the cubic NES**

### 5.2.3 Base Isolation System with Nonlinear Bumpers (IS-NB)

Another passive energy dissipation device installed to reduce the base displacement in this study is the nonlinear bumper device which consists of a nonlinear

spring only. The devices are fixed on the ground and connected to the base directly. The idea behind this strategy is to provide a nonlinear resisting force from these devices whenever there is a movement of the base. By using a nonlinear stiffness, the device is less effective for smaller excitations, allowing the base isolation device to perform normally. Under larger excitations where damage may occur to the base isolator or a surrounding moat wall, the nonlinear bumpers provide more significant restoring forces. The device is assumed to provide a resisting force when it is in compression only and also fully rebound after the compression. One example to realize this device is to adopt a quarter pyramidal bumper made of the material with high Poisson's ratio (Luo et al., 2014) which is shown in Figure 5.13. As the bumper is loaded from the tip, the engaging area resisting the compression increases sharply, and the bumper exhibits a rapidly increasing stiffness which can represent the nonlinearity. Because of this assumption, the devices are arranged around the perimeter of the base which is shown in Figure 5.14.

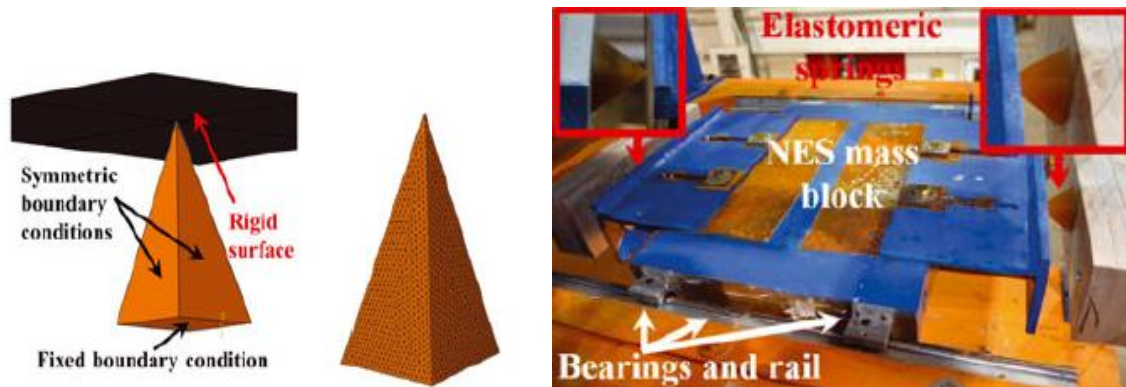


**Figure 5.13 Example of pyramidal nonlinear bumper (Luo et al., 2014)**

Figure 5.15 shows the Simulink model of the nonlinear bumpers in the 8-story three-dimensional structure. To simplify the simulation model, the cubic force-displacement relationship is assumed. The resisting force generated by this device is

$$f_E = k_{NB}x_b^3 \quad (5.27)$$

The relationship between the nonlinear force and the displacement of the nonlinear bumper is shown in Figure 5.16.

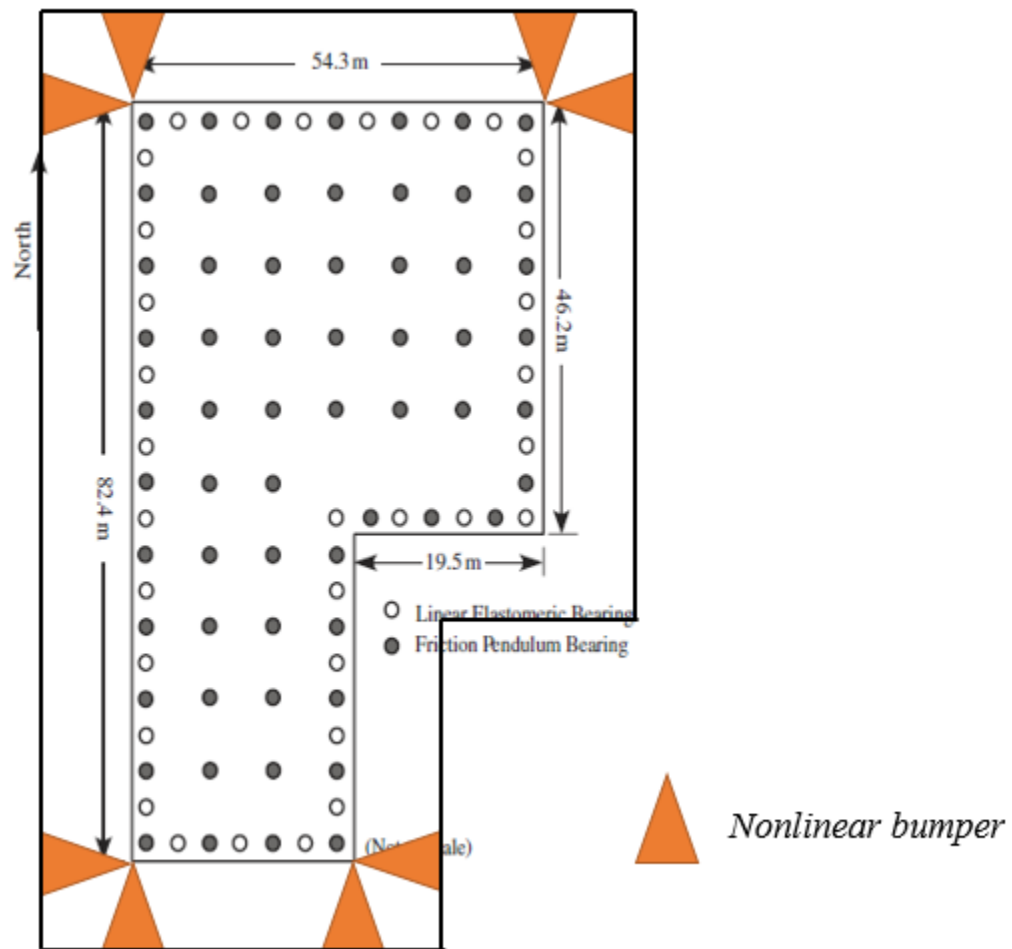


**Figure 5.14 Schematic of the installation of the nonlinear bumper on 8 story structure**

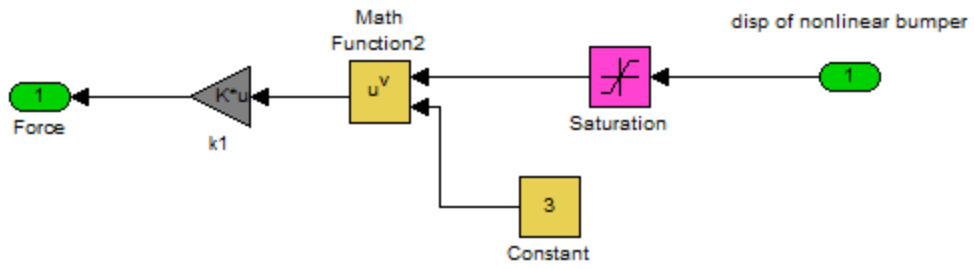


Figure 5.15 Simulink diagram of the nonlinear bumper

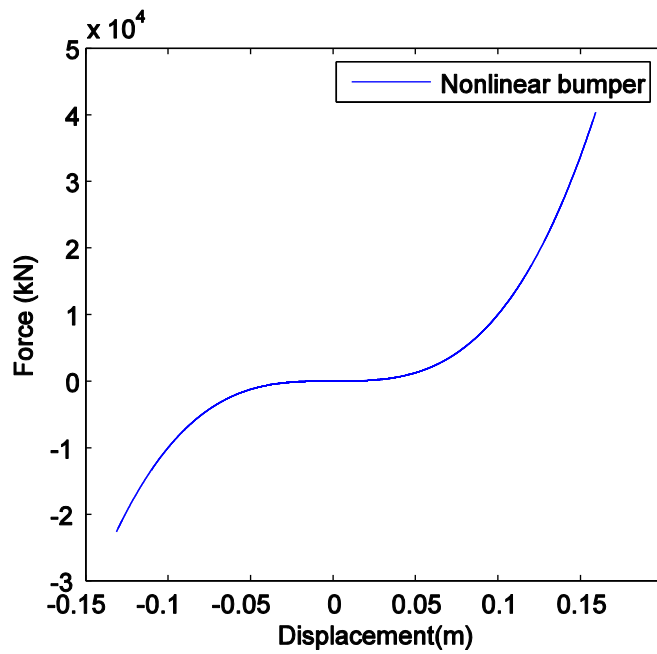


Figure 5.16 Force vs. displacement of the nonlinear bumper

### 5.3 Chapter Summary

Multiple structural control strategies are presented in this chapter in detail, including base isolation and the combination of base isolation and additional control devices. Three types of base isolators are introduced, including the linear elastomeric bearings, the friction pendulum bearings, and the lead rubber bearings. The Bouc-Wen model is also presented to consider the biaxial interaction for the three-dimensional behaviors. The base isolators are assumed to be linear elastomeric bearings only to simplify the Simulink model and save simulation time. The extra devices installed on the base isolated system are the tuned mass damper on the base (IS-TB), tuned mass damper on the roof (IS-TR), cubic nonlinear energy sink (NES) on the base (IS-CN), and nonlinear bumpers connected to the base (IS-NB). The configuration of each device is presented.

## CHAPTER 6 RESULTS AND DATA ANALYSIS

This chapter presents the responses of the 5-story structure and the 8-story three-dimensional structure. The performance of multiple control devices described in Chapter 5 under earthquakes and blast loadings generated in Chapter 4 are investigated. Several evaluation criteria calculated from the resulting structural responses are provided to compare the control performance across different control strategies.

### 6.1 Evaluation Criteria

To evaluate the performance of different control devices under both seismic excitations and blasts, the following evaluation criteria are defined for both 5-story and 8-story structures based on the maximum and root mean square (RMS) responses of the structure systems. For each control design, these criteria are evaluated for all four earthquakes and blast loadings introduced in Chapter 4.

1. Maximum base displacement

$$J_1 = \max_{t \in [0, t_1]} \|d_0(t)\| \quad (6.1)$$

where  $d_0(t)$  is the base displacement of the control system over the time history of each dynamic excitation;  $t_1$  is the duration of the significant response.

2. Maximum RMS base displacement

$$J_2 = \max_{t \in [0, t_1]} \|RMS(d_0(t))\| \quad (6.2)$$



3. Maximum interstory drift of the superstructure

$$J_3 = \max \left\{ \max_{t \in [0, t_1]} \left\| d_i(t) \right\| \right\} \quad (6.3)$$

where  $d_i(t)$  is the interstory drift of the  $i$ -th story of the control system over the time history of each dynamic excitation.

4. Maximum RMS interstory drift of the superstructure

$$J_4 = \max \left\{ \max_{t \in [0, t_1]} \left\| RMS(d_i(t)) \right\| \right\} \quad (6.4)$$

5. Maximum floor-level absolute acceleration of the superstructure

$$J_5 = \max \left\{ \max_{t \in [0, t_1]} \left\| a_i(t) \right\| \right\} \quad (6.5)$$

where  $a_i(t)$  is the absolute acceleration of the  $i$ -th story of the control system over the time history of each dynamic excitation.

6. Maximum RMS floor-level absolute acceleration of the superstructure

$$J_6 = \max \left\{ \max_{t \in [0, t_1]} \left\| RMS(a_i(t)) \right\| \right\} \quad (6.6)$$

7. Maximum base absolute acceleration

$$J_7 = \max_{t \in [0, t_1]} \left\| a_0(t) \right\| \quad (6.7)$$

where  $a_0(t)$  is the base absolute acceleration of the control system over the time history of each dynamic excitation.

8. Maximum RMS base absolute acceleration

$$J_8 = \max_{t \in [0, t_1]} \left\| RMS(a_0(t)) \right\| \quad (6.8)$$

## 9. Maximum base shear

$$J_9 = \max_{t \in [0, t_1]} \|V_0(t)\| \quad (6.9)$$

where  $V_0(t)$  is the base shear of the control system over the time history of each dynamic excitation.

For structures subjected to the ground motions, the base shear is calculated by adding all floor inertia forces above the base as shown in Eq. 6.10. The floor inertia forces are computed as the product of the floor acceleration and the floor mass. For structures subjected to the blasts, the external blast loading on each story should also be taken into account to calculate the base shear as shown in Eq. 6.11.

$$V_0(t) = \sum_{i=1}^n m_i a_i(t) \quad (6.10)$$

$$V_0(t) = \sum_{i=1}^n m_i a_i(t) + \sum_{i=1}^n F_{Bi}(t) \quad (6.11)$$

where  $m_i$  and  $a_i(t)$  are the mass and absolute acceleration of the  $i$ -th floor,  $F_{Bi}(t)$  is the blast loading applied on the  $i$ -th floor.

## 6.2 Performance of Multiple Control Systems for the 5-story Structure

The performance of each control device on the 5-story structure is investigated under both earthquakes and blast loadings introduced in Chapter 4. In the following discussion, the symbols representing the control systems and the reference systems are listed in Table 6.1.

**Table 6.1 Symbols of different systems**

Symbols	Systems
(1%M), (6%M)	Mass of the TMD or cubic NES 1%M – 1% of the total mass of the structure 6%M – 6% of the total mass of the structure
Orig-sys	Fixed base structure system
Orig-sys + TMD	Fixed base structure system with a TMD on the top floor
IS-linear	Base isolated structure system containing linear elastomeric bearings only
IS-TB	Base isolated system with a TMD on the base
IS-TR	Base isolated system with a TMD on the top floor
IS-CN	Base isolated system with a cubic NES on the base
IS-NB	Base isolated system with a nonlinear bumper connected to the base
IS-NB + TMD	Base isolated system with a nonlinear bumper connected to the base plus a TMD on the base level
IS-NB + CN	Base isolated system with a nonlinear bumper connected to the base plus a cubic NES on the base

**Traditional control strategies**

First, traditional control strategies are investigated, including base isolation and the TMD on the top floor. Table 6.2 shows the performance of these control strategies for the 5-story building. The TMD with two different weights and the base isolation system are investigated. It is observed that the traditional TMD underachieves for all excitations even with a higher mass. The base isolation performs well as expected especially under seismic excitations. There is, however, room for improvement, especially when considering the base displacement. The next group of studies will demonstrate

performance gains achieved by combining base isolation with supplemental control devices.

**Table 6.2 Performance of traditional control strategies**

External Excitations	Blast (50 kg)	Blast (100 kg)	El Centro	Kobe	Northridge	Tohoku
<b>J<sub>3</sub>: Maximum Superstructure Interstory Drift (m)</b>						
Orig_sys	0.0451	0.0778	0.0049	0.0122	0.0152	0.0164
Orig_sys+TMD (1% M)	0.0451	0.0778	0.0049	0.0122	0.0151	0.0163
Orig_sys+TMD (6% M)	0.0450	0.0776	0.0048	0.0199	0.0149	0.0159
IS-linear	0.0287	0.0467	0.0011	0.0016	0.0040	0.0017
<b>J<sub>5</sub>: Maximum Superstructure Absolute Acceleration (m/s<sup>2</sup>)</b>						
Orig_sys	299.1326	520.6877	8.1141	19.2747	23.5102	27.8347
Orig_sys+TMD (1% M)	299.1326	520.6877	8.0662	19.1676	23.4553	27.7204
Orig_sys+TMD (6% M)	299.1326	520.6877	7.8346	18.6575	23.1863	27.1950
IS-linear	300.6216	522.9111	1.3153	1.8897	4.6750	2.3688
<b>J<sub>9</sub>: Maximum Base Shear (kN)</b>						
Orig_sys	1,179,500	2,027,000	157,520	394,420	486,550	499,100
Orig_sys+TMD (1% M)	1,179,500	2,027,000	157,140	392,400	485,220	496,820
Orig_sys+TMD (6% M)	1,179,500	2,027,000	155,090	382,840	478,620	486,350
IS-linear	39,558	46,543	47,339	65,219	167,230	67,918

## **Observed improvements through base isolation**

Under earthquakes, base isolation makes an excellent improvement to most evaluation criteria, except for base displacements. Under the blast loadings, the base isolation still performs well in the interstory drift but it cannot make a reduction on maximum absolute acceleration of the superstructure shown in Figure 6.1 and Figure 6.2. This is because the maximum acceleration comes immediately due to the intense loading and without regard for the structural dynamics. That is to say, the frequency content of the blast is much larger than the natural frequencies of the structure for all devices. However, there is still an improvement in the superstructure acceleration by looking at the RMS absolute acceleration of the superstructure. The time histories of the fixed base structure and the base isolated system subject to the 50 kg blast are shown in Figure 6.3. Figure 6.4 shows the base shears of the fixed base structure and the base isolated system under multiple excitations. The base shears are kept at very low levels by base isolation.

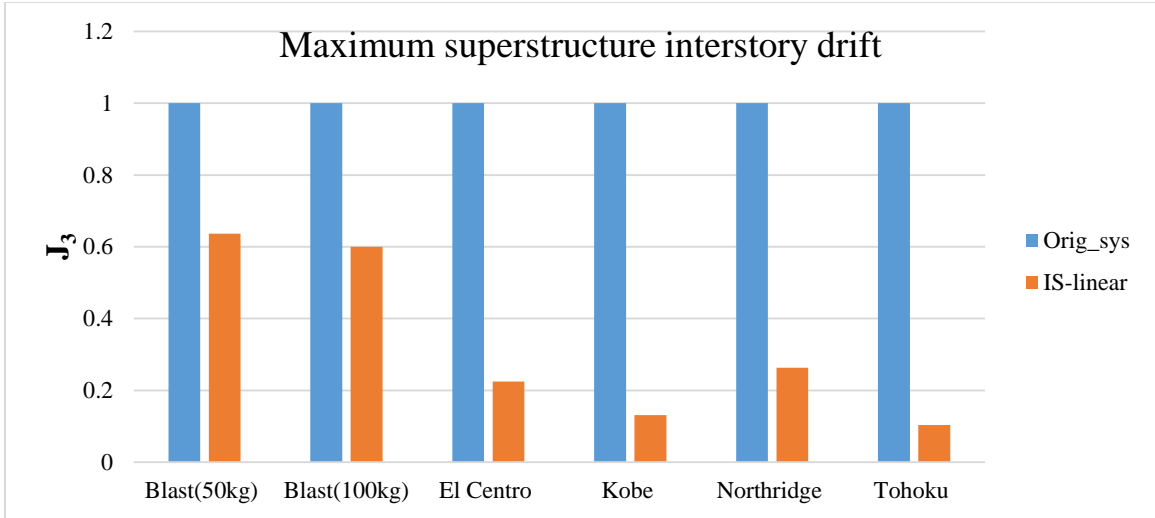


**Figure 6.1 Performance of base isolation on maximum superstructure interstory drift under multiple excitations**

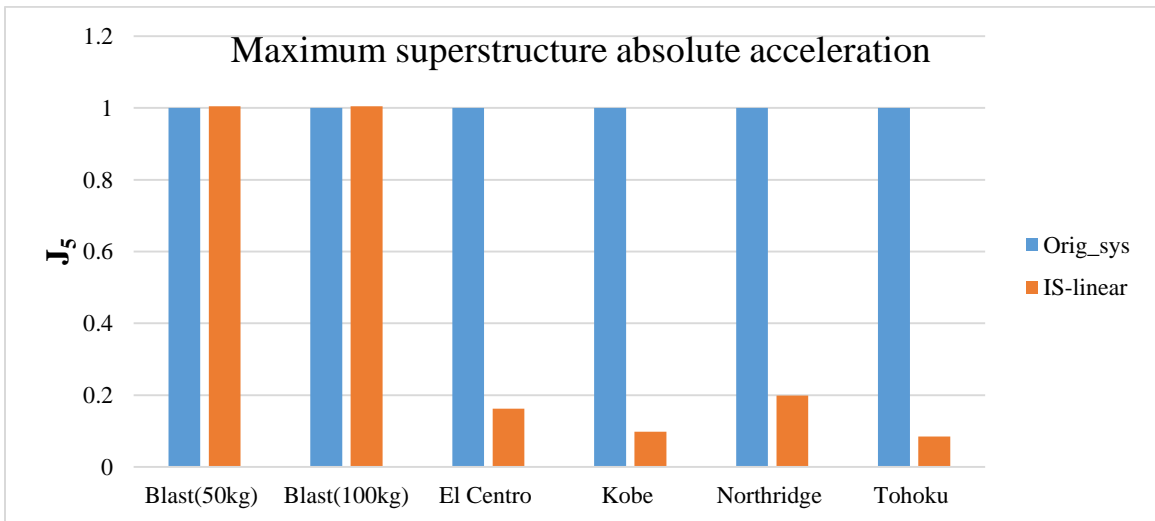


**Figure 6.2 Performance of base isolation on maximum superstructure absolute acceleration under multiple excitations**

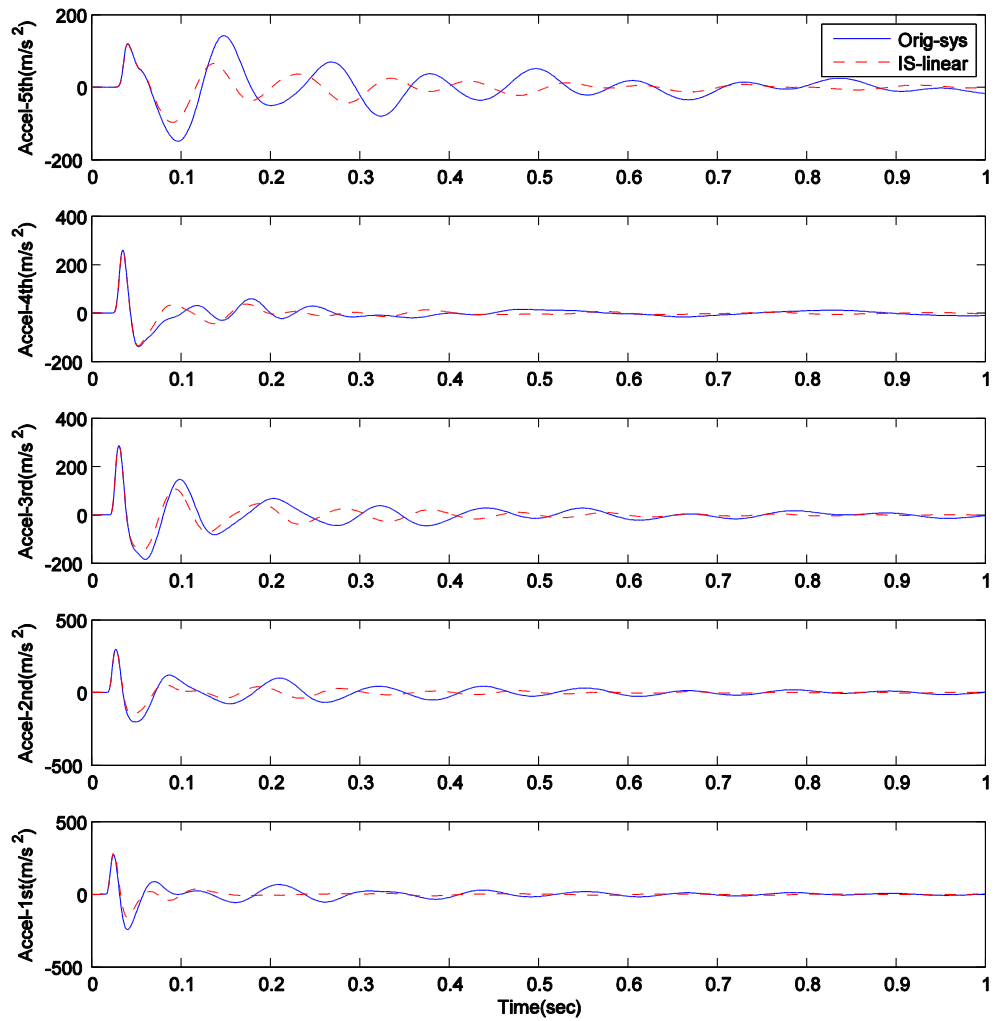


**Figure 6.3 Time history of the superstructure absolute acceleration under explosion of 50 kg TNT**

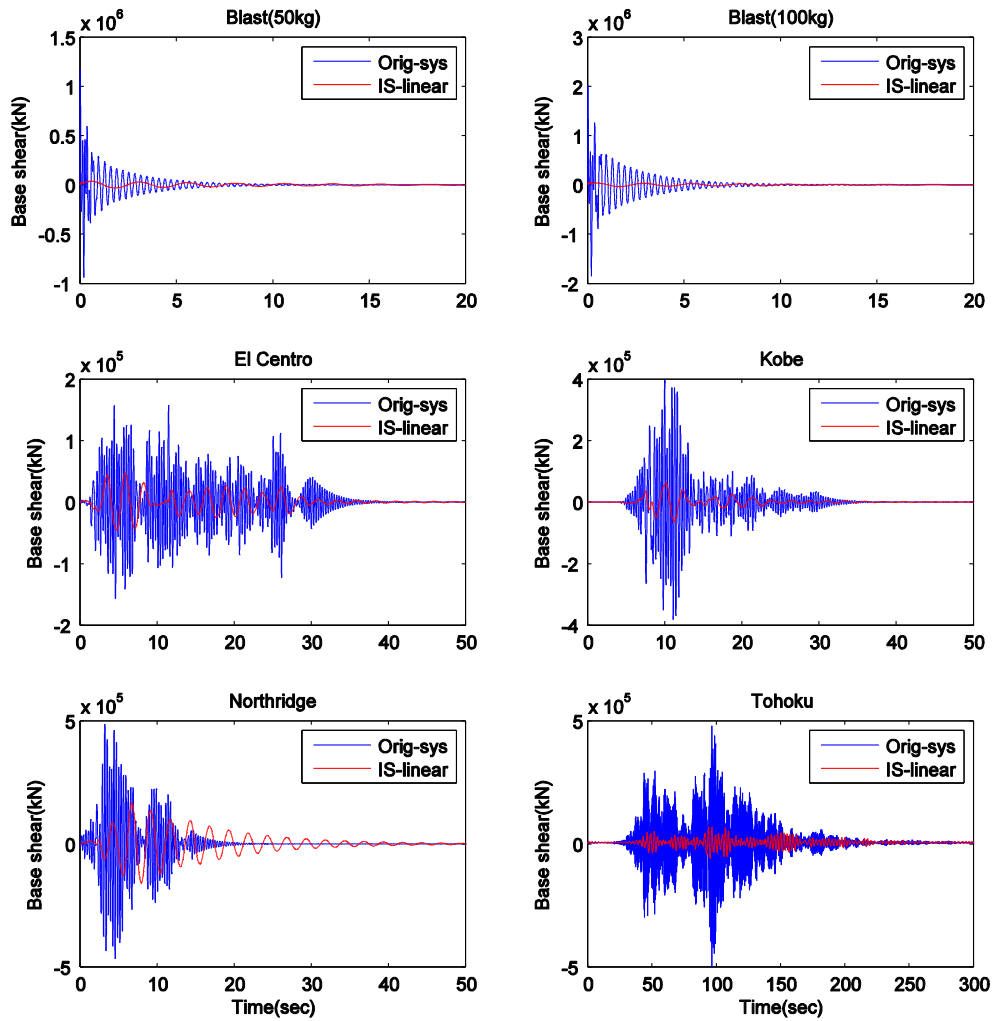


**Figure 6.4 The base shears of base isolation under multiple excitations**

### **Base isolated system with supplemental devices**

To reduce the base displacement of the base isolation system, extra control devices are installed, including the TMD, the cubic NES, and the nonlinear bumper. Figure 6.5 and Figure 6.6 show that the performance of the IS-TR and IS-TB device under Northridge earthquake and 50 kg blast, respectively. Here, the performance criteria



are normalized to the base-isolated structure. Better performance can be achieved when the TMD is installed on the base level instead of the top floor. Thus, all devices are installed on the base level instead of the top floor because the reference system is the base isolated system and the main goal is to reduce the base displacement and concurrently maintain the performance of the base isolation under earthquakes.

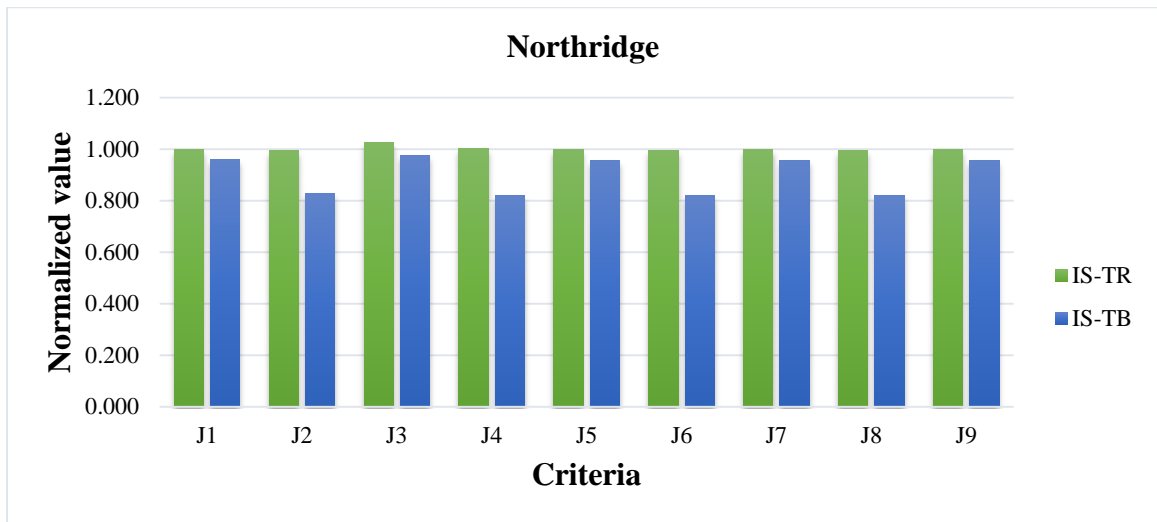


**Figure 6.5 Performance of the IS-TR and IS-TB under Northridge earthquake**

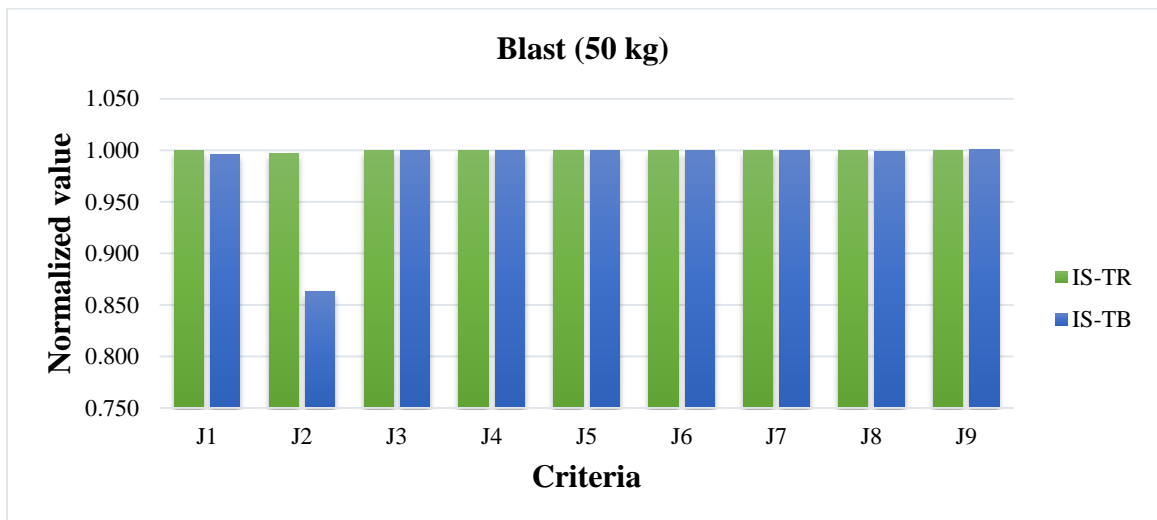


**Figure 6.6 Performance of the IS-TR and IS-TB under explosion of 50 kg TNT**

The tuned mass dampers are set to the fundamental natural frequency of the structure. Conversely, the IS-CN and IS-NB devices have a tunable parameter which influences the structural response. In both cases, the tunable parameter is the cubic stiffness of the device. A sensitivity analysis of the parameter influencing the structural responses is performed and the results for the IS-CN device and IS-NB device are presented in Figure 6.7 through Figure 6.14 and Figure 6.15 through Figure 6.22, respectively. Note that all evaluation criteria are normalized to the base-isolated system.

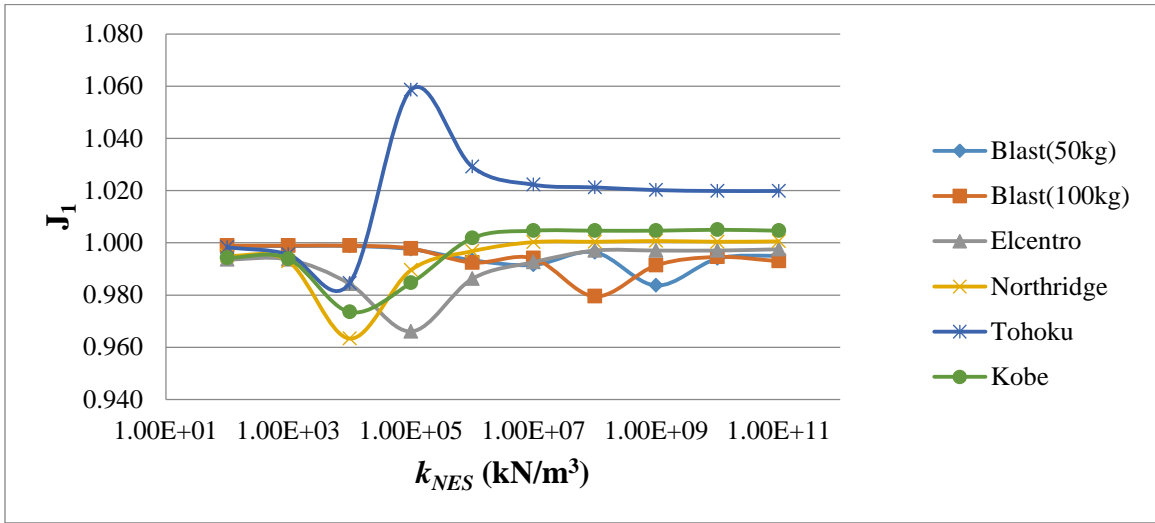


Figure 6.7 Performance of IS-CN on  $J_1$  with varying stiffness

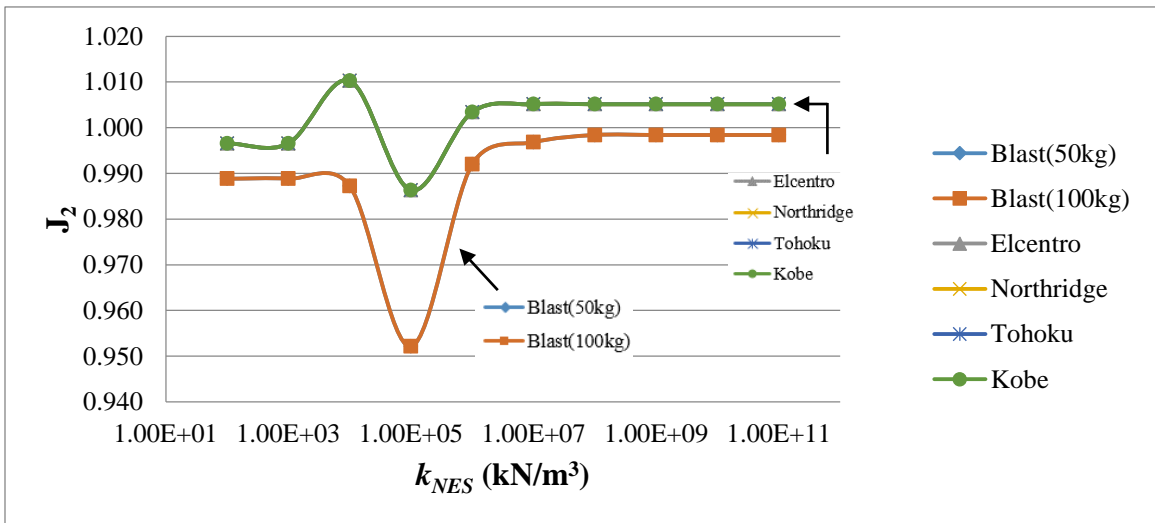


Figure 6.8 Performance of IS-CN on  $J_2$  with varying stiffness

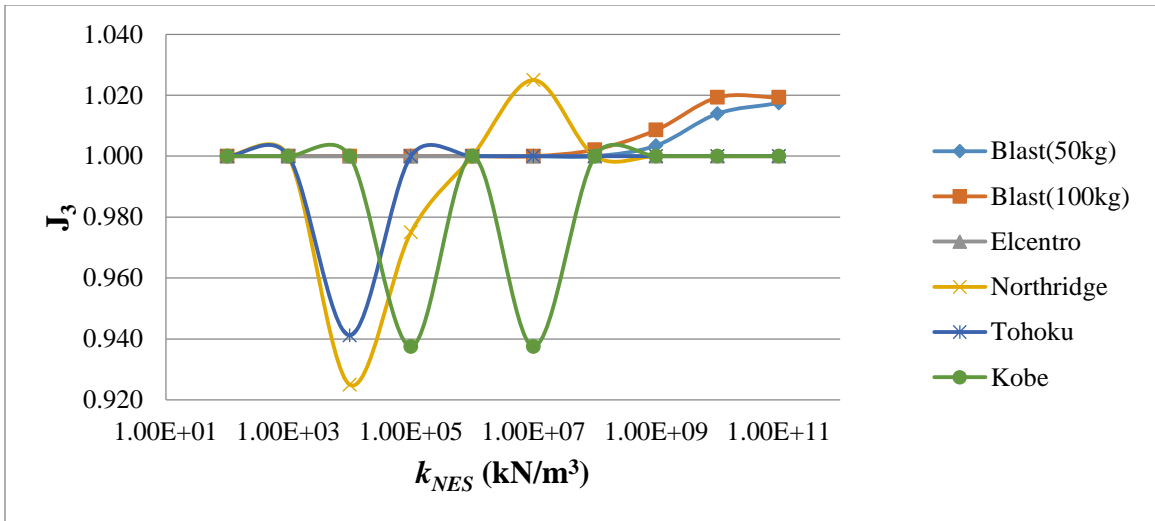


Figure 6.9 Performance of IS-CN on  $J_3$  with varying stiffness

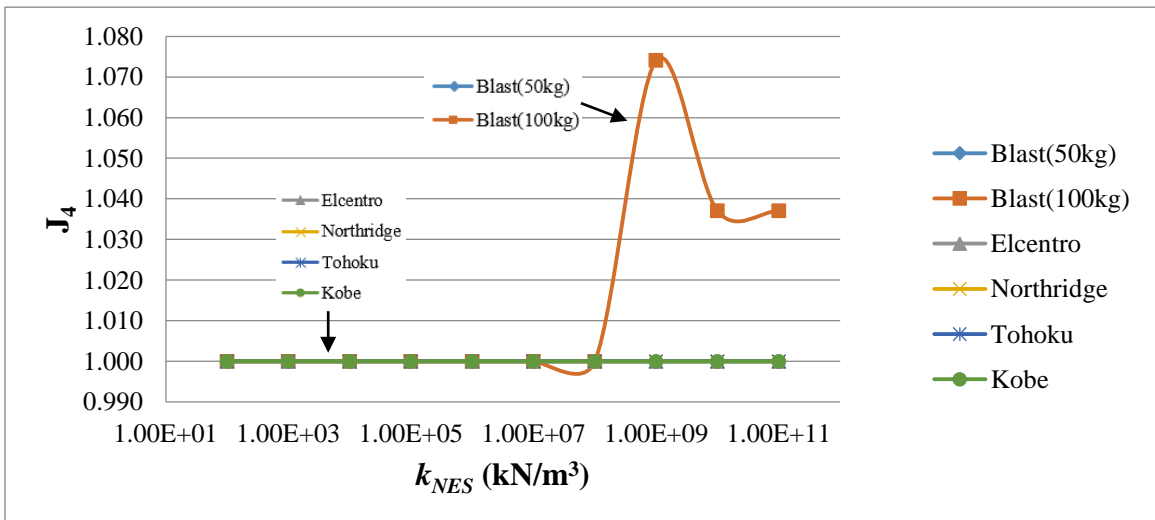


Figure 6.10 Performance of IS-CN on  $J_4$  with varying stiffness

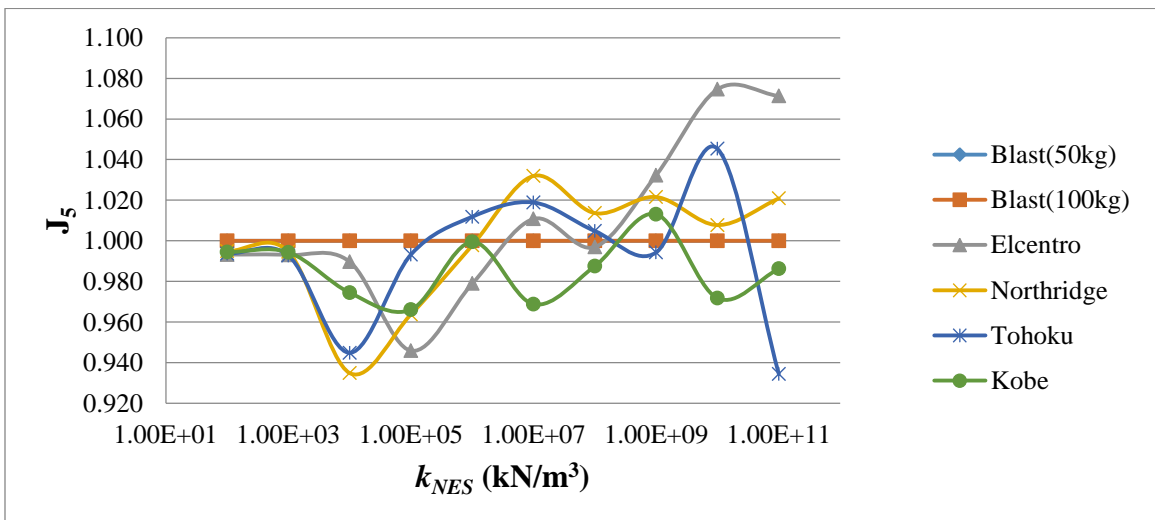


Figure 6.11 Performance of IS-CN on  $J_5$  with varying stiffness

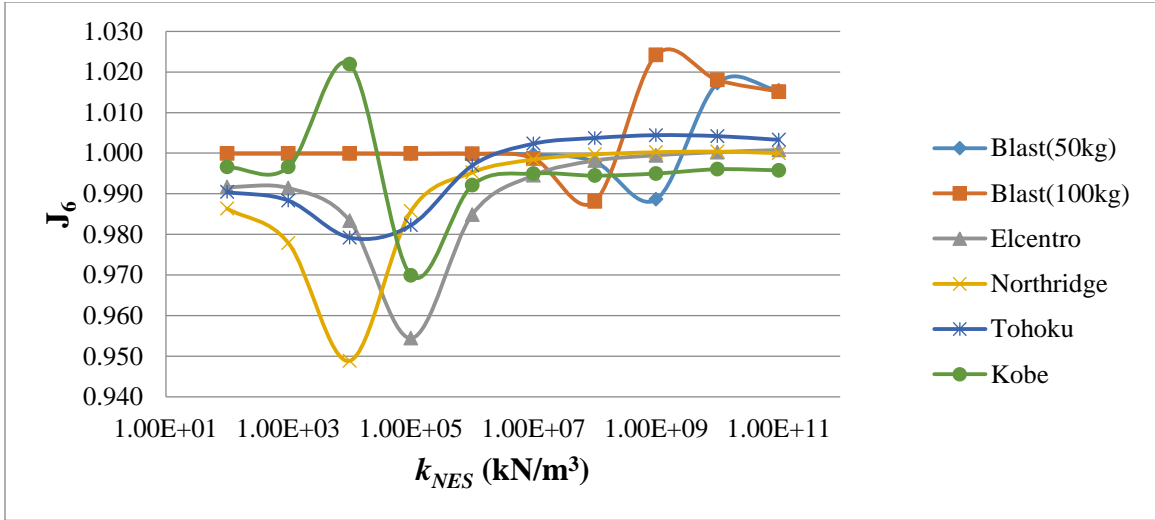


Figure 6.12 Performance of IS-CN on  $J_6$  with varying stiffness

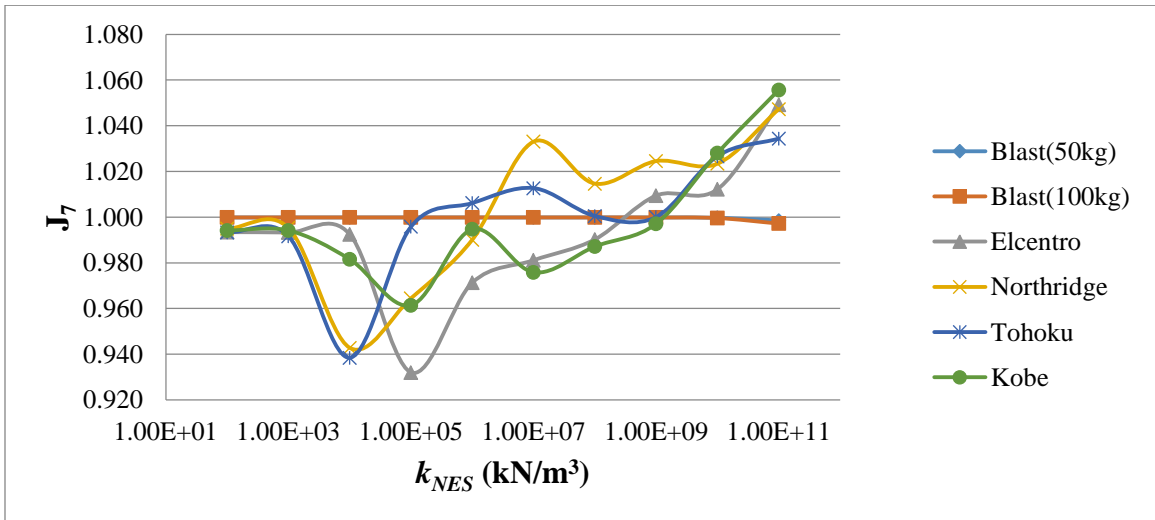


Figure 6.13 Performance of IS-CN on  $J_7$  with varying stiffness

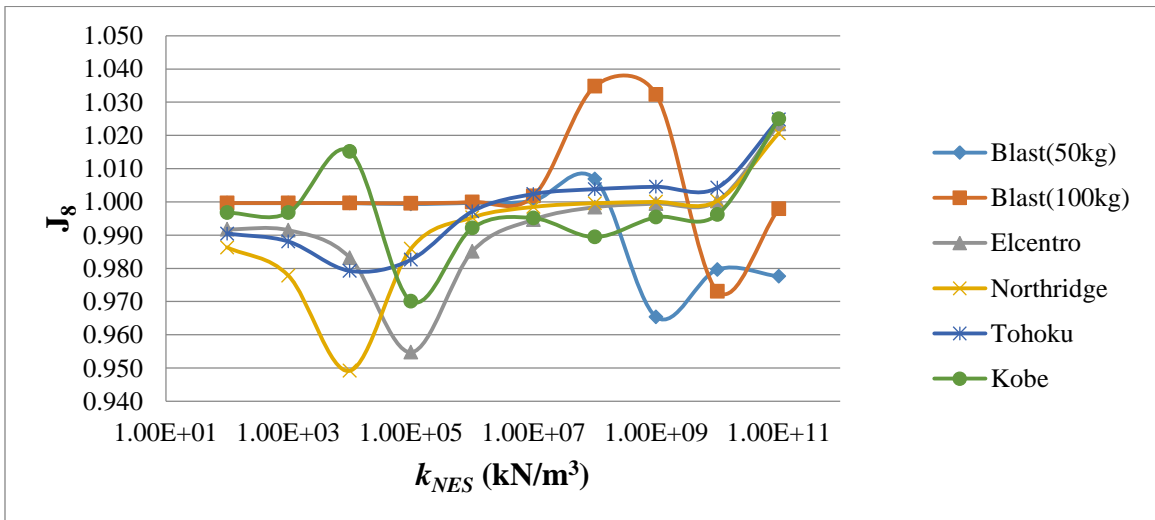
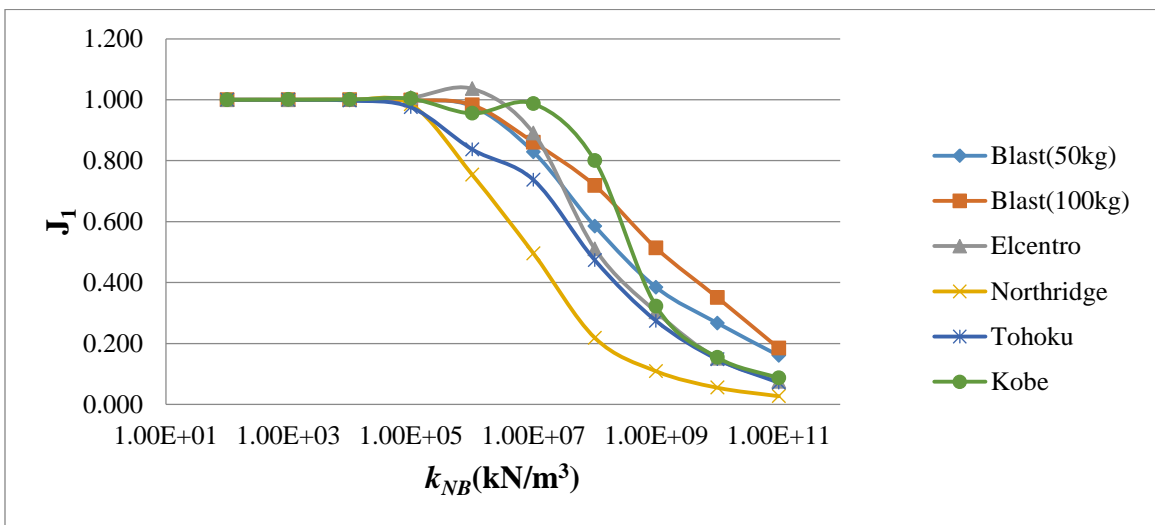
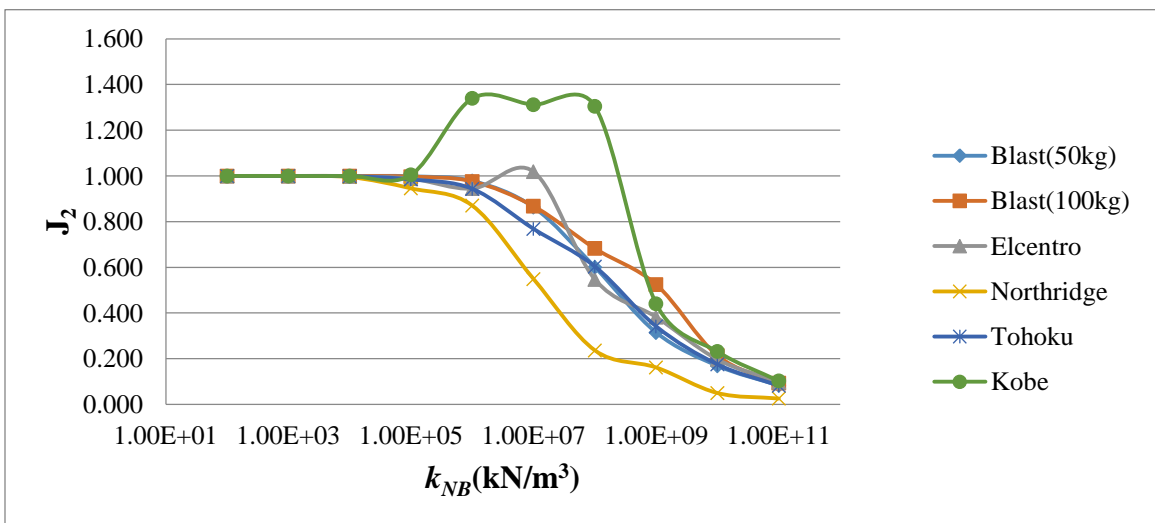


Figure 6.14 Performance of IS-CN on  $J_8$  with varying stiffness

Criteria with a normalized value less than 1 indicate better performance when compared to the base-isolated structure. It is observed through Figure 6.3 to Figure 6.10 that generally the normalized values for all criteria are around 1 even if there are drops and jumps. Although the cubic NES does not make excellent improvement compared to the reference system, the best overall performance of IS-CN under multiple excitations considering all criteria is observed with a stiffness of  $k_{NES} = 10^4 \text{ kN/m}^3$ .



**Figure 6.15 Performance of IS-NB on  $J_1$  with varying stiffness**



**Figure 6.16 Performance of IS-NB on  $J_2$  with varying stiffness**

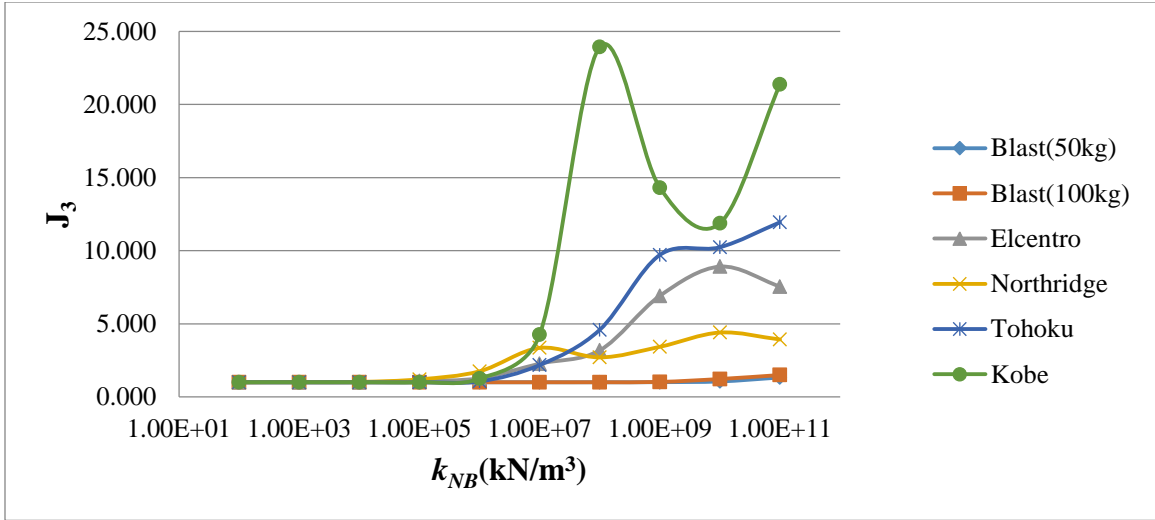


**Figure 6.17 Performance of IS-NB on  $J_3$  with varying stiffness**

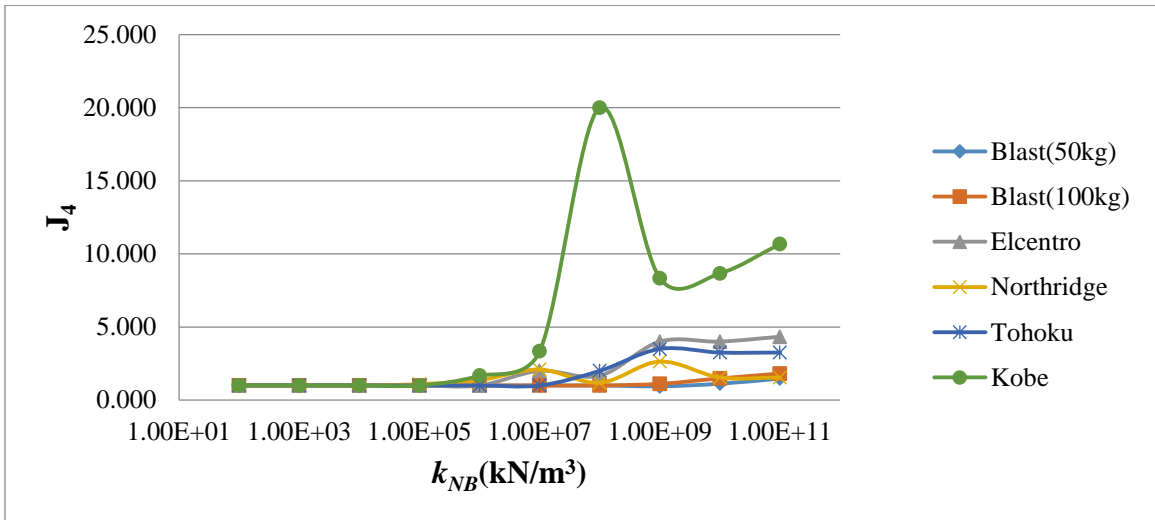


**Figure 6.18 Performance of IS-NB on  $J_4$  with varying stiffness**

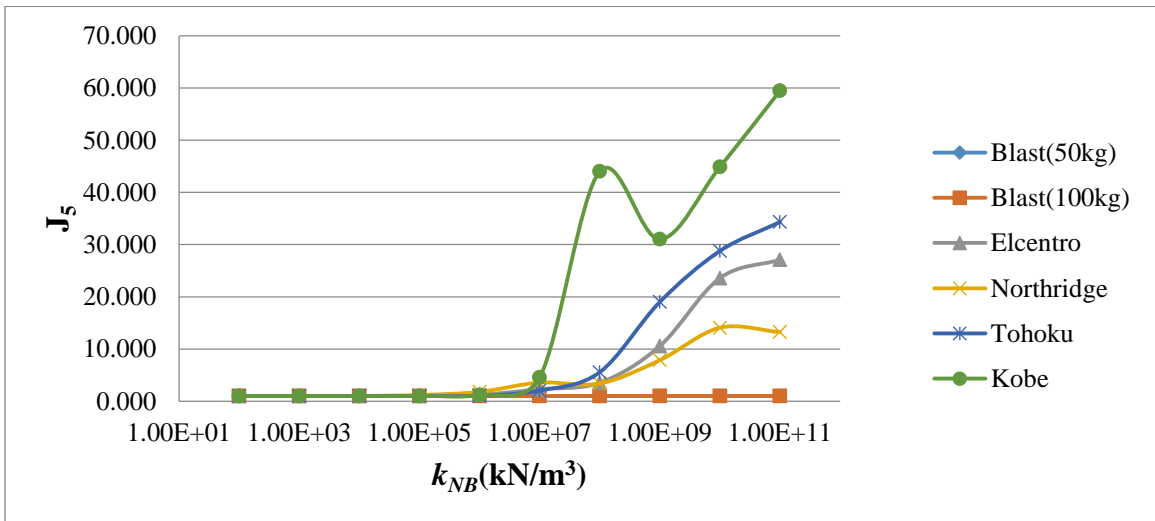


**Figure 6.19 Performance of IS-NB on  $J_5$  with varying stiffness**

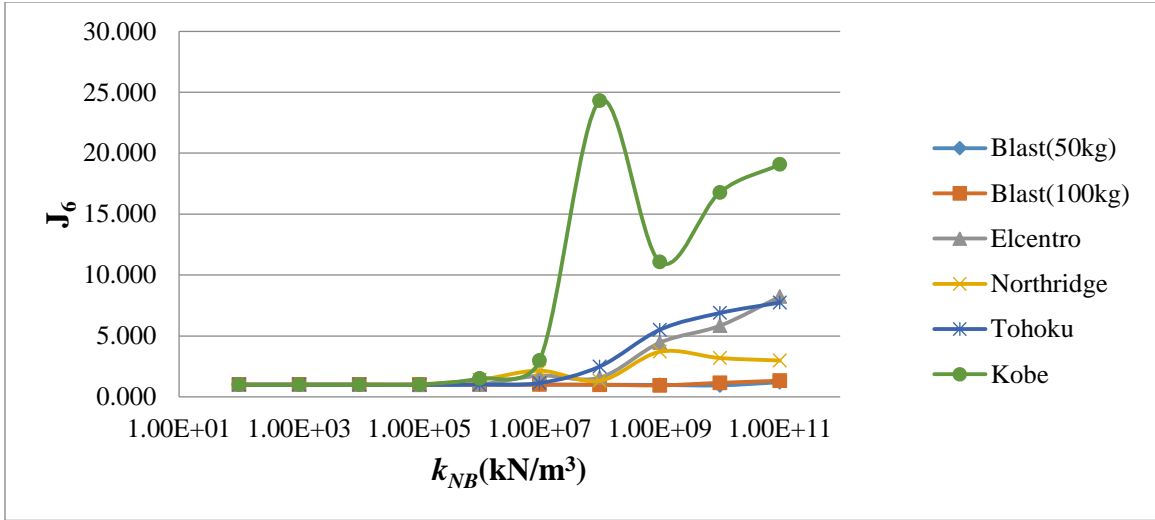


Figure 6.20 Performance of IS-NB on  $J_6$  with varying stiffness

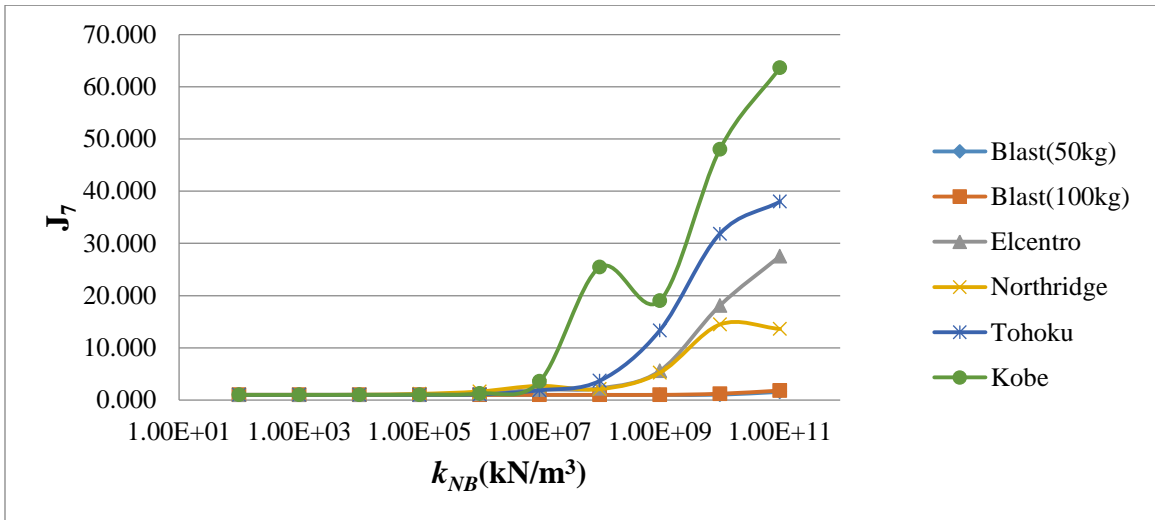


Figure 6.21 Performance of IS-NB on  $J_7$  with varying stiffness

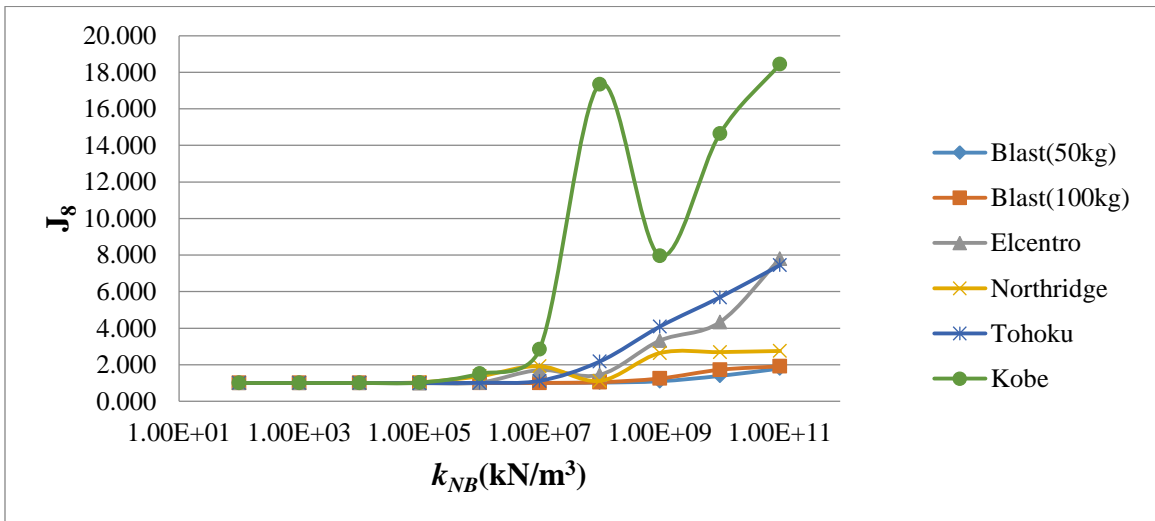


Figure 6.22 Performance of IS-NB on  $J_8$  with varying stiffness

Through Figure 6.15 to Figure 6.22, it is observed that increasing the stiffness of the nonlinear bumper,  $k_{NB}$ , has a general effect of reducing the peak base drift ( $J_1, J_2$ ) under multiple excitations. This reduction comes with amplification on the peak drift of superstructure, absolute acceleration of superstructure, and base absolute acceleration. The amplification is also affected by the frequency content and magnitude of the excitations. Generally, the excitations resulting in an amplification on the peak interstory drift and absolute acceleration, from large to small, are Kobe earthquake, Tohoku earthquake, El Centro earthquake, Northridge earthquake, and blast loadings. The nonlinear bumpers make an excellent improvement in base isolated systems particularly under blast excitations. To maintain good performance of the base isolation under both blast and seismic excitations considering all criteria, a stiffness of  $k_{NB} = 10^7$  kN/m<sup>3</sup> is selected.

With the selected parameters for the IS-CN and IS-NB devices, results across all devices are compared under multiple excitations in Table 6.3. Note that these are the non-normalized performance evaluation criteria.



**Table 6.3 Responses of multiple control systems under blast and earthquakes**

External Excitations	Blast (50 kg)	Blast (100 kg)	El Centro	Kobe	Northridge	Tohoku
Peak Base Displacement (m)						
Orig_sys	NA	NA	NA	NA	NA	NA
IS-linear	0.1653	0.1852	0.2034	0.2795	0.7197	0.2920
IS-TB (1% M)	0.1646	0.1846	0.1913	0.2710	0.6896	0.3055
IS-TB (6% M)	0.1612	0.1819	0.1893	0.2653	0.5550	0.3052
IS-CN (1% M)	0.1651	0.1850	0.2002	0.2721	0.6933	0.2875
IS-CN (6% M)	0.1641	0.1840	0.1954	0.2687	0.6836	0.2809
IS-NB	0.1369	0.1593	0.1810	0.2758	0.3563	0.2151
IS-NB + TMD (1%M)	0.1366	0.1592	0.1783	0.2680	0.3509	0.2014
IS-NB +TMD (6%M)	0.1351	0.1584	0.1642	0.2072	0.3206	0.2085
IS-NB + CN (1%M)	0.1368	0.1568	0.1799	0.2742	0.3515	0.1977
IS-NB + CN (6%M)	0.1362	0.1552	0.1796	0.2701	0.3393	0.2036
RMS Base Displacement (m)						
Orig_sys	NA	NA	NA	NA	NA	NA
IS-linear	0.0591	0.0627	0.0594	0.0584	0.1986	0.0656
IS-TB (1% M)	0.0510	0.0540	0.0552	0.0595	0.1642	0.0618
IS-TB (6% M)	0.0400	0.0421	0.0511	0.0675	0.1170	0.0587
IS-CN (1% M)	0.0584	0.0619	0.0583	0.0590	0.1923	0.0648
IS-CN (6% M)	0.0556	0.0589	0.0565	0.0573	0.1397	0.0612
IS-NB	0.0510	0.0544	0.0605	0.0766	0.1090	0.0504
IS-NB + TMD (1%M)	0.0447	0.0481	0.0565	0.0724	0.0965	0.0483
IS-NB +TMD (6%M)	0.0332	0.0358	0.0464	0.0473	0.0844	0.0438
IS-NB + CN (1%M)	0.0504	0.0544	0.0602	0.0765	0.0962	0.0500
IS-NB + CN (6%M)	0.0480	0.0535	0.0594	0.0732	0.0934	0.0491
Maximum Superstructure Interstory Drift (m)						
Orig_sys	0.0451	0.0778	0.0049	0.0122	0.0152	0.0164
IS-linear	0.0287	0.0467	0.0011	0.0016	0.0040	0.0017
IS-TB (1% M)	0.0287	0.0467	0.0011	0.0015	0.0039	0.0017
IS-TB (6% M)	0.0288	0.0467	0.0010	0.0014	0.0031	0.0016
IS-CN (1% M)	0.0287	0.0467	0.0011	0.0016	0.0037	0.0016
IS-CN (6% M)	0.0287	0.0467	0.0011	0.0015	0.0039	0.0016
IS-NB	0.0287	0.0467	0.0025	0.0068	0.0134	0.0037
IS-NB + TMD (1%M)	0.0287	0.0467	0.0024	0.0064	0.0129	0.0031
IS-NB +TMD	0.0288	0.0468	0.0021	0.0035	0.0101	0.0035

(6%M)							
IS-NB + CN	0.0287	0.0468	0.0024	0.0068	0.0129	0.0030	
(1%M)							
IS-NB + CN	0.0287	0.0469	0.0024	0.0065	0.0118	0.0032	
(6%M)							
	Maximum RMS Superstructure Interstory Drift (m)						
Orig_sys	0.0031	0.0055	0.0012	0.0021	0.0026	0.0021	
IS-linear	0.0017	0.0027	0.0003	0.0003	0.0011	0.0004	
IS-TB (1% M)	0.0017	0.0027	0.0003	0.0003	0.0009	0.0003	
IS-TB (6% M)	0.0017	0.0027	0.0003	0.0003	0.0006	0.0003	
IS-CN (1% M)	0.0017	0.0027	0.0003	0.0003	0.0011	0.0004	
IS-CN (6% M)	0.0017	0.0027	0.0003	0.0003	0.0008	0.0003	
IS-NB	0.0017	0.0027	0.0006	0.0010	0.0023	0.0004	
IS-NB + TMD	0.0017	0.0027	0.0006	0.0009	0.0021	0.0004	
(1%M)							
IS-NB +TMD	0.0017	0.0027	0.0004	0.0005	0.0015	0.0003	
(6%M)							
IS-NB + CN	0.0017	0.0027	0.0006	0.0010	0.0021	0.0004	
(1%M)							
IS-NB + CN	0.0017	0.0027	0.0006	0.0009	0.0018	0.0004	
(6%M)							
	Maximum Superstructure Absolute Acceleration (m/s <sup>2</sup> )						
Orig_sys	299.1326	520.6877	8.1141	19.2747	23.5102	27.8347	
IS-linear	300.6216	522.9111	1.3153	1.8897	4.6750	2.3688	
IS-TB (1% M)	300.6215	522.9110	1.2488	1.7994	4.4634	2.3017	
IS-TB (6% M)	300.6213	522.9105	1.2411	1.6089	3.5249	1.9798	
IS-CN (1% M)	300.6215	522.9110	1.3017	1.8414	4.3705	2.2382	
IS-CN (6% M)	300.6213	522.9105	1.2600	1.8251	4.4901	2.2480	
IS-NB	300.6216	522.9110	3.0272	8.6419	16.7443	4.8543	
IS-NB + TMD	300.6215	522.9110	2.9348	8.0319	16.0844	3.9484	
(1%M)							
IS-NB +TMD	300.6213	522.9105	2.5247	4.2293	12.9225	4.2346	
(6%M)							
IS-NB + CN	300.6215	522.9110	3.0040	8.5265	16.1468	3.7446	
(1%M)							
IS-NB + CN	300.6213	522.9105	2.9277	8.1775	14.8712	3.9707	
(6%M)							
	Maximum RMS Superstructure Absolute Acceleration (m/s <sup>2</sup> )						
Orig_sys	11.5684	19.5206	1.8982	3.2046	4.1978	3.5831	
IS-linear	8.6850	13.9933	0.3841	0.3791	1.2830	0.4282	
IS-TB (1% M)	8.6822	13.9907	0.3553	0.3833	1.0506	0.3981	
IS-TB (6% M)	8.6764	13.9835	0.3185	0.4032	0.7063	0.3491	
IS-CN (1% M)	8.6843	13.9923	0.3777	0.3874	1.2174	0.4193	
IS-CN (6% M)	8.6808	13.9875	0.3651	0.3717	0.9349	0.3982	
IS-NB	8.6870	13.9893	0.6686	1.1336	2.7612	0.4882	
IS-NB + TMD	8.6841	13.9866	0.6412	1.0394	2.4885	0.4606	

(1%M)							
IS-NB +TMD	8.6773	13.9782	0.5127	0.6001	1.799	0.4032	
(6%M)							
IS-NB + CN	8.6863	13.8224	0.6658	1.1198	2.4661	0.4794	
(1%M)							
IS-NB + CN	8.6824	13.8811	0.6593	1.0441	2.2055	0.4651	
(6%M)							
Maximum Base Absolute Acceleration (m/s <sup>2</sup> )							
Orig_sys	NA	NA	NA	NA	NA	NA	NA
IS-linear	152.7872	265.5552	1.2936	1.7653	4.5494	2.1399	
IS-TB (1% M)	152.7662	265.5216	1.2339	1.6773	4.3501	2.0627	
IS-TB (6% M)	152.6612	265.3536	1.1460	1.5214	3.4629	1.8507	
IS-CN (1% M)	152.7670	265.5227	1.2839	1.7328	4.2893	2.0082	
IS-CN (6% M)	152.6659	265.3605	1.2419	1.7045	4.4008	2.0213	
IS-NB	152.7872	265.5551	2.5976	6.3102	12.4065	3.9959	
IS-NB + TMD	152.7662	265.5215	2.5901	5.9060	12.0282	3.5795	
(1%M)							
IS-NB +TMD	152.6612	265.3535	2.3003	3.7732	9.1725	3.8578	
(6%M)							
IS-NB + CN	152.7670	265.5219	2.5779	6.2319	12.0472	3.4405	
(1%M)							
IS-NB + CN	152.6659	265.3597	2.6079	5.9978	11.1780	3.6346	
(6%M)							
RMS Base Absolute Acceleration (m/s <sup>2</sup> )							
Orig_sys	NA	NA	NA	NA	NA	NA	NA
IS-linear	5.2118	8.7170	0.3756	0.3683	1.2570	0.4192	
IS-TB (1% M)	5.2068	8.7122	0.3472	0.3726	1.0290	0.3897	
IS-TB (6% M)	5.1954	8.6972	0.3110	0.3926	0.6907	0.3417	
IS-CN (1% M)	5.2098	8.7140	0.3693	0.3739	1.1931	0.4105	
IS-CN (6% M)	5.2001	8.6989	0.3570	0.3611	0.9138	0.3896	
IS-NB	5.2290	8.7707	0.6413	1.0492	2.4101	0.4692	
IS-NB + TMD	5.2240	8.7658	0.6146	0.9647	2.1735	0.4431	
(1%M)							
IS-NB +TMD	5.2109	8.7489	0.4919	0.5626	1.6135	0.3870	
(6%M)							
IS-NB + CN	5.2264	9.0610	0.6386	1.0378	2.1544	0.4612	
(1%M)							
IS-NB + CN	5.2166	8.9622	0.6322	0.9682	1.9463	0.4475	
(6%M)							

## **Observed improvement through base isolation and supplemental devices**

In the following discussion, the reference system is the base-isolated system. The base displacement can be reduced by installing extra devices on the base isolated system so that the isolation bearings are kept in safer mode. However, for other criteria such as the superstructure interstory drift and the absolute acceleration, slight improvements or even amplifications are obtained. This tradeoff must be considered when designing the structural control system. Based on the responses shown in Table 6.3, the cubic NES cannot make significant improvement in base displacement compared to the reference system even with a larger mass. Better performance can be achieved by additional installation of the TMD, especially under Northridge earthquake with a 23% reduction. The nonlinear bumper performs best in the reduction of the base drift under all excitations, but concurrently leads to amplifications on the interstory drift and the absolute acceleration of the structure. There exists a trade-off between the base displacement and the other criteria as shown in Figure 6.15 to Figure 6.22. However, even with an amplification compared to the base isolated system, the interstory drift and structural accelerations are still below the responses of the fixed base system, as shown in Table 6.4. Although the amplification on the base absolute acceleration is unavoidable, it is still in an acceptable range. Figure 6.23 shows the distribution of peak interstory drifts and accelerations at various floor levels under Northridge earthquake. It is observed that the peak base displacement is reduced by the supplemental devices and the interstory drifts and accelerations are maintained at low levels. Figure 6.24 shows the performance of the extra devices on base displacement. From the time history of each device, we can conclude that the nonlinear bumper demonstrates good performance in reducing the peak

base drift and the TMD has a better overall performance along the time. The RMS base drifts in Table 6.3 also verify this phenomenon. Therefore, the combination of the nonlinear bumper and the TMD is studied and overall better performance is obtained. The extra reductions by the additional devices on base displacement and under multiple excitations are shown in Table 6.4. Almost 20% reduction can be achieved by the combination of nonlinear bumper and TMD under explosions. The reductions by some extra devices are listed in Table 6.4. The mass of TMD used to compare with other devices is 6% total mass of the structure.

**Table 6.4 Reductions on different criteria**

External Excitations	Blast (50 kg)	Blast (100 kg)	El Centro	Kobe	Northridge	Tohoku
Reduction on Peak Base Displacement <sup>a</sup> (%)						
IS-TB (6% M)	2.5	1.8	6.9	5.1	22.9	-4.5
IS-CN (6% M)	0.7	0.6	3.9	3.9	5.0	3.8
IS-NB	17.2	14.0	11.0	1.3	50.5	26.3
IS-NB +TMD (6%M)	18.3	14.5	19.3	25.9	55.5	28.6
Reduction on RMS Base Displacement <sup>a</sup> (%)						
IS-TB (6% M)	32.3	32.9	14.0	-15.6	41.1	10.5
IS-CN (6% M)	5.9	6.1	4.9	1.9	29.7	6.7
IS-NB	13.7	13.2	-1.9	-31.2	45.1	23.2
IS-NB +TMD (6%M)	43.8	42.9	21.9	19.0	57.5	33.2
Reduction on Maximum Superstructure Interstory Drift <sup>b</sup> (%)						
IS-linear	36.4	40.0	77.6	86.9	73.7	89.6
IS-TB (6% M)	36.1	40.0	79.6	88.5	79.6	90.2
IS-CN (6% M)	36.4	40.0	77.6	87.7	74.3	90.2
IS-NB	36.4	40.0	49.0	44.3	11.8	77.4
IS-NB +TMD (6%M)	36.1	39.8	57.1	71.3	33.6	78.7
Reduction on Maximum RMS Superstructure Interstory Drift <sup>b</sup> (%)						
IS-linear	45.2	50.9	75.0	85.7	57.7	81.0
IS-TB (6% M)	45.2	50.9	75.0	85.7	76.9	85.7
IS-CN (6% M)	45.2	50.9	75.0	85.7	69.2	85.7
IS-NB	45.2	50.9	50.0	52.4	11.5	81.0
IS-NB +TMD (6%M)	45.2	50.9	66.7	76.2	42.3	85.7

Reduction on Maximum Superstructure Absolute Acceleration <sup>b</sup> (%)						
IS-linear	-0.5	-0.4	83.8	90.2	80.1	91.5
IS-TB (6% M)	-0.5	-0.4	84.7	91.7	85.0	92.9
IS-CN (6% M)	-0.5	-0.4	84.5	90.5	80.9	91.9
IS-NB	-0.5	-0.4	62.7	55.2	28.8	82.6
IS-NB +TMD (6%M)	-0.5	-0.4	68.9	78.1	45.0	84.8
Reduction on Maximum RMS Superstructure Absolute Acceleration <sup>b</sup> (%)						
IS-linear	24.9	28.3	79.8	88.2	69.4	88.0
IS-TB (6% M)	25.0	28.4	83.2	87.4	83.2	90.3
IS-CN (6% M)	25.0	28.3	80.8	88.4	77.7	88.9
IS-NB	24.9	28.3	64.8	64.6	34.2	86.4
IS-NB +TMD (6%M)	25.0	28.4	73.0	81.3	57.1	88.7

<sup>a</sup>The reference system is the base isolated system.

<sup>b</sup>The reference system is the fixed base system.

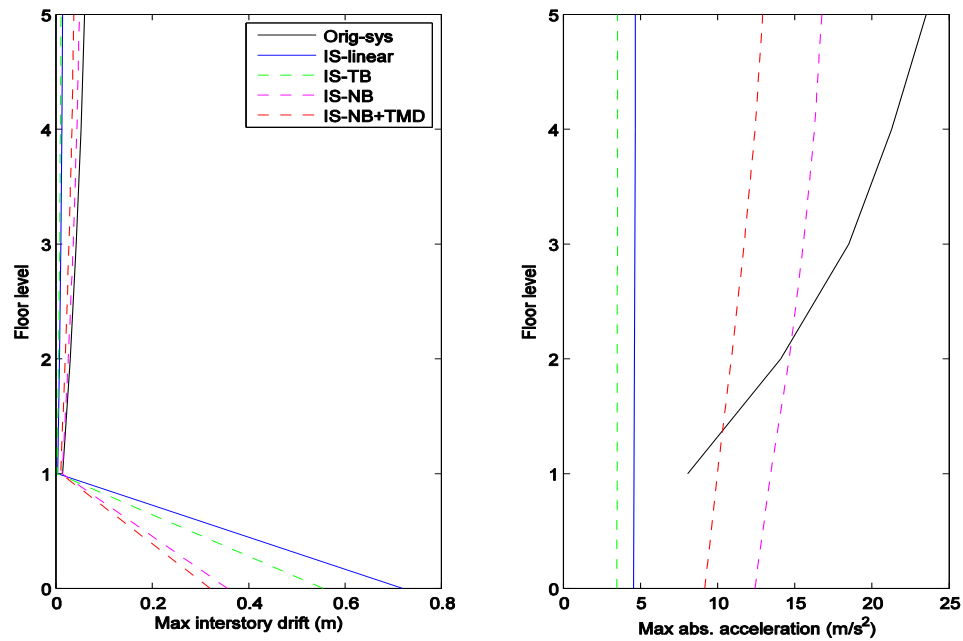


**Figure 6.23 Distribution of peak interstory drifts and absolute accelerations at various floor levels under Northridge**

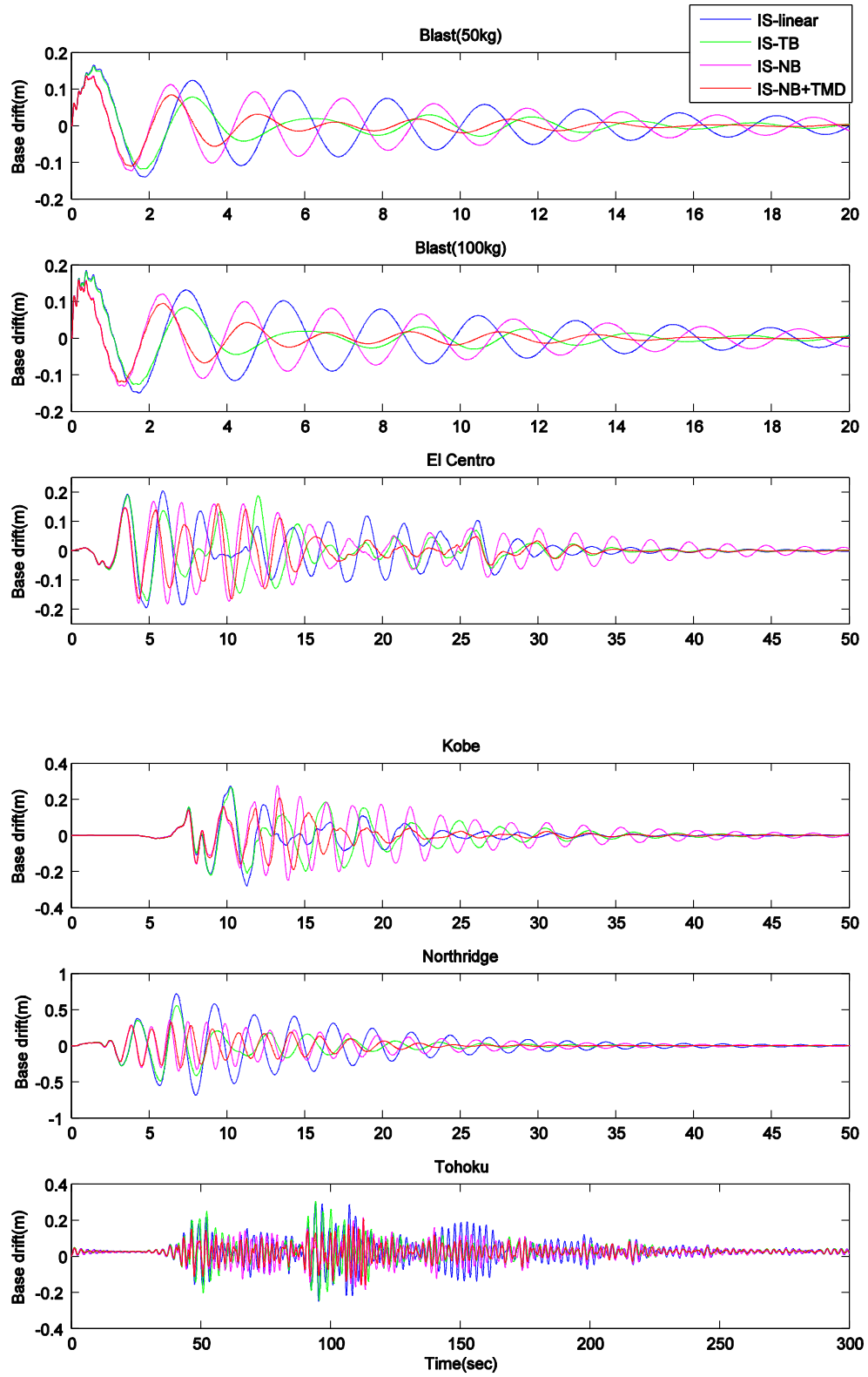


Figure 6.24 Time history of base displacement under multiple excitations



### 6.3 Performance of Multiple Control Systems for the 8-story Structure

In this section, the performance of the control devices on the 8-story structure is investigated. Based on the performance of each device on the simple 5-story structure in the previous section, only the supplemental devices showing significant promise are studied, including IS-NB, and IS-NB + TMD. All control devices are installed in both directions and the parameters are assumed to be same in both directions. The explosion of 2000 kg of TNT introduced in Chapter 4 is used as the excitation input to the structure.

First, a sensitivity analysis of the parameter for the IS-NB device is performed. The processes of parameter tuning in  $x$  and  $y$  direction are shown in Figure 6.25 to Figure 6.32 and Figure 6.33 to Figure 6.40, respectively. All criteria are normalized to the base-isolated system.

From Figure 6.25 to Figure 6.32, it is observed that increasing the stiffness of the nonlinear bumper has a general effect of reducing the peak base displacement under multiple excitations. Although the reduction of the base drift in  $x$  direction is slight under blast loading, the device still performs well in  $y$  direction where the maximum base drift occurs as shown through Figure 6.33 to Figure 6.40. There are also little jumps observed for the base drift under earthquakes across stiffness values. The main cause of this phenomenon is likely the increased stiffness leading to a larger transfer of energy, which is both frequency and amplitude dependent for the nonlinear device. An amplification on the maximum superstructure interstory drift, absolute acceleration, and base absolute acceleration is also seen when a high stiffness is used, similar to the 5-story structure.

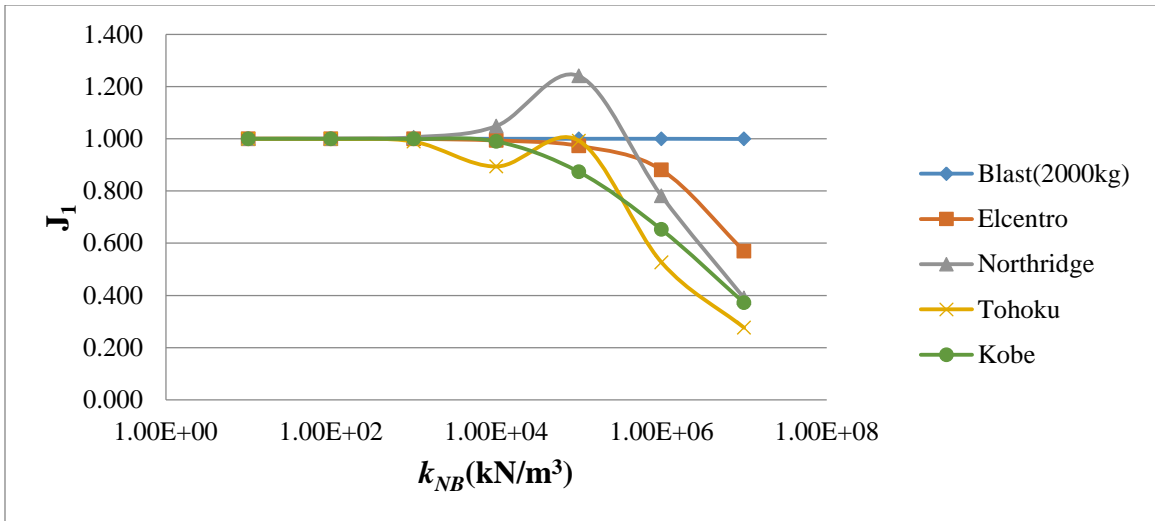


**Figure 6.25 Performance of IS-NB on  $J_1$  with varying stiffness in  $x-d$**

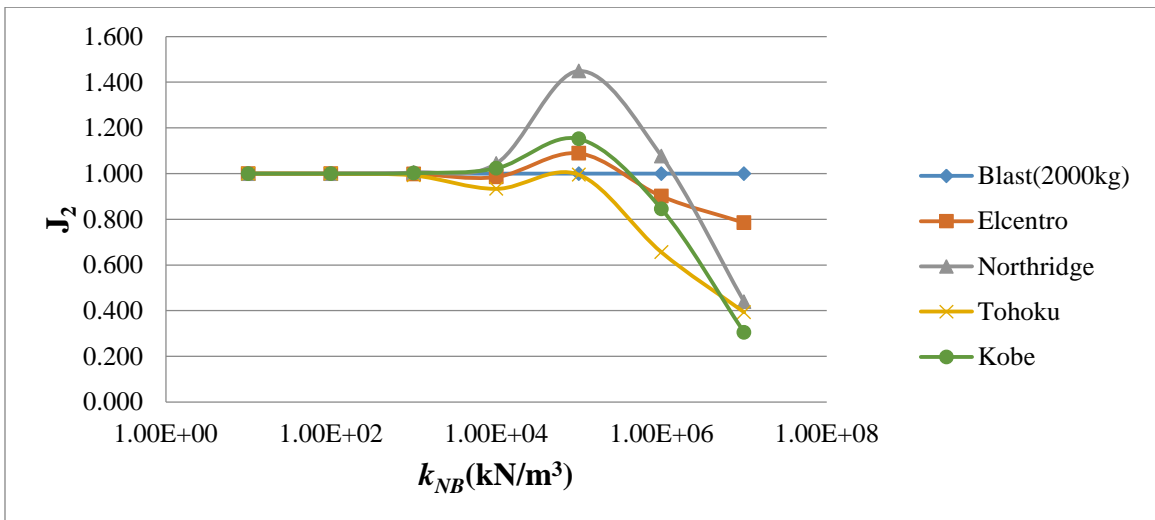


**Figure 6.26 Performance of IS-NB on  $J_2$  with varying stiffness in  $x-d$**

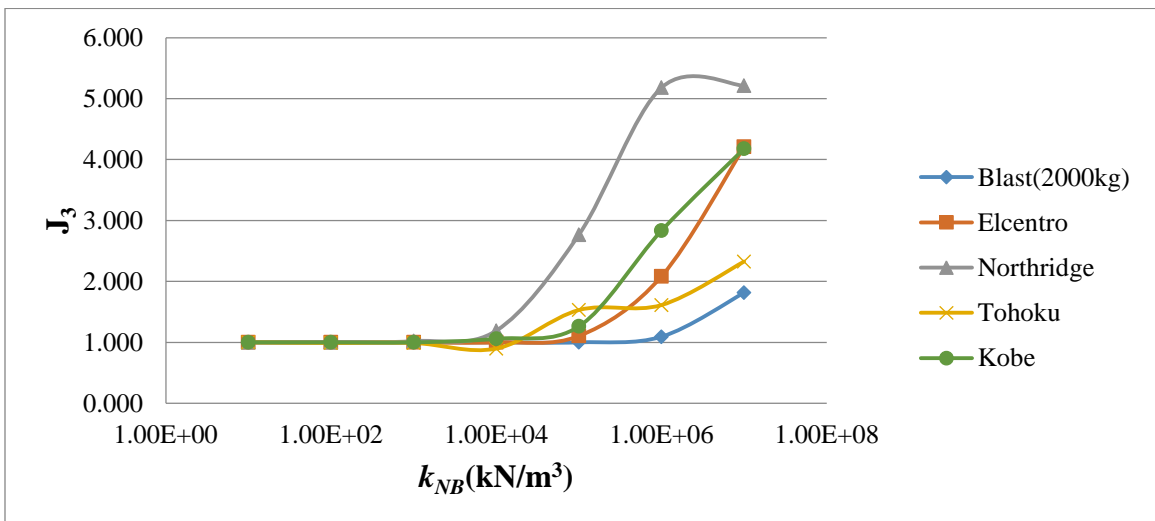


**Figure 6.27 Performance of IS-NB on  $J_3$  with varying stiffness in  $x-d$**

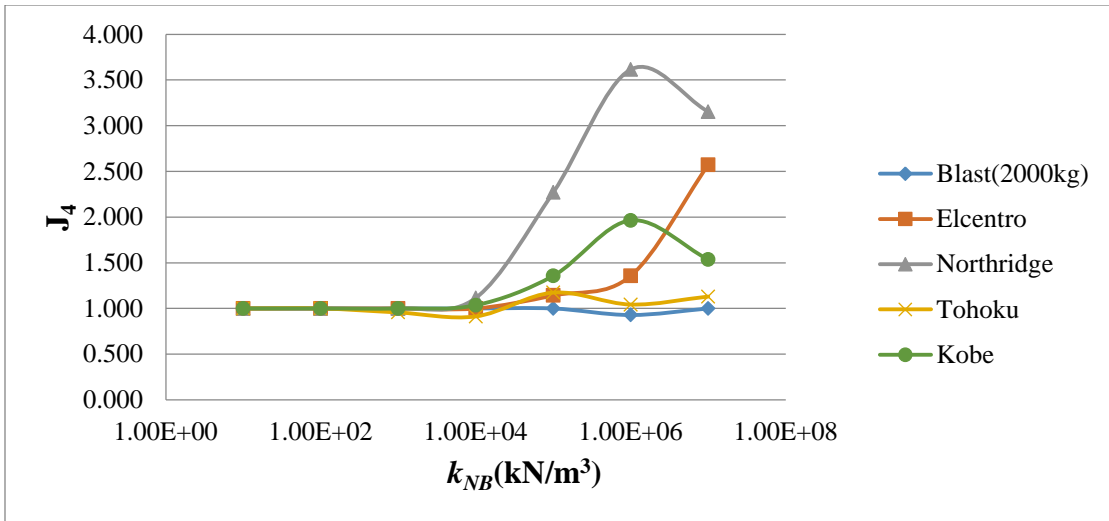


**Figure 6.28 Performance of IS-NB on  $J_4$  with varying stiffness in  $x-d$**

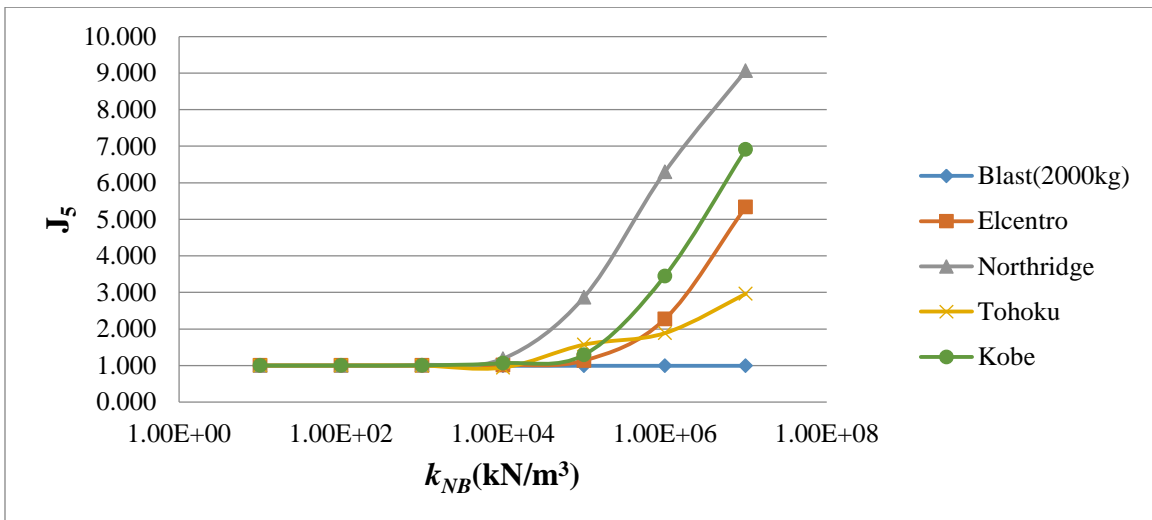


**Figure 6.29 Performance of IS-NB on  $J_5$  with varying stiffness in  $x-d$**

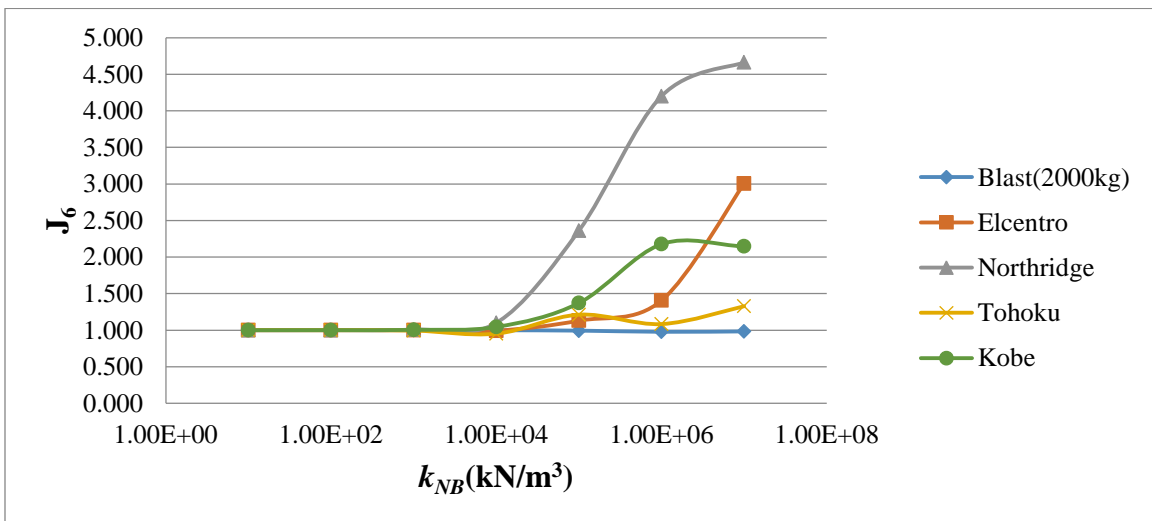


**Figure 6.30 Performance of IS-NB on  $J_6$  with varying stiffness in  $x-d$**

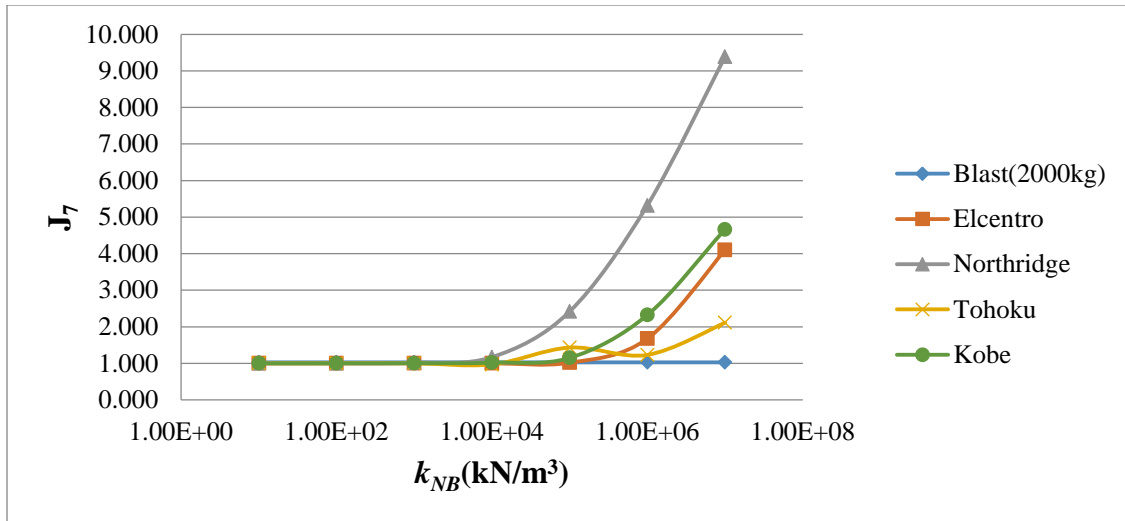


**Figure 6.31 Performance of IS-NB on  $J_7$  with varying stiffness in  $x-d$**

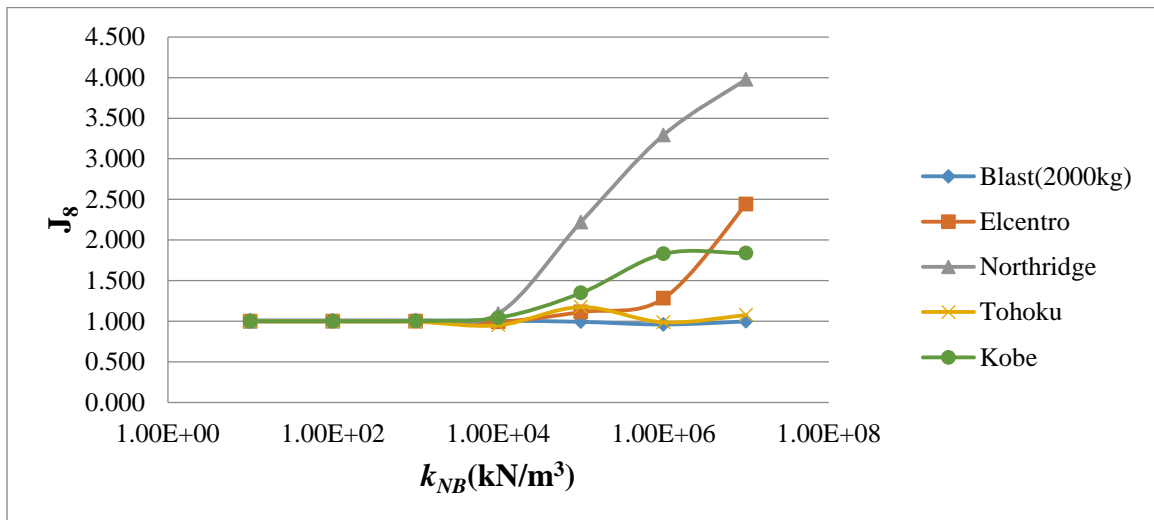


**Figure 6.32 Performance of IS-NB on  $J_8$  with varying stiffness in  $x-d$**

The performance of the IS-NB in  $y$  direction under multiple excitations is shown in Figure 6.33 to Figure 6.40. Same conclusion can be obtained for the parameter study of IS-NB in  $x$  direction. The nonlinear bumpers make an excellent improvement in base isolated systems, particularly under explosions. Based on the performance of IS-NB in both directions under multiple excitations, a stiffness of  $k_{NB} = 10^7$  kN/m<sup>3</sup> is selected. The

responses of the nonlinear bumpers in both directions are shown in Table 6.5 and Table 6.6.

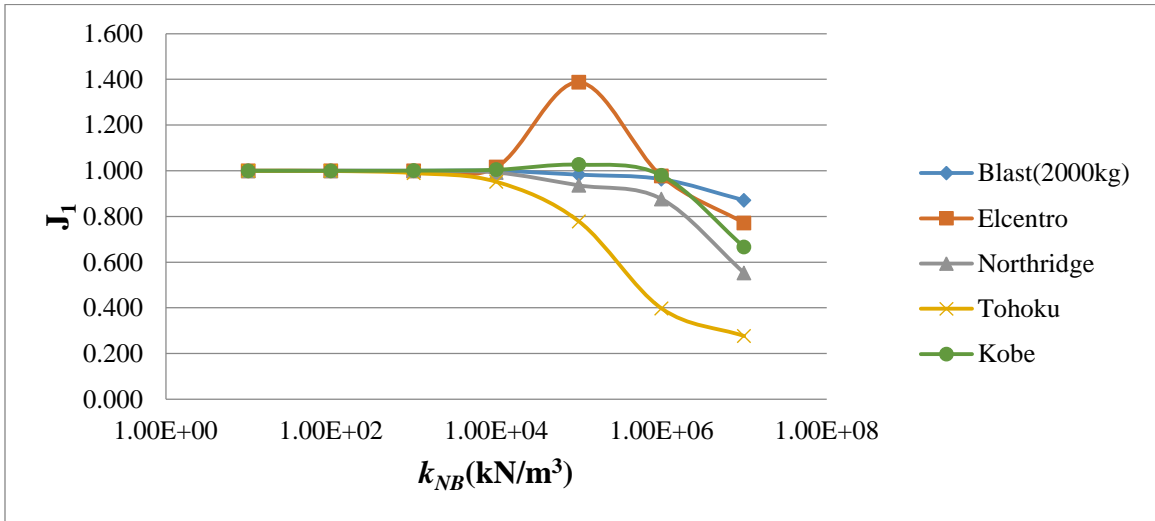


Figure 6.33 Performance of IS-NB on  $J_1$  with varying stiffness in  $y-d$

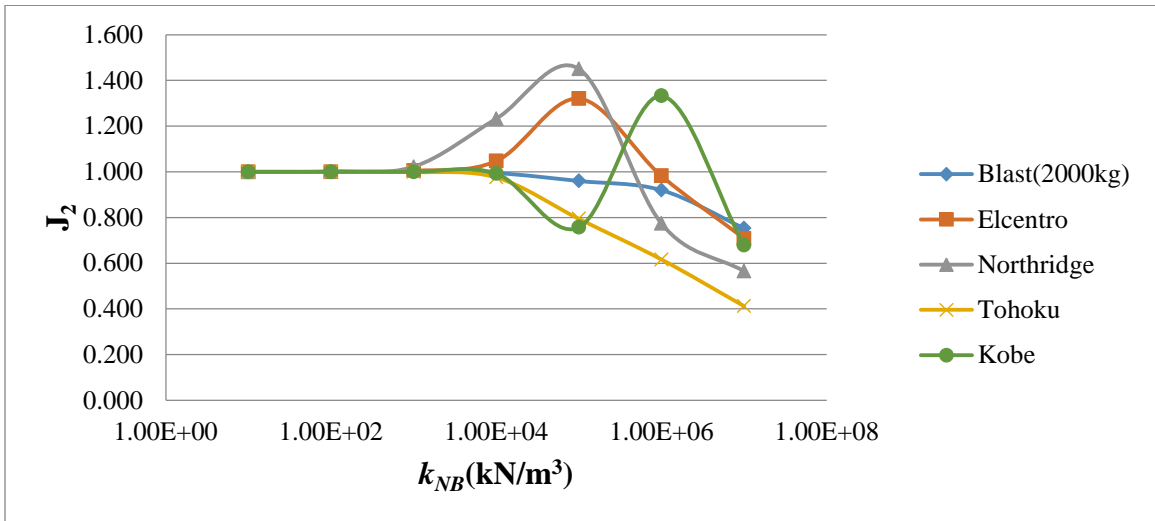
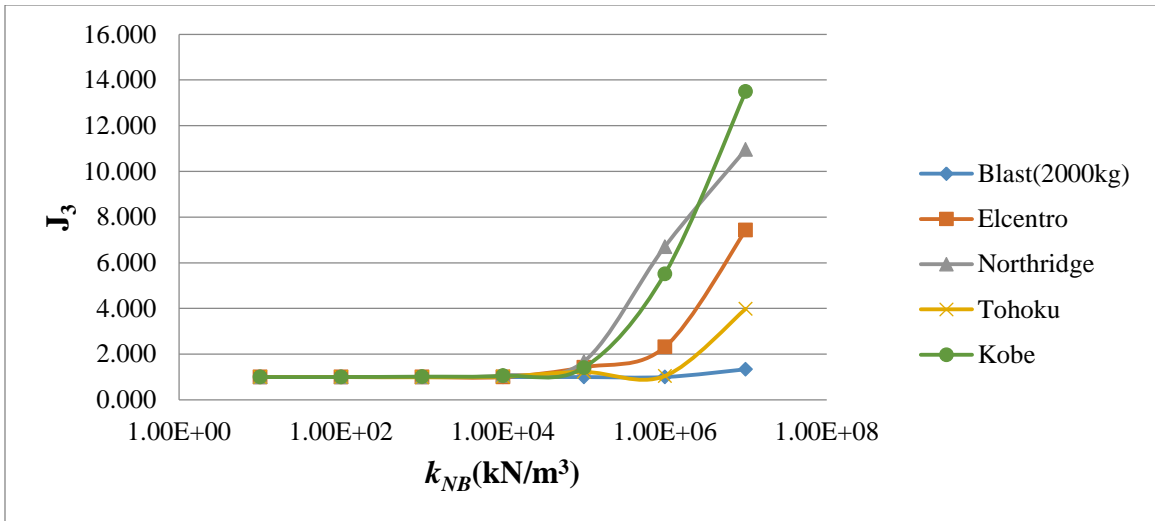
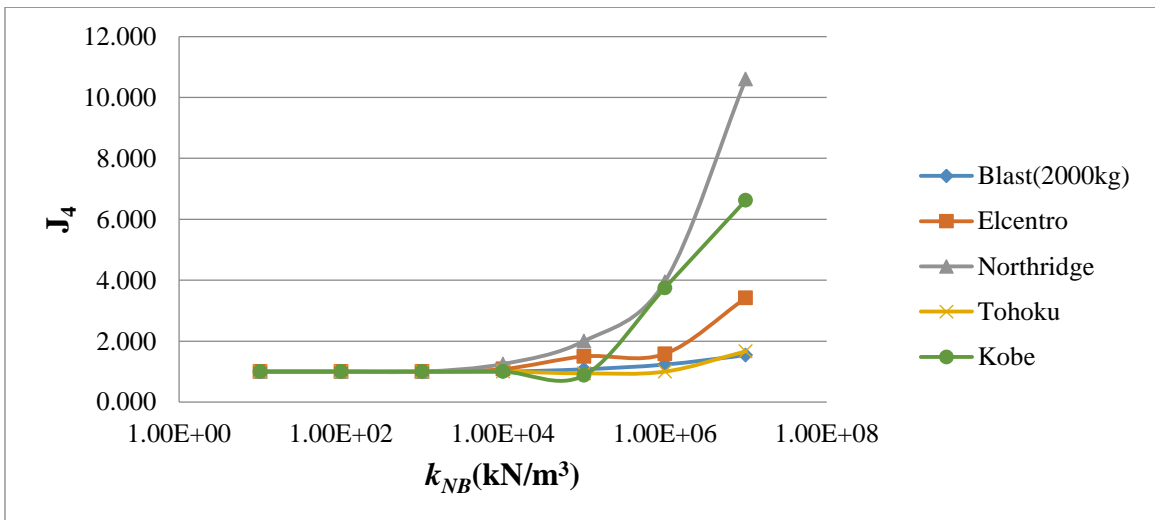


Figure 6.34 Performance of IS-NB on  $J_2$  with varying stiffness in  $y-d$



**Figure 6.35 Performance of IS-NB on  $J_3$  with varying stiffness in  $y-d$**



**Figure 6.36 Performance of IS-NB on  $J_4$  with varying stiffness in  $y-d$**

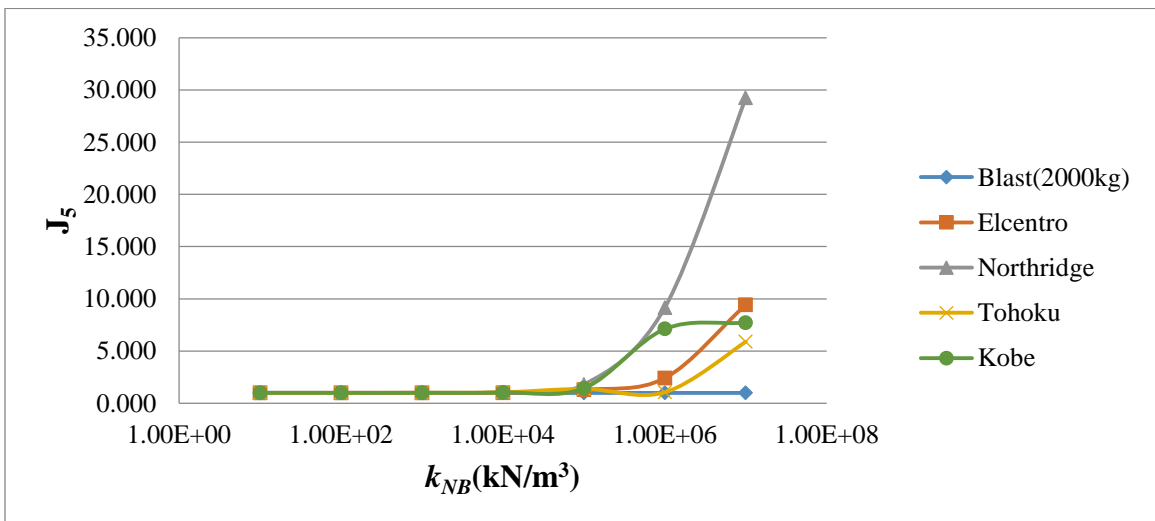


**Figure 6.37 Performance of IS-NB on  $J_5$  with varying stiffness in  $y-d$**

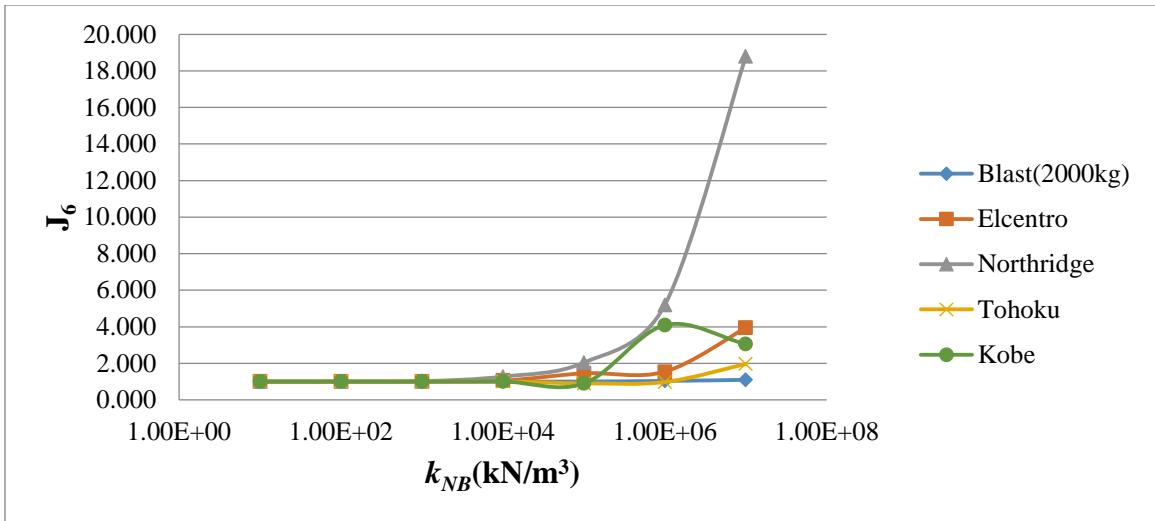


Figure 6.38 Performance of IS-NB on  $J_6$  with varying stiffness in  $y-d$

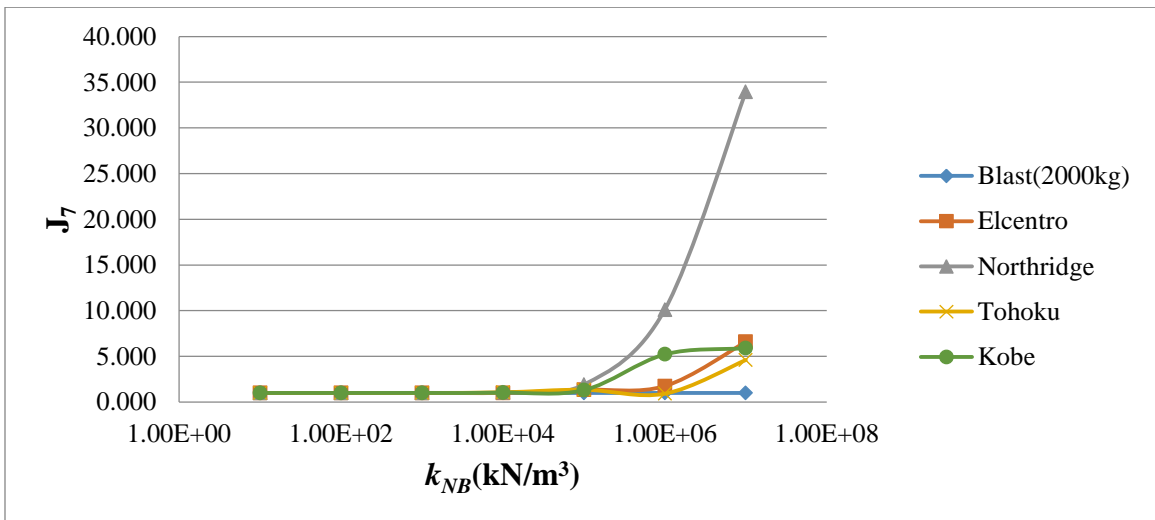


Figure 6.39 Performance of IS-NB on  $J_7$  with varying stiffness in  $y-d$

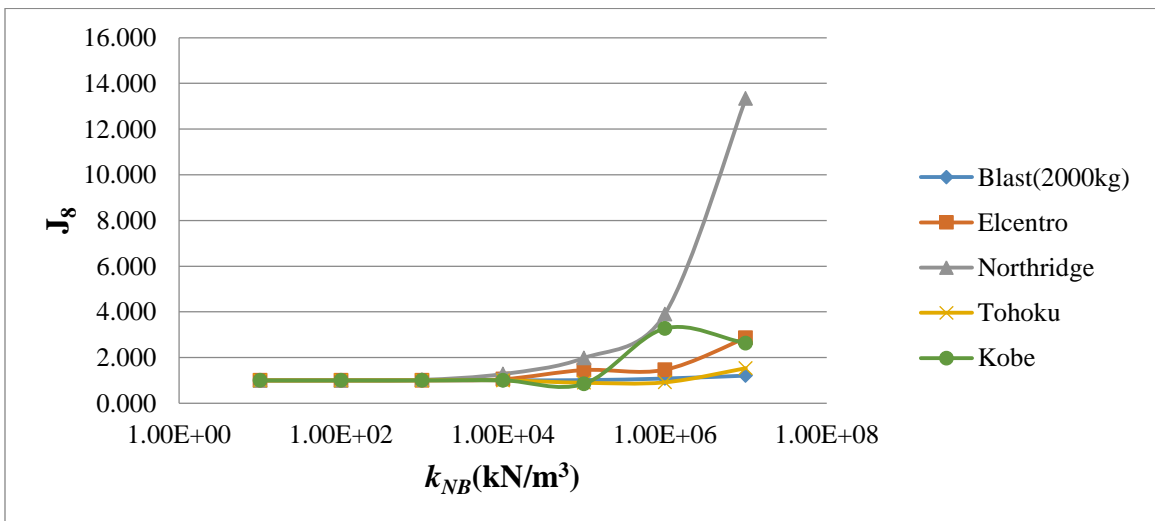


Figure 6.40 Performance of IS-NB on  $J_8$  with varying stiffness in  $y-d$

**Table 6.5 Responses of multiple control systems under blast and earthquakes in  $x-d$** 

External Excitations	Blast (2000 kg)	El Centro	Kobe	Northridge	Tohoku
Peak Base Displacement (m)					
Orig_sys	NA	NA	NA	NA	NA
IS-linear	0.1354	0.2387	0.4587	0.4943	0.5103
IS-NB	0.1353	0.1360	0.1704	0.1927	0.1410
IS-NB + TMD (1%M)	0.0606	0.1352	0.1696	0.1921	0.1412
RMS Base Displacement (m)					
Orig_sys	NA	NA	NA	NA	NA
IS-linear	0.0689	0.0735	0.1523	0.1483	0.1228
IS-NB	0.0346	0.0577	0.0465	0.0651	0.0483
IS-NB + TMD (1%M)	0.0171	0.0565	0.0430	0.0596	0.0487
Maximum Superstructure Interstory Drift (m)					
Orig_sys	0.0120	0.0165	0.0803	0.0436	0.0309
IS-linear	0.0054	0.0048	0.0084	0.0094	0.0098
IS-NB	0.0098	0.0202	0.0351	0.0490	0.0228
IS-NB + TMD (1%M)	0.0114	0.0200	0.0345	0.0488	0.0230
Maximum RMS Superstructure Interstory Drift (m)					
Orig_sys	0.0017	0.0033	0.0129	0.0065	0.0032
IS-linear	0.0014	0.0014	0.0028	0.0026	0.0023
IS-NB	0.0014	0.0036	0.0043	0.0082	0.0026
IS-NB + TMD (1%M)	0.0018	0.0035	0.0040	0.0064	0.0026
Maximum Superstructure Absolute Acceleration ( $m/s^2$ )					
Orig_sys	46.9533	6.1399	26.0664	15.0007	22.0395
IS-linear	47.3927	1.1960	2.056	2.3103	2.5232
IS-NB	47.0207	6.3861	14.2112	20.9382	7.4787
IS-NB + TMD (1%M)	47.1740	6.2774	13.9841	20.7729	7.5096
Maximum RMS Superstructure Absolute Acceleration ( $m/s^2$ )					
Orig_sys	0.9707	1.1158	3.7558	2.1331	1.7046
IS-linear	0.7712	0.3359	0.6713	0.6023	0.5322
IS-NB	0.7581	1.0095	1.4408	2.8079	0.7066
IS-NB + TMD (1%M)	0.8080	0.9972	1.3205	2.1447	0.7013
Maximum Base Absolute Acceleration ( $m/s^2$ )					
Orig_sys	NA	NA	NA	NA	NA
IS-linear	17.4498	1.0225	1.8655	1.7233	2.1674
IS-NB	17.9200	4.1935	8.7025	16.1802	4.5759
IS-NB + TMD (1%M)	17.3793	4.1547	8.5885	16.0500	4.6856



RMS Base Absolute Acceleration (m/s <sup>2</sup> )					
Orig_sys	NA	NA	NA	NA	NA
IS-linear	0.5029	0.2954	0.5912	0.5302	0.4809
IS-NB	0.5021	0.7213	1.0874	2.1081	0.5182
IS-NB + TMD (1%M)	0.5952	0.7095	0.9490	1.6236	0.5167

**Table 6.6 Responses of multiple control systems under blast and earthquakes in *y-d***

External Excitations	Blast (2000 kg)	El Centro	Kobe	Northridge	Tohoku
Peak Base Displacement (m)					
Orig_sys	NA	NA	NA	NA	NA
IS-linear	0.1804	0.2040	0.3632	0.5648	0.6166
IS-NB	0.1571	0.1574	0.2420	0.3123	0.1706
IS-NB + TMD (1%M)	0.0965	0.1566	0.2416	0.3120	0.1699
RMS Base Displacement (m)					
Orig_sys	NA	NA	NA	NA	NA
IS-linear	0.0898	0.0900	0.1060	0.1500	0.1303
IS-NB	0.0676	0.0630	0.0719	0.0833	0.0537
IS-NB + TMD (1%M)	0.0457	0.0614	0.0642	0.0643	0.0513
Maximum Superstructure Interstory Drift (m)					
Orig_sys	0.0129	0.0220	0.0743	0.0810	0.0483
IS-linear	0.0053	0.0035	0.0058	0.0103	0.0090
IS-NB	0.0071	0.0260	0.0783	0.1129	0.0359
IS-NB + TMD (1%M)	0.0095	0.0257	0.0780	0.1125	0.0357
Maximum RMS Superstructure Interstory Drift (m)					
Orig_sys	0.0016	0.0040	0.0120	0.0130	0.0030
IS-linear	0.0013	0.0010	0.0020	0.0020	0.0018
IS-NB	0.0020	0.0041	0.0106	0.0212	0.0030
IS-NB + TMD (1%M)	0.0020	0.0040	0.0095	0.0142	0.0028
Maximum Superstructure Absolute Acceleration (m/s <sup>2</sup> )					
Orig_sys	32.2698	9.0039	26.2168	29.4430	48.1093
IS-linear	32.3496	1.1313	1.8409	3.2150	2.7462
IS-NB	32.1032	10.674	14.2112	94.0013	16.1847
IS-NB + TMD (1%M)	32.4956	10.5313	52.7331	93.6580	16.2484
Maximum RMS Superstructure Absolute Acceleration (m/s <sup>2</sup> )					
Orig_sys	0.8528	1.5860	4.2090	4.4980	2.7328
IS-linear	0.7677	0.3580	0.4710	0.5810	0.5349

IS-NB	0.8418	1.4148	1.4408	10.9175	1.0537
IS-NB + TMD (1%M)	0.8164	1.3863	4.2757	6.8443	1.0112
Maximum Base Absolute Acceleration (m/s <sup>2</sup> )					
Orig_sys	NA	NA	NA	NA	NA
IS-linear	11.4030	0.9458	1.4731	1.9288	2.3686
IS-NB	11.3810	6.2324	8.7025	65.4938	10.9108
IS-NB + TMD (1%M)	11.3845	6.1466	33.9597	65.2615	10.7462
RMS Base Absolute Acceleration (m/s <sup>2</sup> )					
Orig_sys	NA	NA	NA	NA	NA
IS-linear	0.4981	0.3300	0.4100	0.5200	0.4980
IS-NB	0.6027	0.9337	1.0874	6.9396	0.7651
IS-NB + TMD (1%M)	0.5731	0.9130	2.9638	4.6626	0.7065

The responses of all structural control systems in  $x$  and  $y$  direction under multiple excitations are shown in Table 6.5 and Table 6.6, respectively. Base isolation makes an excellent improvement beyond the fixed-base structure but simultaneously leading to a large base displacement. By installing the extra nonlinear bumper devices, the base displacements can be reduced under both explosions and earthquakes. However, the superstructure interstory drift and structural accelerations are amplified. There is a trade-off between the base displacements and other criteria. A finer parameter tuning of the nonlinear bumper can be conducted to obtain a balance responses of the structure, especially for a more narrow range of input loads. The performance is influenced by the magnitude and frequency content of the input excitation. This input dependence is especially seen in the amplifications on acceleration under the Northridge earthquake. .

Based on the experience on the 5-story structure, the TMDs are installed additionally on the IS-NB system in order to improve the performance of the nonlinear bumpers. The additional TMDs significantly further reduce the base displacements under

explosion. Even with amplifications on some criteria, generally, the performance of the combination of the TMDs and nonlinear bumpers are good under multiple excitations except the Kobe earthquake with observed amplification on the maximum superstructure absolute acceleration. The reductions by multiple control strategies are summarized and show in Table 6.7 and Table 6.8.

**Table 6.7 Reductions on different criteria in  $x-d$**

External Excitations	Blast (2000 kg)	El Centro	Kobe	Northridge	Tohoku
Reduction on Peak Base Displacement <sup>a</sup> (%)					
IS-NB	0.1	43.0	62.9	61.0	72.4
IS-NB + TMD (1%M)	55.2	43.4	63.0	61.1	72.3
Reduction on RMS Base Displacement <sup>a</sup> (%)					
IS-NB	49.8	21.5	69.5	56.1	60.7
IS-NB + TMD (1%M)	75.2	23.1	71.8	59.8	60.3
Reduction on Maximum Superstructure Interstory Drift <sup>b</sup> (%)					
IS-linear	55.0	70.9	89.5	78.4	68.3
IS-NB	18.3	-22.4	56.3	-12.4	26.2
IS-NB + TMD (1%M)	5.0	-21.2	57.0	-11.9	25.6
Reduction on Maximum RMS Superstructure Interstory Drift <sup>b</sup> (%)					
IS-linear	17.6	57.6	78.3	60.0	28.1
IS-NB	17.6	-9.1	66.7	-26.2	18.8
IS-NB + TMD (1%M)	-5.9	-6.1	69.0	1.5	18.8

Reduction on Maximum Superstructure Absolute Acceleration <sup>b</sup> (%)					
IS-linear	-0.9	80.5	92.1	84.6	88.6
IS-NB	-0.1	-4.0	45.5	-39.6	66.1
IS-NB + TMD (1%M)	-0.5	-2.2	46.4	-38.5	65.9
Reduction on Maximum RMS Superstructure Absolute Acceleration <sup>b</sup> (%)					
IS-linear	20.6	69.9	82.1	71.8	68.8
IS-NB	21.9	9.5	61.6	-31.6	58.5
IS-NB + TMD (1%M)	16.8	10.6	64.8	-0.5	58.9

<sup>a</sup>The reference system is the base isolated system.

<sup>b</sup>The reference system is the fixed base system.

**Table 6.8 Reductions on different criteria in *y-d***

External Excitations	Blast (2000 kg)	El Centro	Kobe	Northridge	Tohoku
Reduction on Peak Base Displacement <sup>a</sup> (%)					
IS-NB	12.9	22.8	33.4	44.7	72.3
IS-NB + TMD (1%M)	46.5	23.2	33.5	44.8	72.4
Reduction on RMS Base Displacement <sup>a</sup> (%)					
IS-NB	24.7	30.0	32.2	44.5	58.8
IS-NB + TMD (1%M)	49.1	31.8	39.4	57.1	60.6
Reduction on Maximum Superstructure Interstory Drift <sup>b</sup> (%)					
IS-linear	58.9	84.1	92.2	87.3	81.4
IS-NB	45.0	-18.2	-5.4	-39.4	25.7
IS-NB + TMD (1%M)	26.4	-16.8	-5.0	-38.9	26.1

Reduction on Maximum RMS Superstructure Interstory Drift <sup>b</sup> (%)					
IS-linear	18.8	75.0	83.3	84.6	40.0
IS-NB	-25.0	-2.5	11.7	-63.1	0.0
IS-NB + TMD (1%M)	-25.0	0.0	20.8	-9.2	6.7
Reduction on Maximum Superstructure Absolute Acceleration <sup>b</sup> (%)					
IS-linear	-0.2	87.4	93.0	89.1	94.3
IS-NB	0.5	-18.5	45.8	-219.3	66.4
IS-NB + TMD (1%M)	-0.7	-17.0	-101.1	-218.1	66.2
Reduction on Maximum RMS Superstructure Absolute Acceleration <sup>b</sup> (%)					
IS-linear	10.0	77.4	88.8	87.1	80.4
IS-NB	1.3	10.8	65.8	-142.7	61.4
IS-NB + TMD (1%M)	4.3	12.6	-1.6	-52.2	63.0

<sup>a</sup>The reference system is the base isolated system.

<sup>b</sup>The reference system is the fixed base system.

## 6.4 Chapter Summary

This chapter presents the responses of the 5-story structure and the 8-story three-dimensional structure under multiple external excitations.

For the 5-story structure, the performance of multiple control devices is investigated. First, the evaluation criteria are provided to compare the control performance between different devices. The traditional passive control strategies are employed to the fixed base structure and proved that only the base isolation plays a role in reducing structural responses even under blast loadings. However, it leads to a large base displacement which could damage the base isolators. Therefore, some extra control devices are installed on the base isolation system in order to decrease the base drift. The nonlinear bumper demonstrates excellent performance in reducing the peak base drift and the TMD performs better in reducing the RMS base drift. Thus, the combination of these two devices is investigated and the better performance of that is presented. The successful implementation of the nonlinear bumper proves that it is a functional device to decrease the base drift under explosions and concurrently maintain the performance of the base isolation under earthquakes.

For the 8-story structure, promising control alternatives are investigated, including the nonlinear bumper and its combination with the TMD on the base (IS-NB + TMD). Compare to the responses of the 5-story structure, the 8-story structure exhibited more complex structural responses. The nonlinear bumpers are shown to be functional in reducing base displacements under multiple excitations through this study. However, the amplifications on the maximum superstructure interstory drift and absolute accelerations of superstructure and base are significant under some excitations, such as the Northridge

earthquake. The combination of nonlinear bumpers and TMDs exhibits further reduction on peak base displacement, especially under blast excitations. More efforts need to be made on the improvement of the performance on the superstructure interstory drifts and accelerations.

In conclusion, the nonlinear bumper (IS-NB) and its combination with the TMD (IS-NB + TMD) proposed in this dissertation makes an excellent improvement in base displacements of the base isolation systems under explosions and earthquakes and concurrently maintain the performance of base isolation under some earthquakes.

## **CHAPTER 7 CONCLUSIONS AND RECOMMENDATIONS**

### **7.1 Conclusions**

This dissertation investigates the mitigation of blast and the seismic damage on base isolated structures. The main goals of this research are to investigate the potential for base isolated systems under blast loading and improve upon this performance through supplemental passive devices while simultaneously maintaining good performance under seismic excitations.

#### **7.1.1 Conclusions on 5-story Structure**

In this study, base isolation has been implemented and investigated for a simple 5-story structure under both explosions and seismic excitations. Although it was not possible to reduce the peak superstructure floor acceleration caused by the high frequency impact of the blasts, the base isolation is shown to reduce maximum superstructure interstory drifts and RMS superstructure absolute accelerations under blast. However, base-isolation leads to a large base displacement which could damage the isolators. Thus, additional devices installed on the base isolation are proposed. The TMD installed on the base has good performance reducing the RMS base displacement. The nonlinear bumper performs best in the reduction of the peak base displacement under all excitations, but simultaneously leads to amplification on the interstory drift and the absolute acceleration of the superstructure. Though, the responses of superstructure interstory drift and floor acceleration are still below the responses of the fixed base system. Since the nonlinear



bumper is efficient in reducing peak base drift and the TMD is better in terms of overall performance along the time, the combination of these two devices are proposed and investigated. As expected, better performance on reduction of base displacement is obtained through this combination strategy. Therefore, the nonlinear bumper and its combination with TMD installed on base isolation system are proved to be a good option for protecting building structures under both explosions and earthquakes.

### **7.1.2 Conclusions on 8-story Structure**

Three dimensional excitations are utilized to investigate the behaviors of the 8-story structure. All control devices are modeled in both directions to dissipate energy from bi-directional excitations. More complicated responses under the control systems are observed because of the more complicated benchmark structure been studied. As anticipated, base isolation makes an excellent performance by reducing maximum superstructure interstory drifts under explosions and by reducing both superstructure interstory drifts and absolute accelerations under earthquakes but concurrently resulting in a large base displacement. By installing nonlinear bumper device, base displacements are reduced. Further reduction can be achieved by using an additional TMD installed on the base level. However, the superstructure interstory drift and structural accelerations are amplified. Significant amplification occurred under some earthquakes with specific magnitudes and frequency contents like Northridge earthquake in this study. More efforts need to be made to improve the performance on the superstructure interstory drifts and structural accelerations.

In conclusion, generally, the nonlinear bumper (IS-NB) and its combination with the TMD (IS-NB + TMD) proposed in this dissertation are proved to a feasible option in reducing base displacements of base isolation systems under both explosions and earthquakes, concurrently, maintaining the performance of base isolation under some earthquakes.

## **7.2 Future Studies**

Some recommendations for future studies related to this work are:

- The performance of the nonlinear bumper and its combination with TMD is limited on the stage of simulation. The control strategies proposed in this dissertation need to be verified for experimental and full-scale applications.
- The performance of the extra devices is varying under seismic excitations with various frequency contents and magnitudes. The performance of the controlled system should be investigated under more seismic records.
- In this dissertation, the base isolation bearings are assumed to be linear elastomeric bearings. Further studies should focus on the nonlinear base isolation system. The performance of extra devices on the nonlinear base isolation system should be investigated.
- Under some earthquakes, the amplifications of the control systems on the accelerations and superstructure interstory drifts are significant. More efforts need to be made to avoid this phenomenon.

## REFERENCES

- A. S. Whittaker, V. V. Bertero, C. L. Thompson and L. J. Alonso, Seismic testing of steel plate energy dissipation devices, *Earthq. Spectra* **7**(4) (1991) 563–604.
- Baker, W.E. (1973). “Explosions in Air”. University of Texas Press, Austin, Texas.
- Beshara, F.B.A. (1994). “Modelling of Blast Loading on Aboveground Structures-I. General Phenomology and External Blast”, *Computers and Structures*, Vo. 51. No. 5, pp.585-596.
- Brode HL “Numerical solution of spherical blast waves”, *Journal of Applied Physics*, June 1955, No.6.
- Buckle, I., Nagarajaiah, S., Ferrell, K. (2002). "Stability of elastomeric isolation bearings: Experimental study." *Journal of Structural Engineering*, 128(1), 3-11.
- Bulson, P.S., (1997). “Explosive Loading of Engineering Structures”. Chapman and Hall.
- C E Anderson, “An Overview of the Theory of Hydrocodes”, *Int. J. Impact Engng.*, Vol. 5, 1987.
- Dowdell, D.J., and Cherry, S. (1994), Structural Control Using Semi-Active Friction Dampers, *Proc. 1st World Conf. on Struct. Control*, Pasadena, California, FA1:59-68, August 1994.
- Dyke, S. J., Spencer, B. F., Jr., Sain, M. K., Carlson, J. D. (1996a). "Modeling and control of magnetorheological dampers for seismic response reduction." *Smart Materials and Structures*, 5, 565-575.
- Dyke, S. J., Spencer, B. F., Jr., Sain, M. K., Carlson, J. D. (1996b). "Seismic response reduction using magnetorheological dampers." *Proc., IFAC World Congress*, Vol. L., Int. Fed. Of Automatic Control, 145-150.
- G. E. Fairlie. (1998). “The numerical simulation of high explosives using AUTODYN-2D & 3D.”
- Housner, G.W., Bergman, L.A., Caughey, T.K., Chassiakos, A.G., Claus, R.O., Masri, S.F., Skelton, R.E., Soong, T.T., Spencer, B.F., Jr., and Yao, J.T.P. (1997), Structural Control: Past and Present, *Journal of Engineering Mechanics*, ASCE, **123**(9), 897–971.

Inaudi, J.A. (1997), Modulated Homogeneous Friction: A Semi-Active Damping Strategy, *Earthquake Engrg., and Struct. Dyn.*, **26**, 361-376.

Jie Luo, N. E. Wierschem, L. A. Fahnestock, B. F. Spencer Jr., D. Dane Quinn, D. Michael McFarland, A. F. Vakakis, and L. A. Bergman. (2014). "Design, simulation, and large-scale testing of an innovative vibration mitigation device employing essentially nonlinear elastomeric springs." *Earthquake Engrg., and Struct. Dyn.*

Johnson, E. A., Ramallo, J., Spencer, Jr., B. F., and Sain, M. K. (1998). "Intelligent base isolation systems." *Proc., 2nd World Conf. on Structural Control*, Wiley, New York.

J. R. Sladek and R. E. Klinger, Effect of tune mass dampers of seismic response, *J. Struct. Eng. ASCE* **109** (1983) 2004–2009.

K. C. Tsai, H. W. Chen, C. P. Hong and Y. F. Su, Design of steel triangular plate energy absorbers for seismic-resistant construction, *Earthq. Spectra* **9**(3) (1993) 505–528.

Kelly, J. M., Leitmann, G., Soldatos, A. G. (1987). "Robust control of base-isolated structures under earthquake excitation." *Journal of Optimization Theory and Applications*, **53**, 159-180.

Kelly, J. M. (1997). *Earthquake resistant design with rubber*. 2nd ed., Springer, New York.

Kelly, J. M. (1999). "The role of damping in seismic isolation." *Earthquake Engineering and Structural Dynamics*, **28**, 3-20.

Kinney, Gilbert F. and Graham, Kenneth J., (1985). "Explosive Shocks in Air, 2nd Edition". Springer-Verlag, New York Inc.

Kobori, T., Takahashi, M., Nasu, T., Niwa, N., and Ogasawara, K. (1993), Seismic Response Controlled Structure with Active Variable Stiffness System, *Earthquake Engrg., and Struct. Dyn.*, **22**, 925-941.

Kurata, N., Kobori, T., Takahashi, M., Niwa, N., and Midorikawa, H. (1999), Actual Seismic Response Controlled Building with Semi-Active Damper System, *Earthquake Engrg., and Struct. Dyn.*, **28**, 1427-1447.

Kurata, N., Kobori, T., Takahashi, M., Ishibashi, T., Niwa, N., Tagami, J., and Midorikawa, H. (2000), Forced Vibration Test of a Building with Semi-Active Damper System, *Earthquake Engrg., and Struct. Dyn.*, **29**, 629-645.

Lam N, Mendis P and Ngo T (2004). Response spectrum solution for blast loading. *Electronic Journal of Structural Engineering*, 4, eJSE International, pp. 28-44.

Lou, J.Y.K., Lutes, L.D., and Li, J.J. (1994), Active Tuned Liquid Damper for Structural Control, *Proc. 1st World Conf. on Struct. Control*, Pasadena, California, TP1:70-79, August 1994.

Mills, C. A. The design of concrete structure to resist explosions and weapon effects. // *Proceedings of the 1st Int. Conference on concrete for hazard protections*, Edinburgh, UK, pp. 61-73, 1987.

AL-Shudeifat, M. A., Wierschem, N., Quinn, D. D., Vakakis, A. F., Bergman, L. A., & Spencer Jr, B. F. (2013). Numerical and experimental investigation of a highly effective single-sided vibro-impact non-linear energy sink for shock mitigation. *International journal of non-linear mechanics*, 52, 96-109.

Nagarajaiah, S., Ferrell, K. (1999). "Stability of elastomeric seismic isolation bearings." *Journal of Structural Engineering*, 125(9), 946-954.

Narasimhan S, Nagarajaiah S, Johnson EA, Gavin HP. Smart base isolated benchmark building. Part I: problem definition. *Proceedings of the 4th International Workshop on Structural Control and Health Monitoring*, Columbia University, 10–11 June, 2004. CDROM.

Newmark, N. M. and Hansen, R. J., "Design of blast resistant structures", shock and vibration Handbook, Vol. 3, Eds. Harris and Crede. McGraw-Hill, New York, USA. 1961.

Park YJ, Wen YK, Ang AHS. Random vibration of hysteretic systems under bi-directional ground motions. *Earthquake Engineering and Structural Dynamics* 1986; 14(4):543–557.

P. Mahmoodi, Structural dampers, *J. Struct. Div. ASCE* **95** (1969) 1661–1672.

R. Zhang, T. T. Soong and P. Mahmoodi, Seismic response of steel frame structures with added viscoelastic dampers, *Earthq. Eng. Struct. Dynam.* **18**(9) (1989) 389–396.

R. J. McNamara, Tuned mass dampers for buildings, *J. Struct. Div. ASCE* **103** (1977) 1985–1998.

R. W. Luft, Optimal tuned mass dampers for buildings, *J. Struct. Div. ASCE*. **105** (1979) 2766–2772.

Smith, P.D. and Hetherington, J.G., (1994). "Blast and Ballistic Loading of Structures". Butterworth-Heinemann Ltd., Oxford, © 1994.

Spencer Jr., B.F., Suhardjo, J., and Sain, M.K. (1994), Frequency Domain Optimal Control Strategies for Aseismic Protection, *Journal of Engineering Mechanics*, ASCE, **120** (1), 135–159.

Spencer, B.F., Jr., and Sain, M.K. (1997), Controlling Buildings: A New Frontier in Feedback, *IEEE Control Systems Magazine: Special Issue on Emerging Technologies* (Tariq Samad Guest Ed.), **17** (6), 19-35.

Spencer, B.F. Jr., and Soong, T.T. (1999), New Applications and Development of Active, Semi-Active and Hybrid Control Techniques for Seismic and Non-Seismic Vibration in the USA, *Int. Post-SMiRT Conf Seminar on Seismic Isolation, Passive Energy Dissipation and Active Control of Vibration of Structures*, Cheju, Korea, Proceedings, August 23-25, 1999.

Spencer, B. F., Jr., Nagarajaiah, S. (2003). "State of the art of structural control." *Journal of Structural Engineering*, 120(7), 845-856

Soong, T. T., Constantinou, M. C. (1994). *Passive and active structural vibration control in civil engineering*. Springer-Verlag New York, Inc., New York.

Soong, T. T., Dargush, G. F. (1997). *Passive energy dissipation systems in structural engineering*. John Wiley & Sons, Inc., New York.

Soong, T.T., and Spencer Jr., B.F. (2001), Supplemental Energy Dissipation: State-of-the-Art and State-of-the-Practice, *Engineering Structures*, submitted.

TM 5-1300, "Structures to Resist the Effects of Accidental Explosions", U.S. Department of Army, 1990

UFC 3-340-02, "DoD Ammunition and Explosives Safety Standards", U.S. Department of Defense, 5 December 2008.

W & B Pilley (eds.), "Shock and Vibration Computer Programs; SVM-13", SAVIAC, Booz Allen & Hamilton, Virginia, USA, 1995.

Yao, J.T.P. (1972), Concept of Structural Control, *ASCE J. Struct. Div.*, **98**, 1567-1574.